Universidade de Aveiro
2012

Departamento de Química

Patrícia Manuela Ribeiro Pereira

CONJUGADOS FOTOATIVOS PARA TRATAMENTO DO CANCRO DA BEXIGA

Universidade de Aveiro
2012

Departamento de Química

Patrícia Manuela Ribeiro Pereira

CONJUGADOS FOTOATIVOS PARA TRATAMENTO DO CANCRO DA BEXIGA

Dissertação apresentada à Universidade de Aveiro para cumprimento dos requisitos necessários à obtenção do grau de Mestre em Bioquímica com especialização em Métodos Biomoleculares, realizada sob a orientação científica do Doutor João Tomé e da Doutora Rosa Fernandes, respetivamente, investigador auxiliar da Universidade de Aveiro e investigador auxiliar da Universidade de Coimbra.

Dedico esta tese à minha mãe por ser um anjo para mim na terra e
à minha prima Cinda por ser um anjo para mim no céu.

The only source of knowledge is experience.
Albert Einstein

o júri

presidente

Doutor Pedro Miguel Dimas Neves Domingues
Professor Auxiliar da Universidade de Aveiro

Doutora Célia Maria Freitas Gomes
Investigador Auxiliar da Universidade de Coimbra

Doutor João Paulo Costa Tomé
Investigador Auxiliar da Universidade de Aveiro

Doutora Rosa Cristina Simões Fernandes
Investigador Auxiliar da Universidade de Coimbra

agradecimentos

A execução prática e a redação desta tese de mestrado, apenas foram possíveis devido à contribuição de pessoas para as quais quero deixar aqui algumas palavras:

Ao meu orientador, Doutor João Tomé, quero agradecer por ter acreditado em mim logo no primeiro dia em que me conheceu. Um agradecimento especial pelo incentivo, discussões, pelas palavras de apoio, e pela orientação científica.
À minha orientadora, Doutora Rosa Fernandes, agradeço por me ter recebido no seu laboratório, pela confiança que depositou em mim, pela liberdade que me deu na execução de todas as experiências. Agradeço também pelas vezes em que me chamou à razão, pela orientação científica, a amizade e partilha de entusiasmos e desalentos.
Às Doutoras Graça Neves e Graça Marques, obrigado por me terem introduzido no mundo fascinante da ciência.
Ao Doutor Rudolf Schneider quero expressar o meu reconhecimento pelo apoio incondicional e interesse dedicados na realização de parte deste trabalho. Agradeço-lhe a hospitalidade com que me recebeu em Berlim, as palavras de motivação, os ensinamentos científicos e os recursos que me disponibilizou.
À Doutora Sandrina Silva, quero agradecer a amizade, a ajuda no laboratório, as palavras de motivação e o carinho.
Ao Doutor João Carvalho, por me ter recebido em Berlim, pela amizade e pelas valiosas palavras que me deram muita força.
À Doutora Eduarda Silva, agradeço por me ter "encaminhado" para o sítio certo e pela ajuda.
À Doutora Célia Gomes, agradeço os ensinamentos científicos acerca das células estaminais e por ter disponibilizado os recursos que permitiram a realização de uma parte deste trabalho.
À Doutora Amparo Faustino, pela ajuda nos estudos foto-físicos.
À Cláudia Gonçalves quero agradecer as conversas, o apoio, os desabafos e as "trapalhadas" que nos fizeram rir e que acabaram sempre em bem. Com ela, comecei no IBILI esta grande etapa que acima de tudo resultou numa bela amizade. À Andreia Gonçalves quero agradecer por me ter recebido no IBILI e por me ter ajudado em muitas das experiências.

To all the people of the division 1.8 of BAM, for their good work and friendship. Not forgetting the others, I particularly would like to thank Stefanie Gärtner, Sascha Wagner, and André Grasnick, for their help and support. To Sabine Flemig, Doctor Andreas Lehmann and Shireen Weise for help me in the mass spectrometry studies.
A todos os meus amigos e familiares, em especial ao Guido, ao Márcio, à Diana, à Bruna, à Luciana, à Raquel e à Soraia agradeço o valor que me dão e a amizade que temos. *"Thank you for being a friend…Traveled down the road and back again… your heart is true you're a pal and a confidant"*. Agradeço em especial à Diana e ao Guido por terem lido a minha tese. *"I see friends shaking hands.....saying how do you do... They're really saying...I love you.../And I think to myself ....what a wonderful world"*.
À Dona Rosa e Senhor António pelo carinho, pela preocupação e pela ajuda. Agradeço em especial à Dona Rosa pelo incansável apoio em tudo.
Aos meus pais, ao meu Carlitos e à minha Lili por aturarem o meu "mau feitio", por me apoiarem, pelo orgulho que têm em mim e por me amarem incondicionalmente.
Ao Guido Lopes quero agradecer tudo o que me dá todos os dias. *"…Smile when he makes you happy, yell when he makes you mad, and miss him when he's not there..."*

À Universidade de Aveiro, muito em especial ao Departamento de Química.
À Faculdade de Medicina da Universidade de Coimbra, muito em especial ao IBILI.
À Fundação para a Ciência e Tecnologia, a bolsa de investigação.

palavras-chave Terapia Fotodinâmica, Cancro da bexiga, Porfirinas, Ftalocianinas

resumo

A terapia fotodinâmica (PDT) é uma metodologia emergente no tratamento de diversas doenças oncológicas, tendo por base o uso de oxigénio, luz e um fotossensibilizador (PS) para gerar reações citotóxicas no tecido tumoral. Reconhecendo a potencialidade de PSs conjugados com diferentes biomoléculas para serem reconhecidos especificamente por antigénios ou recetores sobrexpressos nas células tumorais, este estudo pretendeu avaliar o potencial fotodinâmico de PSs conjugados com moléculas de galactose (Gal), com a albumina humana e bovina, e com o anticorpo monoclonal anti-CD104. Numa primeira fase (Parte I) foram avaliadas as propriedades foto-químicas e -físicas de uma porfirina (**PorGal$_8$**) e de uma ftalocianina (**PcGal$_{16}$**) conjugadas com moléculas de galactose. Estes compostos mostraram-se solúveis em meio aquoso, fluorescentes, foto-estáveis, geradores de espécies reativas de oxigénio (ROS) após foto-ativação e apresentaram interação com a albumina humana. Nas Partes II e III deste trabalho, foram realizados estudos *in vitro* de PDT com as linhas celulares de cancro da bexiga HT-1376 e UM-UC-3, para avaliar o potencial fotodinâmico da **PorGal$_8$** e **PcGal$_{16}$**. Os conjugados demonstraram toxicidade após foto-ativação, por um mecanismo dependente da formação de ROS. Após PDT, a **PorGal$_8$** induziu alterações ao nível do citoesqueleto das linhas celulares e apresentou-se mais eficaz com a linha celular UM-UC-3. Posteriormente foi demonstrado que a resistência das células HT-1376 à PDT com a **PorGal$_8$** é explicada pela baixa expressão de galectina-1 (proteína capaz de reconhecer a **PorGal$_8$**) e pela presença de células que sobrexpressão a proteína ABCG2 (proteína capaz de bombear a **PorGal$_8$** para fora das células). A **PcGal$_{16}$** apresentou também, inesperadamente, um modo de ação não dependente da sua foto-ativação, sendo capaz de diminuir os níveis de galectina-1 após o seu uptake pelas células. A síntese e o potencial biológico, usando as células UM-UC-3, dos conjugados porfirina-albuminas e porfirina-anti-CD104 são descritos na última parte deste trabalho (Parte IV). Estes conjugados induziram reações citotóxicas após foto-ativação, sendo o conjugado com o anticorpo mais eficaz que os conjugados com as albuminas. Estes resultados obtidos com experiências *in vitro* demonstraram que os conjugados exibem propriedades bio-físico-químicas promissoras e são potenciais PSs para tratamento do cancro da bexiga.

keywords Photodynamic Therapy, Bladder cancer, Porphyrins, Phthalocyanines

abstract

Photodynamic therapy (PDT) is a promising method, which has been studied and applied to improve the treatment of several tumour types. PDT combines molecular oxygen, light and a photosensitizer (PS) to generate cytotoxic reactions in cancer cells. The potential of PSs conjugated with biomolecules which will be recognized by antigens or receptors overexpressed in cancer cells prompted us to validate the photodynamic activity of PSs conjugated with galactose units, human and bovine serum albumins, and the monoclonal antibody anti-CD104.

In Part I, the photo-chemical and -physical properties of a porphyrin (**$PorGal_8$**) and a phthalocyanine (**$PcGal_{16}$**) conjugated with galactose molecules were evaluated. The galacto-conjugates demonstrated to be water soluble, fluorescents, photo-stable, generators of reactive oxygen species (ROS) and able to interact with human serum albumin. The photodynamic potential of **$PorGal_8$** and **$PcGal_{16}$** against human bladder cancer cell lines, HT-1376 and UM-UC-3 is demonstrated in the parts II and III of this thesis. The galacto-conjugates induced phototoxicity in both bladder cancer cell lines by a ROS-mediated mechanism. After photo-activation, **$PorGal_8$** induces changes in actin organization of bladder cancer cells and it was more photo-active against UM-UC-3 cells. The resistance observed in HT-1376 cells after PDT with **$PorGal_8$** was due to the low expression of galectin-1 (able to recognize galactose molecules) and to the presence of cells overexpressing the multi-drug resistant pump ABCG2. Unexpectedly, **$PcGal_{16}$** exhibited also a "dark" mode of action by decreasing galectin-1 after its uptake in cancer cells.

In Part IV, the synthesis of a porphyrin conjugated with bovine and human serum albumins and the monoclonal antibody anti-CD104 is reported, as well as their biological potential against the human bladder cancer cell line UM-UC-3. These conjugates demonstrated high efficacy in destroying the cancer cells, with the mAb anti-CD104 efficacy overruling the albumins one.

The *in vitro* results demonstrated that the conjugates exhibit excellent bio-physic-chemical properties and prompted us to envisage them as novel anticancer drug candidates for bladder cancer treatment.

Contents

Abbreviations and acronyms

BSA	Bovine Serum Albumin
Caf	Caffeine
CSCs	Cancer Stem Cells
CO_2	Carbon dioxide
CIS	Carcinoma *in situ*
DOL	Degree Of porphyrin Labeling
DAPI	4',6-diamidino-2-phenylindole
H_2DCFDA	2´,7´-dichlorohydrofluorescin
DHE	Dihydroethidium
DMF	Dimethylformamide
DMSO	Dimethylsulfoxide
MTT	3-(4,5-Dimethylthiazol-2-yl)-2,5-diphenyltetrazolium bromide
DPBF	1,3-diphenylisobenzofuran
ELISA	Enzyme-Linked Immunosorbent Assay
ER	Endoplasmic Reticulum
ε	Extinction coefficient
Φ_F	Fluorescence quantum yields
HP	Hematoporphyrin
HpD	Hematoporphyrin Derivative
CD104	Human integrin β4
HSA	Human Serum Albumin
IPC_{50}	Intracellular Phototoxic Concentration
LC-UV-MS	Liquid Chromatography coupled to Ultraviolet-Visible and Mass Spectrometric detection
m/z	Mass-to-charge ratio
MALDI-TOF-MS	Matrix-Assisted Laser Desorption/Ionization-Time Of Flight-Mass Spectrometry
mAb	Monoclonal Antibody
nm	nanometers
PBS	Phosphate Buffered Saline
PDT	Photodynamic Therapy
PF	Photofrin
PS	Photosensitizer
$^1PS^*$	Photosensitizer in the excited-singlet-state
^1PS	Photosensitizer in the ground-state
$^3PS^*$	Photosensitizer in the triplet-state
IC_{50}	Photocytotoxic Concentrations
Pc	Phthalocyanine
Por	Porphyrin

ROS	Reactive Oxygen Species
RT	Room Temperature
$^1O_2$	Singlet oxygen
NaN_3	sodium azide
TPP	*meso*-tetraphenylporphyrin
CHOP	Transcription factor C/EBP homologous protein
$^3O_2$	Triplet-state oxygen
UPR	Unfolded Protein Response
ZnPc	Zinc Phthalocyanine

INTRODUCTION
CHAPTER 1

---

1. General overview

Let's suppose that you could have a cancer treatment that maintains your bladder and its physiological function, instead of a surgery that removes a part or your entire organ…

Let's suppose that you could have a cancer treatment made only once, not months of chemotherapy, radiotherapy or surgery…

The choice is pretty objective!!!

Photodynamic Therapy will never be the right or only answer for every type of cancers, but it has a great potential…

Cancer is the term used for describe malignant diseases in which abnormal cells divide without control and are able to invade the tissues and the organs of the body. In European Union, in 2008, over two million (2 457,610) incident cancer cases (all sites but non-melanoma skin) and over one million cancer deaths (1 231,220) were registered [1]. Cancer is an important public health problem and its incidence is likely to increase in the future due to European population ageing. Cancer-associated problems (pain, depression, economic spending, fear, and anxiety) have impact on individuals, families and our society as a whole, making this an alarming situation.

The cancer treatment with conventional modalities, including surgery, radiotherapy and chemotherapy, result in serious side effects caused by the loss of physiological organ function. The advances reported in cancer scientific research imply methods that allow the early detection of the disease, and techniques that avoid the surgical removal of an organ. Photodynamic Therapy (PDT) is a promising and rather non-invasive method, which has been studied and applied to improve the treatment of several tumour types, especially the ones occurring in accessible cavities like the bladder. In PDT, the selective uptake of a photoactive agent by cancer cells followed by light irradiation can result in Reactive Oxygen Species (ROS) production. ROS can trigger chemical and biochemical processes that can lead to *in situ* cell death. Nowadays, the development of compounds for PDT those specifically accumulate in cancer tissues is a lively research field.

2. Bladder cancer

When cancer touches the life, many things can change...

Bladder cancer is one of the most common malignancies in population worldwide and it is characterized by frequent recurrences. This section provides information about the development, incidence, diagnosis and therapy of bladder cancer. Herein, the use of PDT as an emerging modality for bladder cancer treatment is highlighted.

2.1. Bladder cancer development

The bladder is a hollow, balloon shaped organ in the pelvic floor and due to its function (storage of urine) it has flexible and muscular walls [2]. The inside of the bladder is lined with transitional cells (transitional epithelium or urothelium) and squamous cells. Next is lamina propria (a layer of loose connective tissue) that is covered by the bladder muscle. Outside of the bladder is a layer of fat (**Figure 1.1**).

Bladder cancer progression is characterized by four stages [3]. The tumour arises on the inside of the bladder wall (stage 0). Stage 0 tumours can penetrate the lamina propria layer (stage I), spread into the muscular layer (stage II), extend beyond the bladder muscle and into the outer layer (stage III) or spread toward the abdominal or pelvic wall (stage IV) [3, 4]. Cancers confined to the urothelium (stage 0) or lamina propria (stage I) are called superficial bladder cancers or non-muscle invasive. Muscle invasive cancers correspond to cancers that grow into the muscular wall of the bladder [5] (**Figure 1.1**).

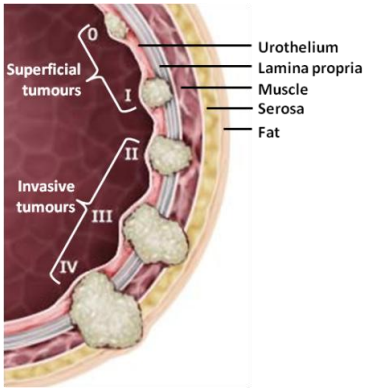

Figure 1.1. Bladder layers and bladder cancer progression (Superficial tumours: stages 0 and I; Invasive tumours: stages II, III, and IV). Adapted from [3].

Muscle invasive cancer may extend through the bladder wall and grow into a nearby organ such as the uterus or vagina (in women) or the prostate gland (in men). It may also

invade the wall of the abdomen. When bladder cancer spreads outside the bladder, cancer cells are often found in nearby lymph nodes. If the cancer reaches these nodes, cancer cells may have spread to other lymph nodes or other organs, such as the lungs, liver, or bones. Metastatic bladder cancer is the term used when cancer extends from its original place to another part of the body [3].

Actually, bladder cancer staging is based on tumour penetration degree into the bladder wall. **Table 1.1** lists penetration stages using the Tumour-Node-Metastases (TNM) classification system, which is the most commonly used and universally accepted classification [6].

Table 1.1. Staging of primary bladder cancer tumours (Tumour-Node-Metastases Classification) [6].

Ta	Non invasive papillary tumour (confined to urothelium)
Tis	CIS carcinoma (high grade "flat tumour" confined to urothelium)
T1	Tumour invades lamina propria
T2	Tumour invades bladder muscle
T2a	Tumour invades superficial bladder muscle
T2b	Tumour invades deep bladder muscle
T3	Tumour invades perivesical fat
T3a	Microscopic perivesical fat invasion
T3b	Macroscopic perivesical fat invasion
T4	Tumour invades prostate, uterus, vagina, pelvic wall or abdominal wall
T4a	Tumour invades adjacent organs (uterus, ovaries, prostate)
T4b	Tumour invades pelvic wall and/or abdominal wall

Ta and Tis (in the urothelium) and T1 (in the lamina propria) are the non-muscle invasive stages. Tis classification is applied for a high grade non-muscle invasive stage known as carcinoma *in situ* (CIS). The CIS is difficult to remove and if untreated will likely progress to muscle invasive disease [5, 6]. Most Ta tumours are low grade and do not progress to invade the bladder muscle. Stage T1 tumours may be much more likely to become muscle invasive. These tumours must be carefully monitored due to their recurrence in a higher and potentially lethal stage [6].

2.2. Bladder cancer statistics

Bladder cancer is the second most common cancer of the genitourinary tract (**Figure 1.2**), with rates of incidence and mortality in European Union of 14.6 and 4.8 per 100,000, respectively [1]. In Portugal, it is the fifth most common cancer among men [1]. Although the improvements seen in the last years, the bladder cancer incidence and mortality rates vary widely across the continents and between sexes [1, 7], with men and those from undeveloped countries at a distinct disadvantage (**Table 1.2**) [8]. Bladder cancer can occur at any age [1], however more than 90% of all patients diagnosed with this type of disease are 55 years of age and older.

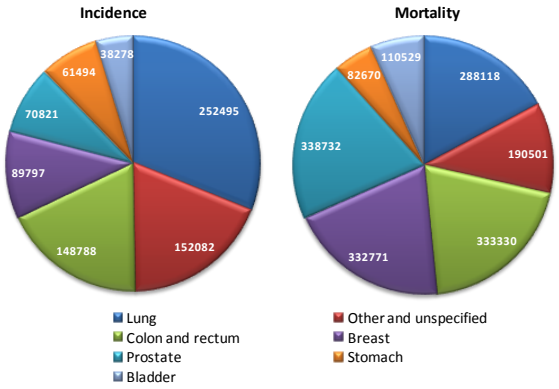

Figure 1.2. Most frequent cancers in European Union (2008). The values correspond to estimated incidence and mortality (both sexes) [1].

Table 1.2. Bladder Cancer in European Union and Portugal (2008) [1]. The values correspond to estimated incidence and mortality. Age standardized rate (European) per 100,000.

		Incidence	Mortality
Portugal	Man	22.6	7.3
	Woman	4.8	1.7
European Union	Man	28.3	8.8
	Woman	5.8	2.0

Fortunately, the majority of bladder cancers diagnosed remains superficial and approximately 75-85% of those are low grade tumours [9]. The probabilities for recurrence of superficial bladder tumours range from 15% to 61% at 1 year and from 31% to 78% at 5 year, according to the European Organisation for Research and Treatment of Cancer [10]. While the majority of superficial bladder tumours does not progress, up to 20% can proceed to muscle invasive or metastatic disease. The rates for progression range from

<1% to 17% at 1 year and from 1% to 45% at 5 year [10]. Due to its frequent recurrence and significant progression risk, patients with non-muscle invasive bladder cancers need to be under medical surveillance. This situation contributes to a large financial expenditure [11].

2.3. Bladder cancer treatment

Transurethral resection and intravesical therapy are used in the treatment of bladder cancer. Cystoscopy, urine cytology and excretory urograms are used as tools for bladder tumours diagnosis [12]. These conventional modalities might cause unwanted side effects and in some cases they are not completely effective [9]. There is an urgent necessity for novel and effective cancer therapies. Identification followed by complete and selective destruction of tumours is the most desirable outcome and may reduce recurrence and progression rates [9], with postulated benefits for both patients and the health care economics.

The clinical urological interest in PDT is focused on the preservation of the bladder and its function. Current scientific research on PDT for bladder cancer treatment is based on the development of tumour selective drugs. Bladder cancers are suitable targets for PDT because their interior can be assessed by endoscopy. The bladder geometry allows a homogeneous light delivery and the bladder tissue is relatively more translucent when compared to other human tissues.

3. Photodynamic Therapy

In oncology, PDT is an emerging modality of cancer treatment. Firstly, a photoactive drug is administrated and accumulated selectively in cancer cells. The exposure of the tumour to light can result in cytotoxicity induced by ROS. This section provides a brief history about PDT and its photoactive component. The clinical applications of PDT in the oncologic field, as well as the mechanisms of cell death induced by PDT are also described.

3.1. Brief history

Perhaps the best way to start is the beginning… A detailed description of the PDT history is too complex to be encompassed here. Nevertheless, some key findings are important to understand the urgent necessity for new and effective PSs.

The idea of combining light and a chemical compound has ancient beginnings. Scientific records of the therapeutic effect of sunlight activation of psoralens extracts date back to approximately 3,000 years ago when this early photochemotherapy was used for repigmentation of vitiligo [13, 14]. The most important discoveries in the history of PDT are described in the following topics, focusing those who encouraged the medical applications of PDT in the oncologic field (**Figure 1.3**).

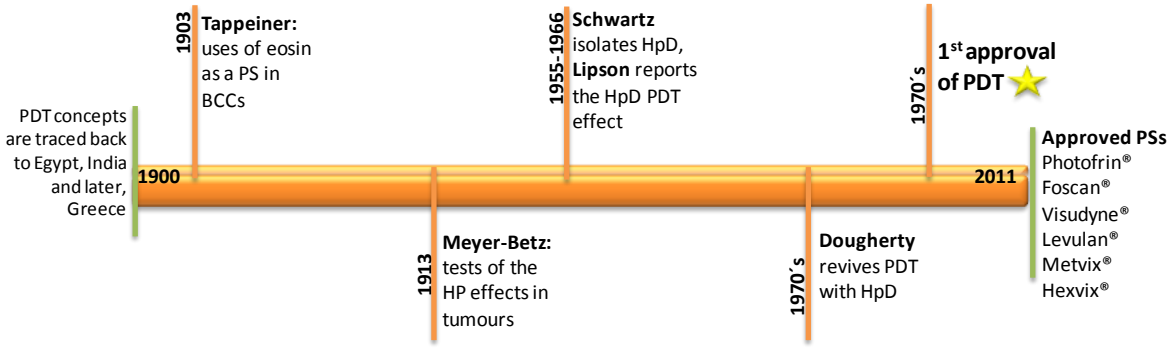

Figure 1.3. Timeline showing selected milestones in the historical development of PDT in oncology.

The first application of PDT in cancer treatment was described by von Tappeiner and Jesionek in 1903 [15], who applied eosin to basal cell carcinomas prior to illumination. Porphyrins (Pors), the most explored class of drugs in PDT, were initially investigated by

Meyer-Betz in 1913 [16]. In these investigations, the PDT effects with Hematoporphyrin (HP) in rat tumours are reported. Meyer-Hertz also performed a heroic self-experiment: he injected himself with HP and irradiated a small area at his forearm. Consequently, exposure to direct sunlight led to phototoxic reactions with swelling and burning sensation [17]. Modern time of PDT applications was stimulated after Schwartz [18] and Lipson´s findings in which the acid treatment of HP yielded a mixture of Pors and other chemical species, termed Hematoporphyrin Derivative (HpD). HpD after red light activation demonstrated better PDT effect than that of HP [14]. Although the chemical characterization of HpD was not completely clear, in 1975 Dougherty [19] reported that the combination of this drug and red light results in mammary tumour eradication. This exciting result encouraged the first clinical experiments with HpD to treat patients with bladder cancer and skin tumours [20, 21]. In the late 1980s, Quadra Logic Technologies Photo Therapeutics (Vancouver, British Columbia, Canada) and Lederle Laboratories (American Cyanamid, Pearl River, NY) formed a partnership to achieve approvals for the clinical use of PDT [14]. The first PDT approval occurred in 1993 (in Canada) using Photofrin® (PF) - a more purified and better characterized version of HpD - for the treatment of bladder cancer [22]. The first Food and Drug Administration approval of PDT in the United States was also obtained with PF, in 1995, for palliation of obstructive esophageal cancer [22]. The results obtained with PF and the PDT approvals generated curiosity in the scientific community, as a brief search on Web of Science for the keyword "photodynamic" for the period 1900-2010. The number of papers increased from 113 in the first half of the century (1900-1955) to more than 10,119 in the second half (1955-2010), with more than 4,000 papers in the last 5 years.

The new recent time of clinical PDT is stimulating organic chemists to develop synthetic pathways that make possible the production of potential PSs.

3.2. Photophysics and Photochemistry

Photosensitization reactions are applied in a wide variety of medical areas. However the photophysical and photochemical mechanisms by which a photo-activated PS induces cytotoxicity are challenges in photobiological and photochemical researches…

From photophysical and photochemical points of view, PDT is not completely clear. Nevertheless, a general overview about the photo-processes involved in PDT will be addressed in the next two points.

3.2.2. Photophysics

A PS molecule in its normal state is in a configuration named ground-state, ^{1}PS. This state corresponds to the lowest possible energy in PS molecule. The absorption of light (at a specific wavelength) by the PS causes its promotion from ground-state to the excited-singlet-state, $^{1}PS^{*}$. The excited-singlet-state is extremely unstable with a half time in the range of 10^{-6} seconds to 10^{-9} seconds. $^{1}PS^{*}$ can decay back to the ^{1}PS emitting fluorescence [23]. However, to obtain the PDT effect, the $^{1}PS^{*}$ must undergo intersystem crossover to an electronically different excited state (10^{-2} seconds), the excited-triplet-state, $^{3}PS^{*}$ [24, 25]. After PS restores its ground-state the cycle is repeated (**Figure 1.4**). The electronic excitation of the PS, after light absorption, can elicit cytotoxic effects by PDT or fluorescence emission which permits to detect the malignant tissue (**Figure 1.4**).

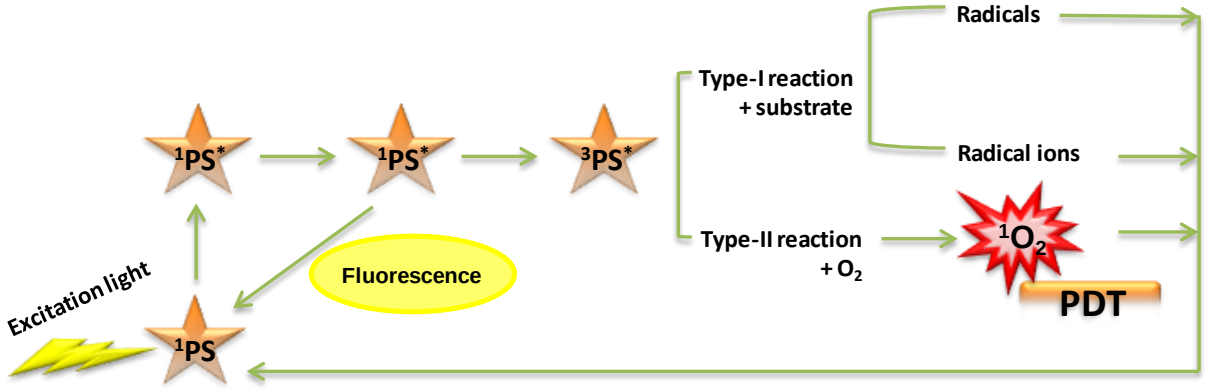

Figure 1.4. The principle of PDT, under photo-chemical and -physical points of view.

Depending on the PS chemistry, visible light at the wavelength range of 400-800 nm can originate the biochemical processes relevant to PDT [23]. However, blue light penetrates less efficiently through tissue than red and infrared radiations. Thus, the maximum absorption of the PS for PDT should correspond to the wavelength range of 650-850 nm, where the light penetration through the tissue is quite high (**Figure 1.5**) and the interference by endogenous chromophores within the body is avoided [23, 26]. Moreover,

with this wavelength range, the energy required for the production of ROS is maintained [23, 26].

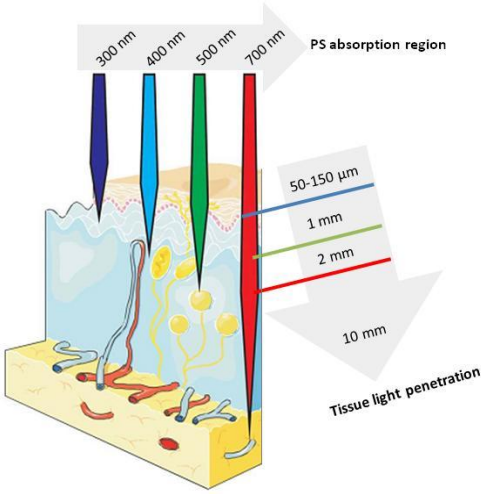

Figure 1.5. Correlation between the absorption of light by the PS molecule and the propagation of light through the tissues. Adapted from [27]**.**

3.2.3. Photochemistry

A light excited PS molecule has a high probability of triplet-state formation ($3PS^*$) [26]. In general, $^3PS^*$ is longer lived than the $^1PS^*$, thus the cytotoxic processes induced by PDT are often mediated by this state. $^3PS^*$ can induce chemical changes in a neighbour molecule *via* two competing pathways: type-I and type-II photochemical reactions [28] (**Figure 1.5**). Type-II is the most predominant process and it is better described in the literature than Type-I.

Type-I photochemical reaction means the transfer of electrons (or protons) to a biological substrate forming radicals and radical ions [26]**.** These radicals can react with molecular oxygen producing ROS [26].

Type-II reaction results in the $^3PS^*$ energy transference to oxygen molecular, causing the excitation of triplet-state oxygen ($^3O_2$) to form singlet oxygen ($^1O_2$) that is a highly reactive chemical specie. The role of $^1O_2$ in the photodynamic effect is controversial between researchers. However, for most PSs currently in investigation, the $^1O_2$-mediated photodynamic mechanism is the model of cytotoxic action usually accepted. In most cellular systems, the $^1O_2$ has a short lifetime [29]**,** ranging from 10 ns to 320 ns. Therefore, its diffusion range is confined to approximately 10-55 nm in cellular media [30, 31]. The diameter of human cells ranges from 10-100 µm, thus $^1O_2$ cannot diffuse more than a

single cell length [32]**.** The site of the primary $^1O_2$ generation determines which sub cellular structures may be accessed and attacked.

3.3. Advances in PSs chemistry (first, second and third generation PSs)

PS is the key element in PDT. Nowadays, none of the existing PSs can be seen as an ideal one.

The design of new PSs with excellent photophysical and biological properties is a lively research field in medicinal chemistry [33-35]. PSs are different in terms of chemical and biological characteristics and are classified in first-, second- and third-generation PSs [36]. An ideal oncologic PS should fulfil the requirements presented in **Table 1.3** [25, 32, 33, 37]. Not only the chemical, physical and biological properties, but also characteristics that meet the patient's needs, have to be taken into account.

Table 1.3. The requirements of an ideal oncologic PS [25, 32, 33, 37].

Toxicity	Able to produce singlet oxygen Not able to produce dark toxicity
Pharmacokinetic elimination	Able to be eliminated itself
Selectivity	Able to be selectively and quickly accumulated in tumour tissue
Activation	Able to be activated at the wavelengths that allow optimal tissue penetration
Sunlight precautions	Not able to produce a high degree of skin photosensitivity
Administration	Able to be dissolved in injectable solvents Not able to produce aggregates in biological environments
Photostability	Able to be photostable and with chemical purity
Reliability	Able to get where you need it and activated when you need it
Pain-free therapy	Not able to induce pain during and after therapy
Availability	Able commercially (and not expensive) Able to be reconstituted by a local pharmacy
Safety	Able to be administrated without patient significant worry
Integrative ability	Able to be used in conjunction with other forms of treatment

3.3.1. First generation PSs

The first family of PSs discovered is based on HP and its derivatives, HpD. After purification and manipulation, HpD was transformed into commercial products like PF (the first approved PS) [38]. PF is the main Por-based drug in both pre-clinical and clinical trials, but it still contains a non homogeneous chemical constitution. By adding, subtracting or substituting Pors structures, new porphyrinic PSs with well characterized composition are being created and they are entitled as first generation PSs.

Pors are aromatic heterocyclic macrocycles composed of four modified pyrrole subunits, interconnected *via* methane bridges. They constitute an important group of pigments (**Figure 1.6**) [39]. The typical absorption spectrum of Pors is characterized by five peaks (**Figure 1.6**), the strongest known as Soret band (about 400 nm) and a set of four progressively smaller absorption bands (as the spectrum moves into the red wavelengths) known as Q-bands (**Figure 1.6**) [40]. Although these compounds are the most commonly used PSs [41] in the oncological clinic, they present three main disadvantages [37, 42]:

- Biological effects after irradiation occur only to a tissue depth of about 5 mm, due to the longest-wave absorption band that appears at 630 nm (with a low extinction coefficient);

- Non-selective accumulation in the tumour due to low specificity to the cancer tissue;

- Long skin photosensitivity due to cutaneous accumulation and slow clearance from the skin.

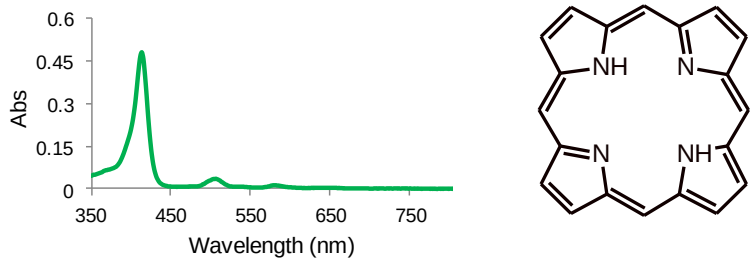

Figure 1.6. Porphyrin structure and absorption spectrum.

3.3.2. Second generation PSs

The limitations of first generation PSs arouse interest amongst organic chemists for the development of second generation PSs with new and improved characteristics based on PF. These new compounds include benzoporphyrin derivates, chlorins, phthalocyanines (Pcs), texaphyrins and naturally occurring compounds such as hypericin and protoporphyrin IX (PPIX) [43]. These PSs absorb light in the red and near-infrared regions of the electromagnetic spectrum (600-800 nm), allowing the treatment of deep tumours. Furthermore, with second generation PSs, the $^1O_2$ production is markedly improved compared with first generation PSs [44].

Pcs consist of a ring with four isoindole units (**Figure 1.7**). The pyrrole groups in Pcs are conjugated to benzene rings, but in contrast to Por, these unities are bridged by nitrogen atoms [43]. Pcs structure causes a strong absorbance in red light with a maximum around 670 nm (**Figure 1.7**) that results in increased tissue light penetration. It has been proved that Pcs are very effective in a variety of cancers [45, 46]. Despite of the improvements referred above, the majority of second generation PSs does not show a localized distribution in the tumour area.

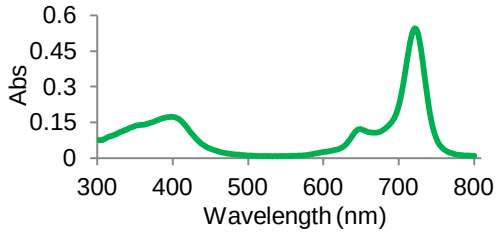

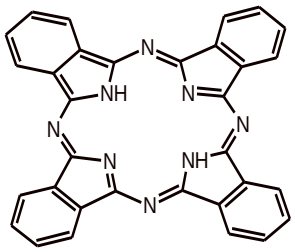

Figure 1.7. Phthalocyanine structure and absorption spectrum.

3.3.3. Third generation PSs

Considering the limitations of first and second generation PSs, the third generation PSs has been developed. These compounds are first or second generation PSs conjugated to/or introduced into biochemical devices that allow biological specificity to deliver/target such PSs to cancer cells [44, 47-49]. Many hypotheses have been proposed for the development of third generation PSs. Although liposomes and nanoparticles can improve tumour accumulation, the biomolecules with specificity for structural motifs overexpressed or enhanced in tumour-associated tissue are being conjugated to PSs showing promising

results [48]. The publications involving third generation PSs refer to PSs conjugated to monoclonal antibodies (mAbs) directed against tumour antigens [50], sugars [51], oligonucleotides to enhance photogenotoxicity [52], hormones, metabolites, cellular signalling species to selectively target an overexpressed enzyme or receptor [53], and also to peptides [54], proteins [55] and amino acids [56]. The tumour selectivity achieved with these PSs is desired in the treatment of bladder tumours, since they have large surface areas to be illuminated [27].

3.3.3.1. Third generation PSs: Immunoconjugates

The conjugation of PSs with monoclonal antibodies (mAbs) is an exciting approach in molecular-targeted PDT. A mAb is a large immunoglobulin molecule with a weight of 150 kDa and is developed specifically against a particular antigen by hybridoma technology [57]. Nowadays, mAbs are being used in a variety of ways in the cancer management, including diagnosis, monitoring, and treatment of the disease. These several applications are due to their unique abilities to recognize and bind to tumour-associated antigens. Antigens can only be present on tumour cells (a rarity) or overexpressed as compared to normal tissue [58, 59]. The main advantages of mAbs employment are their homogeneity and the fact that they can be produced endlessly [60]. The principal disadvantage is that mAbs production can take up to a year or longer, being also considerably expensive [60].

The conjugation of PSs to mAbs has led to some of the most promising results for PDT [48, 61]. The advantages claimed for this approach include mAb specificity (highly specific for their target antigens) and PS specificity (non-toxic to normal organs which did not receive light). The major obstacle is the high PS-to-mAb ratios required, which makes the synthesis and purification steps complicated. The goal of any PS-mAb synthesis should be to retain mAb immunoreactivity and PS phototoxicity.

In **Table 1.4**, are described some results obtained with PS-mAb immunoconjugates.

Table 1.4. Reported experiments of PDT with immunoconjugates.

	Photosensitizer	mAb	Cancer type	Results
Malatesti [62]	Porphyrin derivates	EpCAM CD104	Colon Lung	Conjugates produced cytotoxic effect in lower doses than unconjugated PS
Goff [63]	Chlorin derivative	OC125	Ovarian	After PDT, control mice died and 40% of the treated animals were alive for 50 days Animals treated exhibited a substantial reduction in the amount of ascites
Hudson [64]	Porphyrin derivates	35A7 FSP 77	Colon Ovarian	Conjugates had tumour uptake values and phototoxicity higher than unconjugated PSs
Smith [65]	Porphyrin derivates	CD104 CD146 CD326	Colon Lung	Conjugates caused suppression of tumour growth at lower doses than the commercial PF
Mitsunaga [50]	Phtalocyanine derivate	Trastuzu Panitumu	Subcutaneously xenografted tumours	Conjugates induced rapid cell death *in vitro* by necrosis and were most effective when bound to the target *In vivo* studies showed target specific tumour shrinkage by the conjugates

Malatesti [62] conjugated a Por with the mAbs anti-EpCAM and anti-CD104, which are specific for a human epithelial adhesion molecule and human integrin β4, respectively. These immunoconjugates were tested in human colon adenocarcinoma and human lung carcinoma cell lines and demonstrated ability to bind and photodynamically inactivate cancer cells that expressed the correspondent antigen. Goff [63] reported a study with a chlorin conjugated with a monoclonal than recognizes an antigen expressed in non-mucinous ovarian cancers. The *in vivo* results showed that after PDT, 40% of the treated animals were still alive 50 days and all control animals died between 30 and 50 days. Hudson [64] reported a study with Pors conjugated with mAb anti-FSP 77 directed against the extracellular domain of the erb-B2 receptor (a member of the epithelial growth factor) overexpressed in colon adenocarcinomas, and with mAb anti-35A7 that binds to carcinoembryonic antigen overexpressed in breast and ovarian cancers. Overall, conjugating the Por to mAbs increased the potential for *in vitro* phototoxicity. Smith [65] reported the conjugation of Por with three different mAbs (anti-CD104, anti-CD146 and anti-CD326). *In vivo* studies demonstrated that these conjugates produce suppression of human tumour growth, similar to Photofrin®, but at administered PS doses that were more than two orders of magnitude lower. Mitsunaga [50] reported the conjugation of a Pc with

mAbs targeting epidermal growth factor receptors. The conjugates were effective when bound to the cell membrane and produced no phototoxicity when not bound.

3.3.3.2. Third generation PSs: glycoconjugates

The concept behind PSs conjugated with sugars is quite stimulating in the development of third generation PSs. The carbohydrates can increase therapeutic selectivity because they interact with glycoprotein-based membrane receptors that have carbohydrate recognition domains. Carbohydrates play important roles in biological processes, although carbohydrate and carbohydrate-derived drugs cover only a limited therapeutic area [66].

In our group, at the University of Aveiro, several Por glycoconjugates have been developed [67-72]. Some of these Por glycoconjugates have demonstrated antiviral activity against herpes simplex virus type 1 and 2, after PDT [68, 71]. The corresponding Pc glyconjugates are, however, rather uncommon being thus of great interest to study [72-74].

Additional advantages with glycoconjugates are that the presence of carbohydrates modifies the PS macrocycle amphilicity and specific sugar transporters exist for different monosaccharides in cancer cells [58]. Moreover, the production and characterization of glycoconjugates are easier and cheaper than immunoconjugates. Many glycoconjugates have been synthesized to specifically target the lectin family receptors which are overexpressed in certain malignant cells, since they are involved in cell growth [75], cell adhesion [76], immune response [77] and angiogenesis [78]. Galectins are sugar-binding proteins with a weight of 15-kDa and known to show high affinity for galactose [79, 80]. Extracellular galactose-binding lectins are expressed on the surface of certain cancer cells and actually are one of the most investigated molecular targets for drug development [66]. Galectin-1 (a prototype, dimeric galectin with two identical carbohydrate recognition domains) mRNA levels are increased in most high-grade bladder tumours compared with normal or low-grade tumours and this lectin is able to bind α-galactoside [81, 82]. Therefore, it seems that this may be a valuable cellular target for galactose-based PSs.

The glycoconjugates have demonstrated promising *in vitro* results (**Table 1.5**) and are currently being tested *in vivo*. Maillard reported the synthesis of a glycoconjugated chlorin [83]. This compound displayed good *in vitro* PDT efficacy. Fujimoto [84] reported the conjugation of a porphyrin with galactose and its molecular delivery to hepatocytes

(liver cells). Experiments indicated that the conjugate has a selective uptake by cancer cells. Zheng [85] reported the synthesis and biological evaluation of a β-galactose-conjugate. Laville [86] reported the photoactivity of asymmetric and symmetric glucoconjugated chlorins. The asymmetric glucoconjugated chlorin exhibited superior phototoxicity compared with symmetric glucoconjugated chlorin and sugar-free chlorin. Chen reported the synthesis of Por-saccharide conjugates and their selective uptake to several cancer cells, followed by an investigation of their PDT properties [87]. In a recent study, Tanaka [51] compared the PDT efficacy of a newly developed glycoconjugated chlorin, with Talaporfin, which is clinically used in Japan. The *in vitro* studies showed that this new conjugate was 30 times more cytotoxic to gastric and colon cancer cell lines than Talaporfin. The *in vivo* studies showed that the conjugate accumulation was higher in tumours and this conjugate significantly suppressed tumour growth when compared with Talaporfin.

Table 1.5. Reported experiments of PDT with glycoconjugates.

	Photosensitizer	Sugar	Cancer type	Results
Maillard [83]	Chlorin derivate	Maltose	Colon	Conjugates showed phototoxicity as opposed to unconjugated PS
Fujimoto [84]	Porphyrin derivate	Galactose Glucose	Liver	Galactose conjugate was selectively captured by cancer cells
Zheng [85]	Chlorin derivate	Galactose Lactose	Leucemy	Conjugates produced an increase in photodynamic activity compared with unconjugated PS
Laville [86]	Chlorin derivate	Glucose	Colon	Asymmetric conjugates showed stronger phototoxicity than unconjugated and symmetric conjugates
Chen [87]	Porphyrin derivate	Galactose Glucose	Breast	Glucose conjugate was preferentially accumulated in cancer cells over galactose conjugate
Tanaka [51]	Chlorin derivate	Glucose	Gastric Colon	Conjugates demonstrated a selective accumulation in cancer cells and higher toxicity than Taloporfin

3.4. Clinical applications

Clinical PDT is a two-stage and a dual selective process with the first stage corresponding to the administration of the PS. After a certain period of time, the PS is preferentially retained in tumour (first time selective). The tumour is illuminated with light (second time selective) at a specific wavelength, a process which constitutes the second and final stage in the therapy…

In clinical cancer settings, the PS is typically administered intravenously or topically, followed by light illumination of the anatomical site being treated (**Figure 1.8**).

Initially, there is an uptake of the PS by most normal and hyper-proliferating cells, but it is retained longer in the last ones [88]. After maximum PS accumulation in cancer cells, the tumour is irradiated. The period of time between PS administration and the start of illumination varies from 5 min to 24 h, or more. The combination of PS and light at a specific wavelength can result in $^1O_2$ production which is believed to be responsible for tumour destruction [89]. Total healing of the area after PDT may take from 2 to 6 weeks. During this time, the patient will be light sensitive (due to PS accumulation) and must be protected from direct light. Depending on the PS used, light sensitivity may take from 4 hours to 6 weeks. The rapid cytotoxic reaction resulting in specific tumour destruction makes this therapy attractive to both patient and clinician.

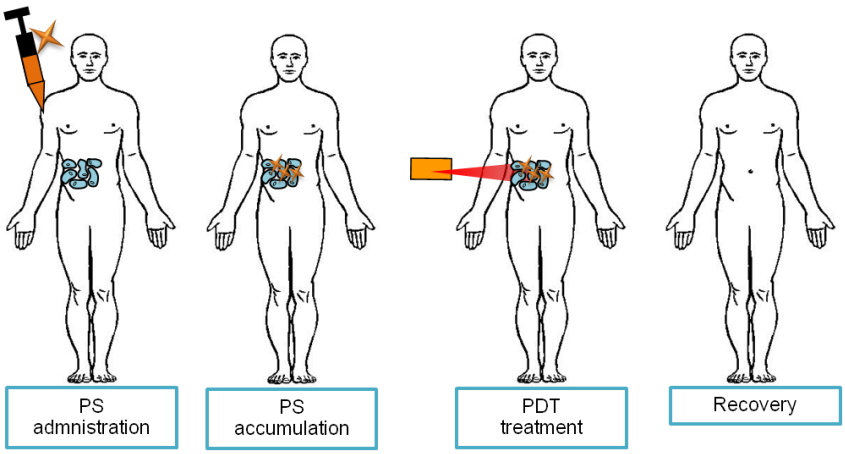

Figure 1.8. Schematic illustration of the mechanism of PDT in oncology.

3.5. Mechanisms of cell death in PDT

Because of short lifetime and limited migration of $^1O_2$ from the site of its formation, sites of damage are closely related to the localization of the PS…

The therapeutic effects of PDT are thought to occur by three different ways: (i) cytotoxic reaction - direct lethal effects on tumour cells, (ii) vasculotoxic reaction - vascular impairment which limits blood supply to the tumour region and (iii) acute inflammation that can stimulate the immune system to recognize and destroy tumour cells [90, 91]. Although PDT can induce many cellular and molecular signalling pathways in cancer cells, its main purpose is to induce cell death (cytotoxic reaction) by apoptosis and necrosis [91, 92]. In these processes, the $^1O_2$ is the fundamental cytotoxic species as outlined in the photochemical section. Singlet oxygen has a very short lifetime in cells and limited migration [29], thus the type of response triggered by activation of the PSs depends on their intracellular localization [93, 94].

3.5.1. Modes of cell death in PDT

Under PDT, cells can undergo at least two distinct types of cell death: necrosis and apoptosis (**Figure 1.9**). Among other factors, the type of cell death induced after PDT depends on the intracellular localization of the PS and on the PDT dose.

Necrosis is a violent and quick form of cell death, characterized by *in vitro* cytoplasm swelling, devastation of organelles and disruption of the plasma membrane, leading to the release of intracellular contents and *in vivo* inflammation. Necrosis has been referred as an accidental cell death way or unprogrammed process [95]. The mechanisms involved in this process are much less studied than in apoptosis [96, 97].

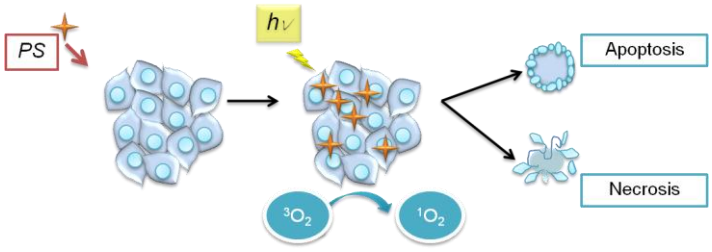

Figure 1.9. The two distinct types of cell death induced by PDT, necrosis and apoptosis.

Apoptosis can be identified in single cells and is characterized by cell shrinkage. Recently, researchers have described many pathways whereby mammalian cells can

undergo apoptosis, and have proposed some of the ways that PDT can initiate these processes *in vitro* [92]. This highly regulated form of cell death results in fast cell destruction, and requires transcriptional activation of specific genes, including the activation of endonucleases, following DNA degradation into fragments, and activation of caspases [92]. Two major apoptotic pathways have been characterized: the death receptor-mediated apoptosis, also referred as extrinsic pathway, and the mitochondria-mediated apoptosis, also named intrinsic pathway [98]. Both events eventually lead to activation of caspase cascades, known as "effector caspases" [99]. Caspases are synthesized as zymogens and these precursors are transformed into active enzymes via oligomerization-induced autoprocessing for initiator caspases (numbers 1, 2, 4, 5, 8, 9, 10, and 14) while effector caspases (numbers 3, 6, and 7) are activated by other proteases and play a key role in initiating and executing apoptotic mechanisms [37].

In the extrinsic pathway, cell death surface receptors from the TNF (Tumour Necrosis Factor) gene family are stimulated after ligand binding, activating the initiator caspase-8 via adaptor and scaffolding proteins. The caspase-8 cleaves Bid (a BH3 only member of the Bcl-2 family).

In the intrinsic pathway, PDT induces release of cytochrome c [100], which occurs as a result of mitochondria outer membrane permeabilization after PDT [99] and is controlled by Bcl-2 family members [27]. The Bcl-2 family includes four anti-apoptotic proteins: BclXL, Bcl-w, A1, Mcll and Bcl-2, and two protein groups that promote apoptosis: the Bax and the BH3-only families pro-apoptotic proteins [99]. Released cytochrome C binds Apaf-1 (apoptosis activating factor-1) and induces its oligomerization, in the presence of dATP. This complex, termed apoptosome, recruits and activates the initiator caspase-9 [101].

In both pathways, the activation of initiator caspases (caspase-8 or caspase-9) leads to the activation of effector caspases (**Figure 1.10**). During apoptosis the cells shrink, the nuclear chromatin becomes pyknotic (irreversible condensation of chromatin), the nuclear membrane condenses and the nucleus break up into apoptotic bodies. Although the cytoplasmic organelles remain intact, DNA is digested at internucleosomal sites, giving rise to fragments [98]. Apoptotic cells and apoptotic bodies are engulfed and cleared by phagocytes [102].

3.5.1.1. Involvement of Bcl2 family of proteins in PDT

There are several reports in the literature showing the involvement of anti-apoptotic and pro-apoptotic proteins in cell death induced by PDT [103-106, 108]. The role of Bcl-2 in the apoptotic response caused by PDT is controversial. In some reports it has been described that cells overexpressing Bcl-2 [103], are sensitive to apoptosis after PDT. It has been demonstrated that PDT induces direct degradation of Bcl-2 without affecting Bax, and the enhanced apoptotic response to PDT is attributed to high Bax:Bcl-2 ratio after PDT [103]. Other studies [104], have described that the Bcl-2 overexpression protects cells against PDT-induced phototoxicity, namely against PDT-induced apoptosis by blocking the activity of caspases 3 and 6. The RIF 1 (radiation-induced fibrosarcome cells), a type of cells resistant to PDT, treated with the antisense oligonucleotide, directed against the coding region of Bcl-2 protein demonstrated an increase of phototoxicity after PDT [105]. Moreover, it was observed that the treatment of these cells with PDT resulted in a significant induction of apoptosis with induction of caspase activity.

The localization of the anti-apoptotic protein Bcl-2 in the endoplasmic reticulum (ER) suggests that this protein controls the intracellular calcium fluxes. It has been reported that after PDT, there are alterations of the Ca^{2+}-binding proteins in the ER [106] leading to Ca^{2+} release and induction of the Ca^{2+} apoptotic processes. The ER stress allows Ca^{2+} to flow from ER stores to the cytosol and mitochondria, leading to induction of apoptosis. In fact, it has been reported that PSs localized in the ER stimulate a rapid increase in calcium concentration after PDT. Moreover, the decrease in ER activity (folding, modifying and sorting newly synthesized proteins) induced after PDT results in the accumulation of unfolded or misfolded proteins activating the adaptive unfolded protein response (UPR) [92]. The excessive accumulation of unfolded or misfolded proteins in ER results in excessive ER stress that can overwhelm the adaptive UPR, triggering cell death. The ALA-based PDT [107] decreased the levels of the ER calcium-binding proteins as well as of Bcl-2, which served to amplify the mechanism ensuring apoptotic cell death.

The role of the pro-apoptotic protein Bax in PDT-induced apoptosis is well reported in [108]. The cells DU-145 (human prostate cancer cells) demonstrated to be resistant to PDT due to the absence of Bax, since apoptosis was restored by the expression of Bax in

these cells. It was observed that in the absence of Bax, the downstream events of the mitochondrial pathway of apoptosis were completely blocked after PDT.

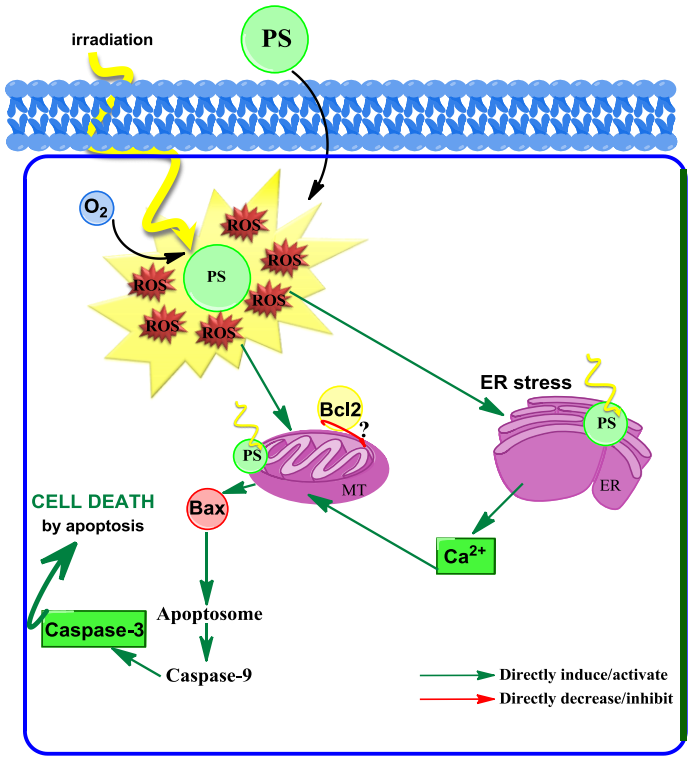

Figure 1.10. Some PDT-associated apoptosis pathways involving mitochondria, ER and Bcl-2 family protein. PS-Photosensitizer, MT-Mitochondria, ER-Endoplasmic Reticulum.

4. PDT in bladder cancer: state of the art

PDT for bladder cancer treatment remains largely investigational with limited use. PDT for bladder cancer is approved in Canada and in some EU nations but has not been approved by the US FDA [27].

Early response rates (from 2-3 months) after PDT have been observed in approximately 50-80% of patients with bladder cancer, with longer term (from 1 year to 2 years) durable responses noted in 20-60% of patients [27]. PF is the most commonly used PS in bladder cancer treatment and its clinical use dates to the late 1970s, when HpD effects in 5 patients were published [21]. PDT with HpD was used to treat 50 transitional cell carcinomas in 37 patients and a 74% complete response rate was achieved [109]. Another study reported the PDT effects with HpD in 34 patients with CIS. In this trial a 73.5% complete response rate at 3 months was achieved [110]. However, by 2 years, 77.8% of these patients had recurrence. In these studies, treatment of superficial bladder cancer with PDT was generally well tolerated, with dysuria (painful urination), hematuria (blood in the urine), and skin photosensitivity being the most common acute toxicities. Bladder wall fibrosis and diminished bladder capacity have been and continue to be problems in some PDT treated patients. It was demonstrated that PDT with sulfonated Pc in a rat bladder cancer produces a superficial necrosis without muscle damage [111]. With the use of PF as a PS, researchers observed complete response rates as high as 60% for patients with CIS or superficial bladder cancer [112, 113]. Several experiments have demonstrated that suitable results can be achieved by combination of PDT to another therapeutic modality. Namely, studies combining intravesical immunotherapies or chemotherapies with PDT demonstrated that these therapies may significantly enhance the treatment of bladder tumours [114, 115]. In a recent small pilot study performed by Lee [116], 5 patients with non-muscle invasive bladder cancer were treated by PDT using a chlorin derivative. At a median follow-up of 29 months, 2 patients where disease free, 2 patients developed recurrence and 1 patient progressed to muscle invasive disease.

In terms of immunoconjugates for bladder cancer therapy, promising results were obtained with the conjugation of the monoclonal antibody Erbitux (cetuximab), that binds to an antigen overexpressed in bladder cancer cells [117]. In terms of glycoconjugates for bladder cancer therapy, no experiments have been reported.

5. Objectives of this thesis

The objectives of this thesis were:

- Study the photo-physical and -chemical properties of new galacto-conjugates, already synthesized: a porphyrin conjugated with eight galactose molecules (**$PorGal_8$**) and a phthalocyanine conjugated with sixteen galactose molecules (**$PcGal_{16}$**);
- Conjugate a porphyrin with human and bovine albumins, and with an mAb against CD104;
- Validate the photodynamic potential of the aforementioned conjugates against two human bladder cancer cell lines, UM-UC-3 and HT-1376:
- Determine the uptake of the bioconjugates by cells,
    - Verify the toxicity of the conjugates in darkness and after light activation,
    - Quantify the levels of ROS after PSs-PDT,
    - Clarify the nature of the phototoxicity for each bioconjugates,
    - Identify the molecular mechanisms underlying cell death induced after **$PorGal_8$**-PDT.

References

1. *European Cancer Observatory. Cancer: bladder. International Agency for Research on CancerWeb site.* Available from: http://eu-cancer.iarc.fr/cancer-20-bladder.html,en, accessed on December 2011.
2. Kenneth, S., *Human Anatomy' 2007 Ed.2007 Edition*: Rex Bookstore, Inc.
3. Syrigos, K. N. and Skinner, D. G. *Bladder cancer: biology, diagnosis, and management*. 1999: Oxford University Press.
4. Blandy, J. and Kaisary, A. *Urology*. 2009: John Wiley & Sons.
5. Bassi, P. and Pagano, F. *Invasive Bladder Cancer*. 2007: Springer.
6. Greene, F.; Balch, C.; Haller, D. and Morrow, M., *AJCC Cancer Staging Manual (6th Edition)*. 2002: Springer.
7. *Bladder cancer survival statistics. Cancer Research UK Website.* Available from: http://nfo.cancerresearchuk.org/cancerstats/types/bladder/#survival, accessed on December 2011.
8. Shah, A.; Rachet, B.; Mitry, E.; Cooper, N.; Brown, C. M. and Coleman, M. P. *Survival from bladder cancer in England and Wales up to 2001*. Br J Cancer, **2008**, 99, p. 86-89.
9. Witjes, J. A.; Redorta, J. P.; Jacqmin, D.; Sofras, F.; Malmstrom, P. U.; Riedl, C.; Jocham, D.; Conti, G.; Montorsi, F.; Arentsen, H. C.; Zaak, D.; Mostafid, A. H. and Babjuk, M. *Hexaminolevulinate-guided fluorescence cystoscopy in the diagnosis and follow-up of patients with non-muscle-invasive bladder cancer: review of the evidence and recommendations*. Eur Urol, **2010**, 57(4), p. 607-614.
10. Sylvester, R. J.; van der Meijden, A. P.; Oosterlinck, W.; Witjes, J. A.; Bouffioux, C.; Denis, L.; Newling, D. W. and Kurth, K. *Predicting recurrence and progression in individual patients with stage Ta T1 bladder cancer using EORTC risk tables: a combined analysis of 2596 patients from seven EORTC trials*. Eur Urol, **2006**, 49(3), p. 466-465.
11. Botteman, M. F.; Pashos, C. L.; Redaelli, A.; Laskin, B. and Hauser, R. *The health economics of bladder cancer: a comprehensive review of the published literature*. Pharmacoeconomics, **2003**, 21(18), p. 1315-1330.
12. Herr, H. W. *Natural history of superficial bladder tumors: 10- to 20-year follow-up of treated patients*. World J Urol, **1997**, 15(2), p. 84-88.
13. Fitzpatrick, T. B. and Pathak, M. A. *Historical aspects of methoxsalen and other furocoumarins*. J Invest Dermatol, **1959**, 32, p. 229-231.
14. Moan, J. and Peng, Q. *An outline of the hundred-year history of PDT*. Anticancer Res, **2003**, 23, p. 3591-3600.
15. von Tappeiner, H. and Jesionek, H. *Therapeutische versuche mit fluoreszierenden stoffen*. Munch Med Wochenschr, **1903**, 47, p. 2042-2044.
16. Meyer-Betz, F. *Untersuchungen über die biologische (photodynamische) Wirkung des Hämatoporphyrins und anderer Derivate des Blut- und Gallenfarbstoffs*. Dtsch Arch Klin Med, **1913**, 112, p. 476–503.

17. Kick, G.; Messer, G. and Plewig, G. *Historische Entwicklung der Photodynamischen Therapie*. Der Hautarzt, **1996**, 47(8), p. 644-649.
18. Schwartz, S.; Absolon, K. and Vermund, H. *Some relationship of porphyrins, X-rays and tumors.* Univ Minn Med Bull, **1955**, 27, p. 1-37.
19. Dougherty, T. J.; Grindey, G. B.; Fiel, R.; Weishaupt, K. R. and Boyle, D. G. *Photoradiation Therapy .2. Cure of Animal Tumors with Hematoporphyrin and Light*. Journal of the National Cancer Institute, **1975**, 55(1), p. 115-121.
20. Dougherty, T. J.; Kaufman, J. E.; Goldfarb, A.; Weishaupt, K. R.; Boyle, D. and Mittleman, A. *Photoradiation Therapy for Treatment of Malignant-Tumors.* Cancer Res, **1978**, 38(8), p. 2628-2635.
21. Kelly, J. F. and Snell, M. E. *Hematoporphyrin derivative: a possible aid in the diagnosis and therapy of carcinoma of the bladder*. J Urol, **1976**, 115(2), p. 150-151.
22. Huang, Z. *A review of progress in clinical photodynamic therapy*. Technol Cancer Res Treat, **2005**, 4(3), p. 283-293.
23. Celli, J. P.; Spring, B. Q.; Rizvi, I.; Evans, C. L.; Samkoe, K. S.; Verma, S.; Pogue, B. W. and Hasan, T. *Imaging and Photodynamic Therapy: Mechanisms, Monitoring, and Optimization*. Chem Rev, **2010**, 110(5), p. 2795-2838.
24. Calin, M. A. and Parasca, S. V. *Photodynamic therapy in oncology*. Journal of Optoelectron Adv M, **2006**, 8(3), p. 1173-1179.
25. Luksiene, Z. *Photodynamic therapy: mechanism of action and ways to improve the efficiency of treatment*. Medicina (Kaunas), **2003**, 39(12), p. 1137-1150.
26. Plaetzer, K.; Krammer, B.; Berlanda, J.; Berr, F. and Kiesslich, T. *Photophysics and photochemistry of photodynamic therapy: fundamental aspects*. Lasers Med Sci, **2009**, 24(2), p. 259-268.
27. Agostinis, P.; Berg, K.; Cengel, K. A.; Foster, T. H.; Girotti, A. W.; Gollnick, S. O.; Hahn, S. M.; Hamblin, M. R.; Juzeniene, A.; Kessel, D.; Korbelik, M.; Moan, J.; Mroz, P.; Nowis, D.; Piette, J.; Wilson, B. C. and Golab, J. *Photodynamic therapy of cancer: an update*. CA Cancer J Clin, **2011**, 61(4), p. 250-281.
28. Foote, C. S. *Definition of type I and type II photosensitized oxidation*. Photochem Photobiol, **1991**, 54(5), p. 659.
29. Moan, J. and Berg, K. *The photodegradation of porphyrins in cells can be used to estimate the lifetime of singlet oxygen*. Photochem Photobiol, **1991**, 53(4), p. 549-553.
30. Sharman, W. M.; Allen, C. M. and van Lier, J. E. *Role of activated oxygen species in photodynamic therapy*. Methods Enzymol, **2000**, 319, p. 376-400.
31. Dysart, J. S. and Patterson, M. S. *Characterization of Photofrin photobleaching for singlet oxygen dose estimation during photodynamic therapy of MLL cells in vitro*. Phys Med Biol, **2005**, 50(11), p. 2597-2616.
32. Ethirajan, M.; Chen, Y.; Joshi, P. and Pandey, R. K. *The role of porphyrin chemistry in tumor imaging and photodynamic therapy*. Chem Soc Rev, **2011**, 40(1), p. 340-362.

33. Detty, M. R.; Gibson, S. L. and Wagner, S. J. *Current clinical and preclinical photosensitizers for use in photodynamic therapy*. J Med Chem, **2004**, 47(16), p. 3897-3915.
34. Nyman, E. S. and Hynninen, P. H. *Research advances in the use of tetrapyrrolic photosensitizers for photodynamic therapy*. J Photochem Photobiol B, **2004**, 73(1-2), p. 1-28.
35. Garland, M. J.; Cassidy, C. M.; Woolfson, D. and Donnelly, R. F. *Designing photosensitizers for photodynamic therapy: strategies, challenges and promising developments*. Future Med Chem, **2009**, 1(4), p. 667-691.
36. Allison, R. R. and Sibata, C. H. *Oncologic photodynamic therapy photosensitizers: a clinical review*. Photodiagnosis Photodyn Ther, **2010**, 7(2), p. 61-75.
37. Castano, A. P.; Demidova, T. N. and Hamblin, M. R. *Mechanisms in photodynamic therapy: part one - photosensitizers, photochemistry and cellular localization*. Photodiagnosis Photodyn Ther, **2004**, 1, p. 279-293.
38. Bonnett, R. and Berenbaum, M. C. *HPD - a study of its components and their properties*. Adv Exp Med Biol, **1983**, 160, p. 241-250.
39. Battersby, A. R.; Fookes, C. J.; Matcham, G. W. and McDonald, E. *Biosynthesis of the pigments of life: formation of the macrocycle*. Nature, **1980**, 285(5759), p. 17-21.
40. Bonnett, R. and Berenbaum, M. *Porphyrins as photosensitizers*. Ciba Found Symp, **1989**, 146, p. 40-53.
41. Dougherty, T. J. *An update on photodynamic therapy applications*. J Clin Laser Med Surg, **2002**, 20(1), p. 3-7.
42. Wohrle, D.; Hirth, A.; Bogdahn-Rai, T.; Schnurpfeil, G. and Shopova, M. *Photodynamic therapy of cancer: second and third generations of photosensitizers*. Russ Chem Bt, **1998**, 47(5), p. 807-816.
43. van Lier, J. E. and Spikes, J. D. *The chemistry, photophysics and photosensitizing properties of phthalocyanines*. Ciba Found Symp, **1989**, 146, p. 17-26; discussion 26-32.
44. Moser, J. G. *Photodynamic Tumour Therapy: 2nd and 3rd generation photosensitizers*. 1998, Weinheim Harwood Academic Publishers.
45. Xia, C. H.; Wang, Y.; Gao, Y.; Zhang, C. X.; Wang, Y. C.; Li, T.; Chen, W.; Bai, L. M. and Li, X. L. *Photodynamic Therapy of New Amphiphilic Phthalocyanine Zinc Inhibits the Proliferation of Human Hepatoma Bel-7402 Cells through the Induction of Apoptosis*. Proceedings of the 2009 2nd International Conference on Biomedical Engineering and Informatics, Vols 1-4, **2009**, p. 1134-1137.
46. Longo, J. P.; Lozzi, S. P.; Simioni, A. R.; Morais, P. C.; Tedesco, A. C. and Azevedo, R. B. *Photodynamic therapy with aluminum-chloro-phthalocyanine induces necrosis and vascular damage in mice tongue tumors*. J Photochem Photobiol B, **2009**, 94(2), p. 143-146.
47. Sibani, S. A.; McCarron, P. A.; Woolfson, A. D. and Donnelly, R. F. *Photosensitiser delivery for photodynamic therapy. Part 2: systemic carrier platforms*. Expert Opin Drug Deliv, **2008**, 5(11), p. 1241-1254.

48. Bugaj, A. M. *Targeted photodynamic therapy--a promising strategy of tumor treatment*. Photochem Photobiol Sci, **2011**, 10(7), p. 1097-1109.
49. Josefsen, L. B. and Boyle, R. W. *Photodynamic therapy: novel third-generation photosensitizers one step closer?* Br J Pharmacol, **2008**, 154(1), p. 1-3.
50. Mitsunaga, M.; Ogawa, M.; Kosaka, N.; Rosenblum, L. T.; Choyke, P. L. and Kobayashi, H. *Cancer cell-selective in vivo near infrared photoimmunotherapy targeting specific membrane molecules*. Nat Med, **2011**, 17(12), p. 1685-1691.
51. Tanaka, M.; Kataoka, H.; Mabuchi, M.; Sakuma, S.; Takahashi, S.; Tujii, R.; Akashi, H.; Ohi, H.; Yano, S.; Morita, A. and Joh, T. *Anticancer effects of novel photodynamic therapy with glycoconjugated chlorin for gastric and colon cancer*. Anticancer Res, **2011**, 31(3), p. 763-769.
52. Balaz, M.; Steinkruger, J. D.; Ellestad, G. A. and Berova, N. *5'-Porphyrin-oligonucleotide conjugates: neutral porphyrin-DNA interactions*. Org Lett, **2005**, 7(25), p. 5613-5616.
53. Schneider, R. L.; Schmitt, F.; Frochot, C.; Fort, Y.; Lourette, N.; Guillemin, F.; Muller, J. F. and Barberi-Heyob, M. *Design, synthesis, and biological evaluation of folic acid targeted tetraphenylporphyrin as novel photosensitizers for selective photodynamic therapy*. Bioorg Med Chem, **2005**, 13(8), p. 2799-2808.
54. Nuno Silva, J.; Haigle, J.; Tome, J. P.; Neves, M. G.; Tome, A. C.; Maziere, J. C.; Maziere, C.; Santus, R.; Cavaleiro, J. A.; Filipe, P. and Morliere, P. *Enhancement of the photodynamic activity of tri-cationic porphyrins towards proliferating keratinocytes by conjugation to poly-S-lysine*. Photochem Photobiol Sci, **2006**, 5(1), p. 126-133.
55. Conlon, K. A. and Berrios, M. *Site-directed photoproteolysis of 8-oxoguanine DNA glycosylase 1 (OGG1) by specific porphyrin-protein probe conjugates: a strategy to improve the effectiveness of photodynamic therapy for cancer*. J Photochem Photobiol B, **2007**, 87(1), p. 9-17.
56. Serra, V. V.; Zamarron, A.; Faustino, M. A.; Cruz, M. C.; Blazquez, A.; Rodrigues, J. M.; Neves, M. G.; Cavaleiro, J. A.; Juarranz, A. and Sanz-Rodriguez, F. *New porphyrin amino acid conjugates: synthesis and photodynamic effect in human epithelial cells*. Bioorg Med Chem, **2010**, 18(16), p. 6170-6178.
57. Kohler, G. and Milstein, C. *Continuous cultures of fused cells secreting antibody of predefined specificity*. Nature, **1975**, 256(5517), p. 495-497.
58. Wojtyk, J. T. C.; Goyan, R.; Gudgin-Dickson, E. and Pottier, R. *Exploiting tumour biology to develop novel drug delivery strategies for PDT*. Med Laser Appl, **2006**, 21(4), p. 225-238.
59. Konan, Y. N.; Gurny, R. and Allemann, E. *State of the art in the delivery of photosensitizers for photodynamic therapy*. J Photochem Photobiol B, **2002**, 66(2), p. 89-106.
60. Antibodies, C. o. M. o. P. M.; Research, I. f. L. A. and Council, N. R., *Monoclonal Antibody Production*. 1999: The National Academies Press.

61. van Dongen, G. A. M. S.; Visser, G. W. M. and Vrouenraets, M. B. *Photosensitizer-antibody conjugates for detection and therapy of cancer*. Adv Drug Deliv Rev, **2004**, 56(1), p. 31-52.
62. Malatesti, N.; Smith, K.; Savoie, H.; Greenman, J. and Boyle, R. W. *Synthesis and in vitro investigation of cationic 5,15-diphenyl porphyrin-monoclonal antibody conjugates as targeted photodynamic sensitisers*. Int J Oncol, **2006**, 28(6), p. 1561-1569.
63. Goff, B. A.; Blake, J.; Bamberg, M. P. and Hasan, T. *Treatment of ovarian cancer with photodynamic therapy and immunoconjugates in a murine ovarian cancer model*. Br J Cancer, **1996**, 74(8), p. 1194-1198.
64. Hudson, R.; Carcenac, M.; Smith, K.; Madden, L.; Clarke, O. J.; Pelegrin, A.; Greenman, J. and Boyle, R. W. *The development and characterisation of porphyrin isothiocyanate-monoclonal antibody conjugates for photoimmunotherapy*. Br J Cancer, **2005**, 92(8), p. 1442-1449.
65. Smith, K.; Malatesti, N.; Cauchon, N.; Hunting, D.; Lecomte, R.; van Lier, J. E.; Greenman, J. and Boyle, R. W. *Mono- and tri-cationic porphyrin-monoclonal antibody conjugates: photodynamic activity and mechanism of action*. Immunology, **2011**, 132(2), p. 256-265.
66. Ernst, B. and Magnani, J. L. *From carbohydrate leads to glycomimetic drugs*. Nat Rev Drug Discov, **2009**, 8(8), p. 661-677.
67. Silva, A. M. G.; Tome, A. C.; Neves, M. G. P. M. S.; Cavaleiro, J. A. S.; Perrone, D. and Dondoni, A. *Porphyrins in 1,3-dipolar cycloadditions with sugar azomethine ylides. Synthesis of pyrrolidinoporphyrin glycoconjugates*. Synlett, **2005**, (5), p. 857-859.
68. Tome, J. P.; Silva, E. M.; Pereira, A. M.; Alonso, C. M.; Faustino, M. A.; Neves, M. G.; Tome, A. C.; Cavaleiro, J. A.; Tavares, S. A.; Duarte, R. R.; Caeiro, M. F. and Valdeira, M. L. *Synthesis of neutral and cationic tripyridylporphyrin-D-galactose conjugates and the photoinactivation of HSV-1*. Bioorg Med Chem, **2007**, 15(14), p. 4705-4713.
69. Lourenco, L. M.; Tome, J. P.; Domingues, M. R.; Domingues, P.; Costa, P. J.; Felix, V.; Neves, M. G. and Cavaleiro, J. A. *Synthesis and differentiation of alpha- and beta-glycoporphyrin stereoisomers by electrospray tandem mass spectrometry*. Rapid Commun Mass Spectrom, **2009**, 23(21), p. 3478-3483.
70. Gomes, A. T. P. C.; Leao, R. A. C.; da Silva, F. C.; Neves, M. G. P. M. S.; Faustino, M. A. F.; Tome, A. C.; Silva, A. M. S.; Pinheiro, S.; de Souz, M. C. B. V.; Ferreira, V. F. and Cavaleiro, J. A. S. *Synthesis of new glycoporphyrin derivatives through carbohydrate-substituted alpha-diazoacetates*. Journal of Porphyr and Phthalocya, **2009**, 13(2), p. 247-255.
71. Tome, J. P.; Neves, M. G.; Tome, A. C.; Cavaleiro, J. A.; Mendonca, A. F.; Pegado, I. N.; Duarte, R. and Valdeira, M. L. *Synthesis of glycoporphyrin derivatives and their antiviral activity against herpes simplex virus types 1 and 2*. Bioorg Med Chem, **2005**, 13(12), p. 3878-3888.

72. Silva, S.; Pereira, P. M.; Silva, P.; Paz, F. A.; Faustino, M. A.; Cavaleiro, J. A. and Tome, J. P. *Porphyrin and phthalocyanine glycodendritic conjugates: synthesis, photophysical and photochemical properties*. Chem Commun (Camb), **2012**, 48(30), p. 3608-3610.
73. Soares, A. R.; Tome, J. P.; Neves, M. G.; Tome, A. C.; Cavaleiro, J. A. and Torres, T. *Synthesis of water-soluble phthalocyanines bearing four or eight D-galactose units*. Carbohydr Res, **2009**, 344(4), p. 507-510.
74. Ribeiro, A. O.; Tome, J. P. C.; Neves, M. G. P. M. S.; Tome, A. C.; Cavaleiro, J. A. S.; Iamamoto, Y. and Torres, T. *[1,2,3,4-tetrakis(alpha/beta-D-galactopyranos-6-yl)-phthalocyaninato]zinc(II): a water-soluble phthalocyanine*. Tetrahedron Lett, **2006**, 47(52), p. 9177-9180.
75. Yang, R. Y. and Liu, F. T. *Galectins in cell growth and apoptosis*. Cell Mol Life Sci, **2003**, 60(2), p. 267-276.
76. Brewer, C. F.; Miceli, M. C. and Baum, L. G. *Clusters, bundles, arrays and lattices: novel mechanisms for lectin-saccharide-mediated cellular interactions*. Curr Opin Struct Biol, **2002**, 12(5), p. 616-623.
77. Rabinovich, G. A.; Baum, L. G.; Tinari, N.; Paganelli, R.; Natoli, C.; Liu, F. T. and Iacobelli, S. *Galectins and their ligands: amplifiers, silencers or tuners of the inflammatory response?* Trends Immunol, **2002**, 23(6), p. 313-320.
78. Riss, D.; Jin, L.; Bayliss, J. M.; Kovacs, K.; Vidal, S.; Scheithauer, B. W. and Lloyd, R. V. *Galectin-3 expression in pituitary tumors*. Lab Invest, **2003**, 83(1), p. 109a-109a.
79. Barondes, S. H.; Cooper, D. N.; Gitt, M. A. and Leffler, H. *Galectins. Structure and function of a large family of animal lectins*. J Biol Chem, **1994**, 269(33), p. 20807-20810.
80. Sharon, N. and Lis, H. *Lectins as cell recognition molecules*. Science, **1989**, 246(4927), p. 227-234.
81. Cindolo, L.; Benvenuto, G.; Salvatore, P.; Pero, R.; Salvatore, G.; Mirone, V.; Prezioso, D.; Altieri, V.; Bruni, C. B. and Chiariotti, L. *galectin-1 and galectin-3 expression in human bladder transitional-cell carcinomas*. Int J Cancer, **1999**, 84(1), p. 39-43.
82. Miller, M. C.; Ribeiro, J. P.; Roldos, V.; Martin-Santamaria, S.; Canada, F. J.; Nesmelova, I. A.; Andre, S.; Pang, M.; Klyosov, A. A.; Baum, L. G.; Jimenez-Barbero, J.; Gabius, H. J. and Mayo, K. H. *Structural aspects of binding of alpha-linked digalactosides to human galectin-1*. Glycobiology, **2011**, 21(12), p. 1627-1641.
83. Maillard, P.; Hery, C. and Momenteau, M. *Synthesis, characterization and photocytotoxicity of a glycoconjugated meso-monoarylbenzochlorin*. Tetrahedron Lett, **1997**, 38(21), p. 3731-3734.
84. Fujimoto, K.; Miyata, T. and Aoyama, Y. *Saccharide-directed cell recognition and molecular delivery using macrocyclic saccharide clusters: Masking of*

hydrophobicity to enhance the saccharide specificity. J Am Chem Soc, **2000**, 122(14), p. 3558-3559.

85. Zheng, G.; Graham, A.; Shibata, M.; Missert, J. R.; Oseroff, A. R.; Dougherty, T. J. and Pandey, R. K. *Synthesis of beta-galactose-conjugated chlorins derived by enyne metathesis as galectin-specific photosensitizers for photodynamic therapy*. J Org Chem, **2001**, 66(26), p. 8709-8716.
86. Laville, I.; Figueiredo, T.; Loock, B.; Pigaglio, S.; Maillard, P.; Grierson, D. S.; Carrez, D.; Croisy, A. and Blais, J. *Synthesis, cellular internalization and photodynamic activity of glucoconjugated derivatives of tri and tetra(meta-hydroxyphenyl)chlorins*. Bioorg Med Chem, **2003**, 11(8), p. 1643-1652.
87. Chen, X.; Hui, L.; Foster, D. A. and Drain, C. M. *Efficient synthesis and photodynamic activity of porphyrin-saccharide conjugates: targeting and incapacitating cancer cells*. Biochemistry, **2004**, 43(34), p. 10918-10929.
88. Henderson, B. W. and Dougherty, T. J. *How Does Photodynamic Therapy Work*. Photochem Photobiol, **1992**, 55(1), p. 145-157.
89. MacDonald, I. J. and Dougherty, T. J. *Basic principles of photodynamic therapy*. J Porphyr Phthalocya, **2001**, 5(2), p. 105-129.
90. Almeida, R. D.; Manadas, B. J.; Carvalho, A. P. and Duarte, C. B. *Intracellular signaling mechanisms in photodynamic therapy*. Biochim Biophys Acta, **2004**, 1704(2), p. 59-86.
91. Robertson, C. A.; Evans, D. H. and Abrahamse, H. *Photodynamic therapy (PDT): a short review on cellular mechanisms and cancer research applications for PDT*. J Photochem Photobiol B, **2009**, 96(1), p. 1-8.
92. Buytaert, E.; Dewaele, M. and Agostinis, P. *Molecular effectors of multiple cell death pathways initiated by photodynamic therapy*. Biochim Biophys Acta, **2007**, 1776(1), p. 86-107.
93. Tijerina, M.; Kopeckova, P. and Kopecek, J. *Mechanisms of cytotoxicity in human ovarian carcinoma cells exposed to free Mce6 or HPMA copolymer-Mce6 conjugates*. Photochem Photobiol, **2003**, 77(6), p. 645-652.
94. Kessel, D.; Luguya, R. and Vicente, M. G. *Localization and photodynamic efficacy of two cationic porphyrins varying in charge distributions*. Photochem Photobiol, **2003**, 78(5), p. 431-435.
95. Davids, L. M.; Kleemann, B.; Kacerovska, D.; Pizinger, K. and Kidson, S. H. *Hypericin phototoxicity induces different modes of cell death in melanoma and human skin cells*. J Photochem Photobiol B, **2008**, 91(2-3), p. 67-76.
96. Fisher, A. M.; Ferrario, A.; Rucker, N.; Zhang, S. and Gomer, C. J. *Photodynamic therapy sensitivity is not altered in human tumor cells after abrogation of p53 function.* Cancer Res, **1999**, 59(2), p. 331-335.
97. Carthy, C. M.; Granville, D. J.; Jiang, H.; Levy, J. G.; Rudin, C. M.; Thompson, C. B.; McManus, B. M. and Hunt, D. W. *Early release of mitochondrial cytochrome c and expression of mitochondrial epitope 7A6 with a porphyrin-derived photosensitizer: Bcl-2 and Bcl-xL overexpression do not prevent early mitochondrial*

events but still depress caspase activity. Laboratory Investigation, **1999**, 79(8), p. 953-965.
98. Hengartner, M. O. *The biochemistry of apoptosis*. Nature, **2000**, 407(6805), p. 770-776.
99. Mroz, P.; Yaroslavsky, A.; Kharkwal, G. B. and Hamblin, M. R. *Cell Death Pathways in Photodynamic Therapy of Cancer*. Cancers, **2011**, 3(2), p. 2516-2539.
100. Oleinick, N. L.; Morris, R. L. and Belichenko, I. *The role of apoptosis in response to photodynamic therapy: what, where, why, and how*. Photochem Photobiol Sci, **2002**, 1(1), p. 1-21.
101. Zou, H.; Li, Y.; Liu, X. and Wang, X. *An APAF-1.cytochrome c multimeric complex is a functional apoptosome that activates procaspase-9*. J Biol Chem, **1999**, 274(17), p. 11549-11556.
102. Krieser, R. J. and White, K. *Engulfment mechanism of apoptotic cells*. Curr Opin Cell Biol, **2002**, 14(6), p. 734-738.
103. Kim, H. R.; Luo, Y.; Li, G. and Kessel, D. *Enhanced apoptotic response to photodynamic therapy after bcl-2 transfection*. Cancer Res, **1999**, 59(14), p. 3429-3432.
104. Granville, D. J.; Jiang, H.; An, M. T.; Levy, J. G.; McManus, B. M. and Hunt, D. W. *Bcl-2 overexpression blocks caspase activation and downstream apoptotic events instigated by photodynamic therapy*. Br J Cancer, **1999**, 79(1), p. 95-100.
105. Srivastava, M.; Ahmad, N.; Gupta, S. and Mukhtar, H. *Involvement of Bcl-2 and Bax in photodynamic therapy-mediated apoptosis. Antisense Bcl-2 oligonucleotide sensitizes RIF 1 cells to photodynamic therapy apoptosis*. J Biol Chem, **2001**, 276(18), p. 15481-15488.
106. Grebenova, D.; Halada, P.; Stulik, J.; Havlicek, V. and Hrkal, Z. *Protein changes in HL60 leukemia cells associated with 5-aminolevulinic acid-based photodynamic therapy. Early effects on endoplasmic reticulum chaperones*. Photochem Photobiol, **2000**, 72(1), p. 16-22.
107. Grebenova, D.; Kuzelova, K.; Smetana, K.; Pluskalova, M.; Cajthamlova, H.; Marinov, I.; Fuchs, O.; Soucek, J.; Jarolim, P. and Hrkal, Z. *Mitochondrial and endoplasmic reticulum stress-induced apoptotic pathways are activated by 5-aminolevulinic acid-based photodynamic therapy in HL60 leukemia cells*. J Photochem Photobiol B, **2003**, 69(2), p. 71-85.
108. Chiu, S. M.; Xue, L. Y.; Usuda, J.; Azizuddin, K. and Oleinick, N. L. *Bax is essential for mitochondrion-mediated apoptosis but not for cell death caused by photodynamic therapy*. Br J Cancer, **2003**, 89(8), p. 1590-1597.
109. Prout, G. R., Jr.; Lin, C. W.; Benson, R., Jr.; Nseyo, U. O.; Daly, J. J.; Griffin, P. P.; Kinsey, J.; Tian, M. E.; Lao, Y. H.; Mian, Y. Z. and et al. *Photodynamic therapy with hematoporphyrin derivative in the treatment of superficial transitional-cell carcinoma of the bladder*. N Engl J Med, **1987**, 317(20), p. 1251-1255.

110. Uchibayashi, T.; Koshida, K.; Kunimi, K. and Hisazumi, H. *Whole bladder wall photodynamic therapy for refractory carcinoma in situ of the bladder*. Br J Cancer, **1995**, 71(3), p. 625-628.
111. Pope, A. J. and Bown, S. G. *The morphological and functional changes in rat bladder following photodynamic therapy with phthalocyanine photosensitization*. J Urol, **1991**, 145(5), p. 1064-1070.
112. D'Hallewin, M. A. and Baert, L. *Long-term results of whole bladder wall photodynamic therapy for carcinoma in situ of the bladder*. Urology, **1995**, 45(5), p. 763-767.
113. Nseyo, U. O.; Shumaker, B.; Klein, E. A. and Sutherland, K. *Photodynamic therapy using porfimer sodium as an alternative to cystectomy in patients with refractory transitional cell carcinoma in situ of the bladder. Bladder Photofrin Study Group*. J Urol, **1998**, 160(1), p. 39-44.
114. Pinthus, J. H.; Bogaards, A.; Weersink, R.; Wilson, B. C. and Trachtenberg, J. *Photodynamic therapy for urological malignancies: past to current approaches*. J Urol, **2006**, 175(4), p. 1201-1207.
115. Skyrme, R. J.; French, A. J.; Datta, S. N.; Allman, R.; Mason, M. D. and Matthews, P. N. *A phase-1 study of sequential mitomycin C and 5-aminolaevulinic acid-mediated photodynamic therapy in recurrent superficial bladder carcinoma*. BJU Int, **2005**, 95(9), p. 1206-1210.
116. Lee, L. S.; Thong, P. S.; Olivo, M.; Chin, W. W.; Ramaswamy, B.; Kho, K. W.; Lim, P. L. and Lau, W. K. *Chlorin e6-polyvinylpyrrolidone mediated photodynamic therapy--A potential bladder sparing option for high risk non-muscle invasive bladder cancer*. Photodiagnosis Photodyn Ther, **2010**, 7(4), p. 213-220.
117. Bhuvaneswari, R.; Gan, Y.; Soo, K. and Olivo, M. *Targeting EGFR with photodynamic therapy in combination with Erbitux enhances in vivo bladder tumor response*. Molecular Cancer, **2009**, 8(1), p. 94.

RESULTS AND DISCUSSION
CHAPTER 2

Galacto-conjugated porphyrin $PorGal_8$ and phthalocyanine $PcGal_{16}$:
Photo-chemical and -physical characterization
Part I

1. Galacto-conjugated porphyrin **PorGal$_8$** and phthalocyanine **PcGal$_{16}$**: photo-chemical and -physical characterization

1.1. General overview

Porphyrins (Pors) and phthalocyanines (Pcs) are well known first and second generation PSs, respectively. The conjugation of PSs with galactose units increases their water solubility [1-8] and provides the possibility for specific interaction of the resulting galacto-conjugate with galectins overexpressed in cancer cells. In this thesis, Pors and Pcs conjugated with galactose units (already synthesized) were evaluated as new PSs for PDT of bladder cancer cells. The photo-chemical and -physical properties (mentioned below) of these galacto-conjugates were assessed before their *in vitro* validation, since these are important parameters in the development of new PSs.

This section includes the UV-Visible and fluorescence characterization, water solubility, $^1O_2$ production ability, photostability and interaction with human serum albumin (HSA) (**Figure 2.1**) of a Pc conjugated with sixteen galactose units **PcGal$_{16}$** and a Por conjugated with eight galactose units **PorGal$_8$**. These results are already published [9].

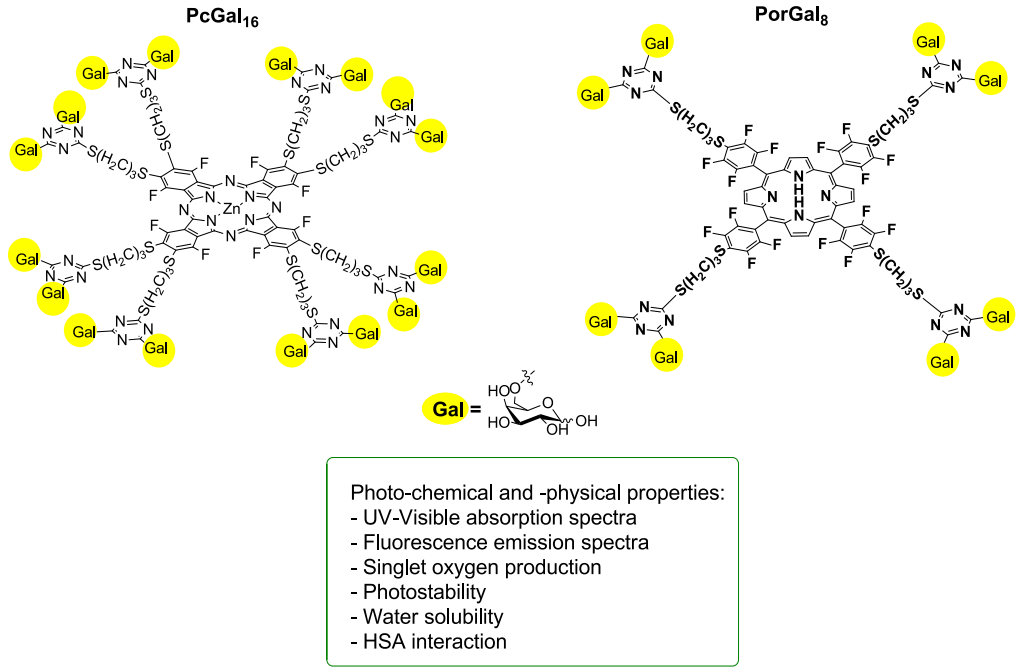

Figure 2.1. Schematic overview of this section including the photo-chemical and -physical characterization of two galacto-conjugates, **PcGal$_{16}$** and **PorGal$_8$**. The galacto-conjugates were synthesized and gently provided by Doctor Sandrina Silva [9].

1.2. UV-Visible characterization, water solubility and fluorescence emission of galacto-conjugates

The electronic absorption spectra of the galacto-conjugates were measured in DMF and DMSO (**Figure 2.2**) and their extinction coefficients (ε) in these two organic solvents are summarized in **Table 2.1**. **PcGal$_{16}$** and **PorGal$_8$** at 2 µM (in DMSO or DMF) exhibit a very sharp Soret band (at 415 nm) and Q band (at 720 nm), respectively, which is typical of non-aggregated PSs. To determine the solubility of the galacto-conjugates in aqueous buffered solution, their absorption spectra were also acquired in PBS. In this solvent, **PorGal$_8$** and **PcGal$_{16}$** demonstrated a lowering intensity and a broadening of the Soret and Q bands (**Figure 2.2**), which are related with reasonable water solubility.

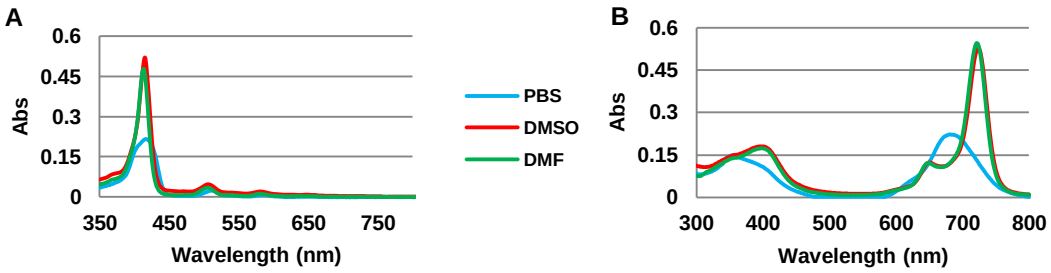

Figure 2.2. Electronic absorption spectra of **PorGal$_8$** (**A**) and **PcGal$_{16}$** (**B**) at 2 µM in DMF, DMSO, and PBS.

To evaluate the water solubility range of the galacto-conjugates, UV-Visible studies with increasing concentrations of the conjugates in PBS solution (**PcGal$_{16}$**: 0 µM to 9 µM, **PorGal$_8$**: 0 µM to 19 µM) were performed (**Figure 2.3**). The galacto-conjugates strictly follow the Beer-Lambert law at the studied concentrations (**Figure 2.3 B and D**) suggesting no aggregation in PBS at concentrations below 19 µM for **PorGal$_8$** and 9 µM for **PcGal$_{16}$**. The PSs´ solubility in aqueous solution is a critical parameter for their PDT application, since PSs´ aggregation compromises their ROS production and their uptake by cells [8].

These results demonstrate that concentrations of **PorGal$_8$** and **PcGal$_{16}$** in PBS below 19 µM and 9 µM, respectively, can be used for the *in vitro* PDT assays without compromising their phototoxic effectiveness.

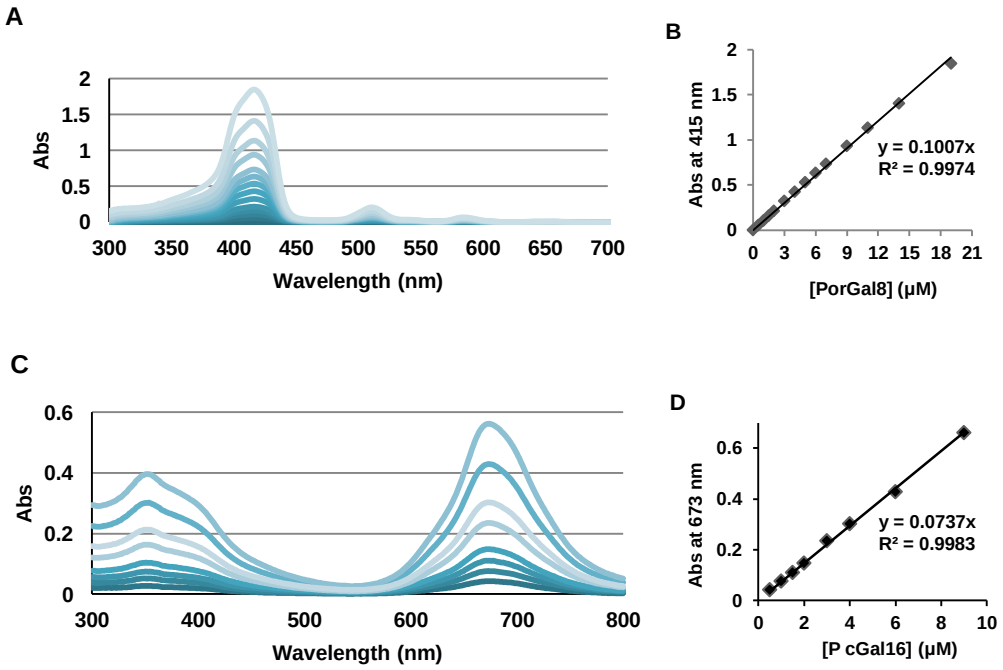

Figure 2.3. UV-Visible spectra of **PorGal$_8$** (**A**) and **PcGal$_{16}$** (**C**) in PBS at different concentrations (**PcGal$_{16}$**: 0 μM to 9 μM, **PorGal$_8$**: 0 μM to 19 μM). The inset plots the **PorGal$_8$**-Soret band (**B**) at 415 nm and **PcGal$_{16}$** Q-band (**D**) at 673 nm *versus* concentration of the respective galacto-conjugate in PBS.

The steady-state fluorescence emission spectra of **PorGal$_8$** and **PcGal$_{16}$** were acquired in DMF and the fluorescence quantum yields (Φ_F) were determined (**Table 2.1**) using *meso*-tetraphenylporphyrin (TPP) as standard (Φ_F = 0.11 in DMF [10]). These studies demonstrated that the galacto-conjugates shown fluorescence emission bands in the red spectral region - **PcGal$_{16}$**: 734 nm and 805 nm, **PorGal$_8$**: 659 nm and 703 nm - which can be used to determine the concentration of these PSs inside the cells.

Table 2.1. UV-Visible data of the galacto-conjugates in DMF and DMSO. Fluorescence data of **PorGal$_8$** and **PcGal$_{16}$** in DMF.

Galacto-conjugate	Solvent	$\lambda_{absorption\ bands}$ [nm] (log ε)[a]	$\lambda_{emission}$ (nm)	Φ_F	Δ_{Stokes} (nm)
PcGal$_{16}$	DMF	391 (5.34), 649 (5.30), 722 (5.45)	734, 805	0.13[b]	12
	DMSO	399 (5.16), 650 (5.26), 723 (5.40)	___	___	___
PorGal$_8$	DMF	413 (5.10), 504 (3.39), 577 (3.27), 655 (2.30)	659, 703	0.09[b]	4
	DMSO	415 (5.24), 505 (4.20), 575 (3.80), 655 (2.00)	___	___	___

[a] log ε $M^{-1}.cm^{-1}$
[b] Reference: TPP in DMF Φ_F = 0.11 [10] excitation at 601 nm
[c] ΔStokes is the Stokes shift, corresponding to the difference between wavelengths of maxima absorption and emission

1.3. Photostability and singlet oxygen production of galacto-conjugates

To evaluate the potentiality of the galacto-conjugates as new PSs, their photostability and ability to generate $^1O_2$ (the main cytotoxic specie involved in PDT) were determined. For the photobleaching studies, the intensity of the Soret band of **PorGal$_8$** and Q band of **PcGal$_{16}$** was monitored after irradiation with white light at a fluence rate of 150 mW.cm^{-2} (**Table 2.2**).

These results demonstrate that the galacto-conjugates are photostable when exposed to UV-Visible light and molecular oxygen over the investigated irradiation period (30 min).

Table 2.2. Photostability of 19 µM of **PorGal$_8$** and 9 µM of **PcGal$_{16}$** in PBS, after irradiation with white light at a fluence rate of 150 mW.cm^{-2} for different periods of time (0-30 min). The results are presented in percentage calculated by the ratio of residual absorbance (at 673 nm for **PcGal$_{16}$** and at 415 nm for **PorGal$_8$**) at different periods of time and absorbance before irradiation.

Galacto-conjugate	**Irradiation time (min)**									
	0	1	3	4	5	10	15	20	25	30
PcGal$_{16}$	100	100	100	99	99	98	98	98	98	97
PorGal$_8$	100	99	99	99	99	99	98	98	97	97

The generation of $^1O_2$ by galacto-conjugates was determined in DMF:H_2O (9:1) using DPBF (1,3-diphenylisobenzofuran) as $^1O_2$ scavenger [11]. The well known $^1O_2$ generators, TPP and ZnPc (zinc phthalocyanine) were used as references [12] for **PorGal$_8$** and **PcGal$_{16}$**, respectively. **PorGal$_8$** and TPP (both at 0.67 µM), **PcGal$_{16}$** and ZnPc (both at 0.1615 µM) were able to photo-oxidize DPBF (at 16.15 µM) (**Figure 2.4**).

The galacto-conjugates demonstrated to be potent generators of $^1O_2$ and at 0.67 µM **PorGal$_8$** was able to decompose 77.5% of DPBF, after 20 min of irradiation. For **PcGal$_{16}$** at 0.1615 µM, the DPBF breakdown was about 96.1%, after 5 min of irradiation. The galacto-conjugates have shown similar ability to photo-oxidize DPBF when compared to the corresponding references TPP and ZnPc.

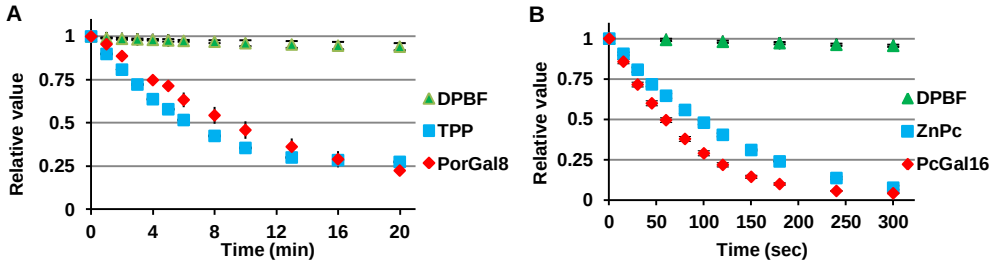

Figure 2.4. Photo-oxidation of DPBF (16.15 µM) in DMF:H_2O (9:1) with or without **PorGal$_8$** or TPP at 0.67 µM (**A**); **PcGal$_{16}$** or ZnPc at 0.1615 µM (**B**), after irradiation with white light filtered through a cut-off filter for wavelengths <540 nm (4.5 mW.cm^{-2}). The DPBF absorbance was recorded at 415 nm.

1.4. Affinity of galacto-conjugates to Human Serum Albumin

To elucidate the pharmacological properties of the galacto-conjugates [13], their interaction with the abundant plasma protein HSA was studied. The fluorescence quenching of tryptophan residues in 2.0 µM of HSA samples, after addition of **PorGal$_8$** and **PcGal$_{16}$** at increasing concentrations (0-30 µM) was determined. PSs´ addition to HSA samples produced fluorescence quenching of the tryptophan residues (**Figure 2.5**). The effects of DMSO on HSA fluorescence quenching were tested, since the stock solutions of the galacto-conjugates were prepared in this solvent. Over a concentration range of 0-0.5 % (v/v), DMSO did not quench HSA fluorescence (data not shown). The binding constant (K_a) and the number of binding sites (n) of galacto-conjugates to HSA were determined as described in the literature [14]. The values of K_a and n for **PorGal$_8$** were 1.544 x 10^4 M^{-1} and 1.2, respectively. For **PcGal$_{16}$** were 2.351 x 10^5 M^{-1} and 1.4, respectively. These results indicate that there is only one binding site for the galacto-conjugates closes to the tryptophan residues of HSA.

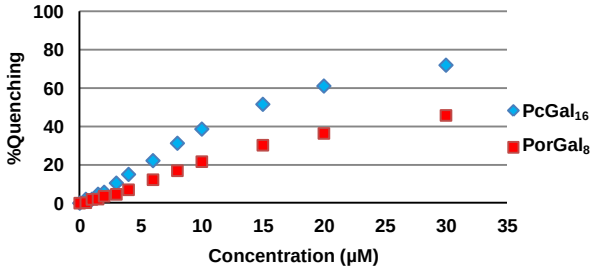

Figure 2.5. Fluorescence quenching curves of 2 µM of HSA, after addition of the galacto-conjugates at several concentrations (between 0 µM to 30.0 µM). *Quenching (%)=(F_0-F)/F_0*, where F_0 and F are the HSA fluorescence intensities in the absence and presence of the conjugates ($\lambda_{excitation}$ at 280 nm and wavelength emission range between 300 nm to 400 nm).

Galacto-conjugated porphyrin PorGal$_8$:
Photoactive agent against bladder cancer cells
Part II

2. Galacto-conjugated porphyrin **PorGal$_8$**: photoactive agent against bladder cancer cells

2.1. General overview

Porphyrins are the most commonly used drugs in cancer treatment by PDT. Porphyrins decorated with carbohydrates, like galactose units, should allow for improved PDT treatment. Galactose-binding lectins, especially galectin-1 and galectin-3 are overexpressed in the surface of bladder tumours [15] and can be exploited in the development of new molecular-targeted PSs for cancer treatment. As demonstrated in part I, **PorGal$_8$** is water soluble up to 19 μM, stable after light irradiation, efficient generator of $^1O_2$ and binds to HSA protein [9]. In this part of the work (**Figure 2.6**), the effectiveness of **PorGal$_8$** to induce phototoxicity in two human bladder cancer cell lines HT-1376 and UM-UC-3 will be reported. Due to the presence of carbohydrate moieties in the PS, the involvement of galecin-1 target specificity of the **PorGal$_8$** was addressed. Additionally, the presence of cancer stem cells (CSCs) in these cell lines was exploited. The ROS generation after **PorGal$_8$**-PDT (in the presence and absence of quenchers) was evaluated. The alterations of F-actin and the cell death pathways induced after **PorGal$_8$**-PDT were also addressed.

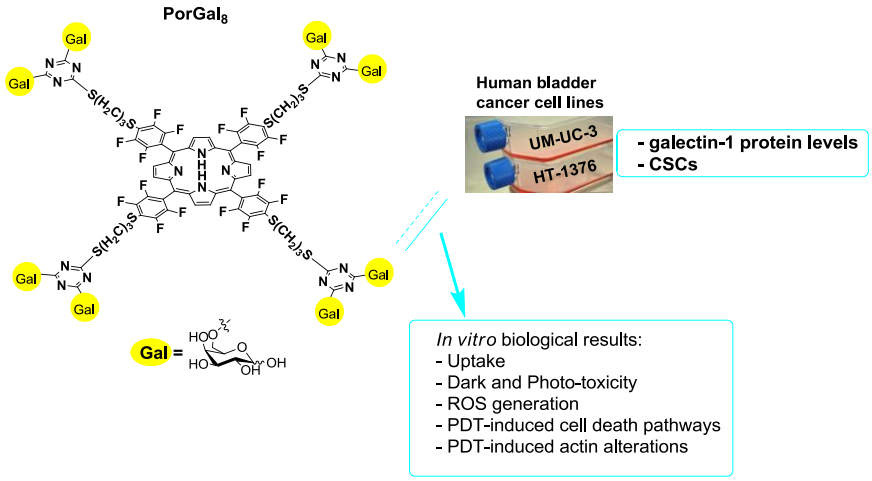

Figure 2.6. Schematic overview of this section including the *in vitro* results obtained with **PorGal$_8$** against the human bladder cancer cell lines, UM-UC-3 and HT-1376.

2.2. Galectin-1 protein levels in HT-1376 and UM-UC-3 bladder cancer cells

The *in vitro* validation of the compounds studied in this thesis, namely **PorGal$_8$**, was performed in bladder cancer cell lines (HT-1376 and UM-UC-3, **Figure 2.7 A and B**) derived from transitional cell carcinoma, which is the most common malignant tumour arising from the urothelium. The morphology of HT-1376 is defined by tightly adherent cuboidal cells growing as colonies. The morphology of UM-UC-3 cells is defined by poorly adherent cells displaying a stellate morphology. UM-UC-3 cells have been associated with the epithelial to mesenchimal phenotype, which is an event implicated in neoplastic progression [16]. It has been reported that UM-UC-3 cells have an invasive phenotype, while HT-1376 cells have an epithelial morphology associated with a non-invasive phenotype [16].

For the PSs conjugated with galactose units it was thought that galactose around the core of PSs has interaction with galactose-binding lectins (galectins) overexpressed on the surface of certain types of cancer cells, promoting somehow its uptake [16]. Among galectins, the expression of galectin-1 is correlated with the cancer staging and cell metastatic potential [15] and can be exploited in the development of new conjugated PSs for cancer treatment.

The galectin-1 protein levels were determined in both cell lines by western blotting and they were significantly higher in UM-UC-3 than in HT-1376 cells (**Figure 2.7 C and D**). The expression of galectin-1 is known to be correlated with the degree of malignancy in rat thyroid cell lines transformed with several viral oncogenes [17]. The mRNA (messenger ribonucleic acid) levels of galectin-1 were 20-fold higher in low tumourigenic and 100-fold higher in highly tumourigenic cells, than in normal cells [17].

These results demonstrate that UM-UC-3 and HT-1376 cells have a different morphology and galectin-1 protein levels. UM-UC-3 cells seem to correspond to a more aggressive and invasive phenotype.

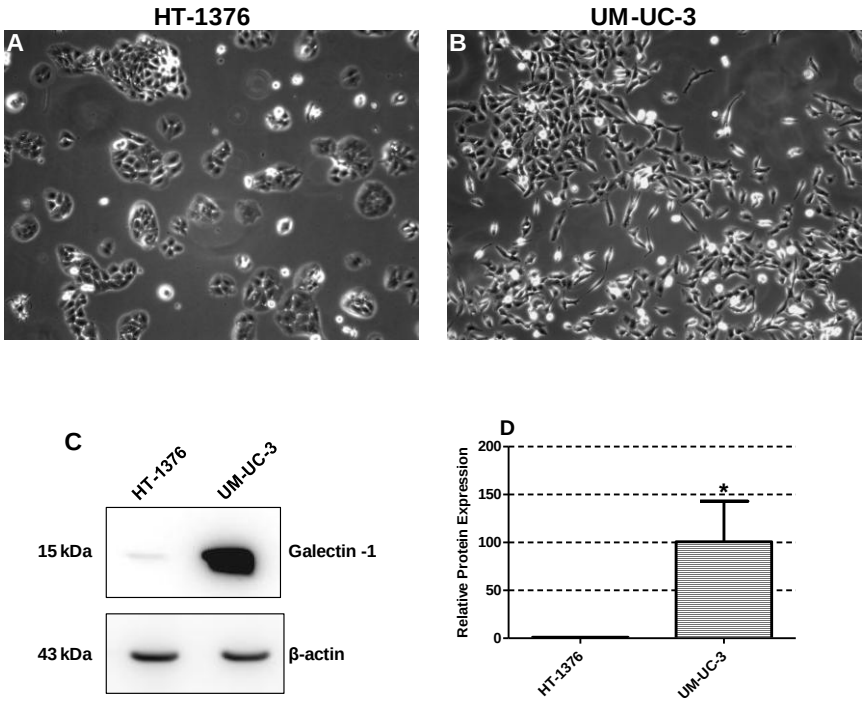

Figure 2.7. Bright field images of monolayer culture of HT-1376 (**A**) and UM-UC-3 (**B**) human bladder cancer cell lines. Original magnification: 200x. (**C**) Western blotting analysis of galectin-1 protein levels in HT-1376 and UM-UC-3 cells. β-actin was blotted as loading control. (**D**) Quantitative analysis of galectin-1 (normalized to β -actin) expressed as a ratio of the levels found in HT-1376 cells. Data represents mean ± S.D. of five independent experiments. *Significantly different from HT-1376 cells ($p<0.05$).

2.3. Uptake of **PorGal$_8$** by HT-1376 and UM-UC-3 bladder cancer cells

The concentration of **PorGal$_8$** inside the HT-1376 and UM-UC-3 cells was measured by fluorescence spectroscopy, in order to determine the optimum concentration of **PorGal$_8$** and incubation time to be used in the following assays. Bladder cancer cell lines were incubated in the dark at various periods of time (0.5, 1, 2, and 4 h) with increasing concentrations of water soluble **PorGal$_8$** (0.5, 2.5, 5, 10, and 12.5 μM) in PBS.

In both cell lines a fast uptake of **PorGal$_8$** occurred during the first 1.5 h, followed by a slower steady increase (**Figure 2.8**). **PorGal$_8$** uptake profile as a function of the incubation time was higher in UM-UC-3 cells than in HT-1376 cells. Thus, the higher uptake of **PorGal$_8$** by UM-UC-3 cells when compared with HT-1376 cells can in some way be attributed to the protein levels of galectin-1 (**Figure 2.7 C and D**). Galectin-1 may serve as docking sites for **PorGal$_8$** on the cell membrane and probably, facilitating entry of **PorGal$_8$**.

The results can support our hypothesis, that the presence of galactose units in

PorGal$_8$ should allow for improved uptake of this PS in cancer cells and galectin-1 may have an important role in that process.

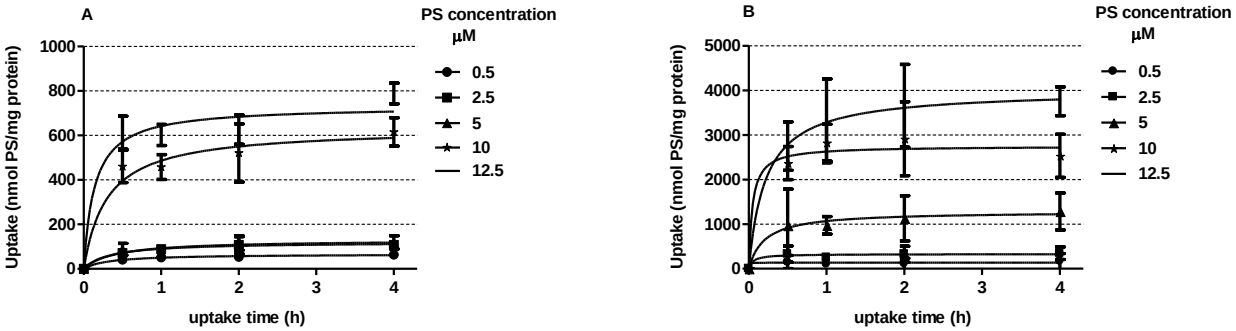

Figure 2.8. Intracellular uptake of **PorGal$_8$** by HT-1376 (**A**) and UM-UC-3 (**B**) cells, at various concentrations (0.5, 2.5, 5, 10, and 12.5 µM) in function of the uptake time (0, 1, 2, 3, and 4 h). **PorGal$_8$** concentration was determined using fluorescence spectroscopy and the results were normalized to protein quantity. Data are the mean ± S.D. of at least three independent experiments performed in triplicates.

The intracellular uptake of **PorGal$_8$** in bladder cancer cells was also confirmed by confocal fluorescence microscopy (**Figure 2.9**). The cells were incubated with **PorGal$_8$** at 10 µM for 1.5 h (in darkness) and cell nuclei were stained with DAPI. In both cell lines, the fluorescence of **PorGal$_8$** was clearly observed throughout the cytoplasm of cancer cells with some small bright spots. The strong fluorescent signal of **PorGal$_8$** inside the UM-UC-3 cells (**Figure 2.9**) confirms its higher uptake in these cells than in HT-1376 cells, as previously obtained by fluorescence spectroscopy (**Figure 2.8**).

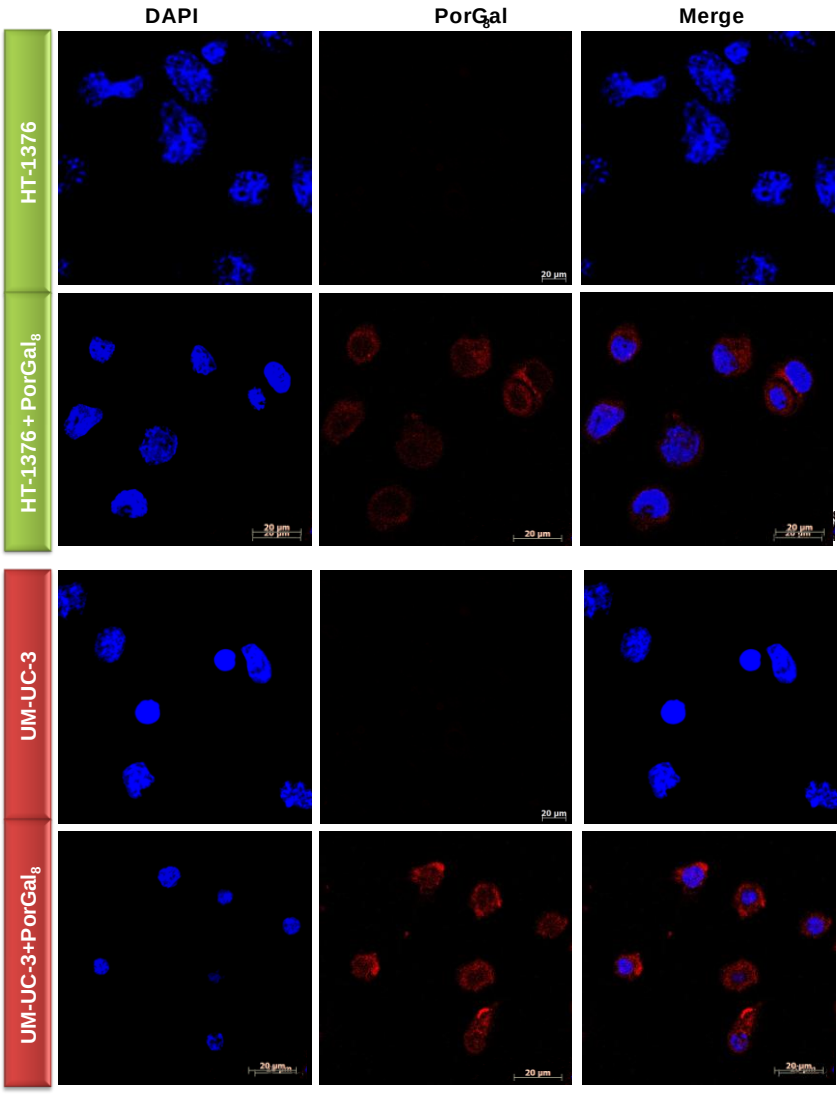

Figure 2.9. Representative fluorescence images of HT-1376 and UM-UC-3 cells incubated for 1.5 h with 10 µM of **PorGal$_8$** in darkness (red) with nucleus stained with DAPI (blue). Control fluorescence images (no **PorGal$_8$** fluorescence) were acquired after cells´ incubation with PBS for 1.5 h in the dark and staining the nucleus with DAPI (blue). Scale bars are indicated on images. Original magnification: 400x.

2.4. Dark toxicity and phototoxicity of **PorGal$_8$** in HT-1376 and UM-UC-3 bladder cancer cells

The current PSs, at the working concentrations, are non-toxic unless and until activation by light at a specific wavelength. Thus, after confirming the uptake of **PorGal$_8$** by bladder cancer cells, its cytotoxicity in darkness was determined. Bladder cancer cell lines, HT-1376 and UM-UC-3, were incubated in darkness at various periods of time (0.5, 1, 2, and 4 h) with increasing concentrations of **PorGal$_8$** (0.5, 2.5, 5, 10, and 12.5 µM) in PBS. The cells viability was determined 24 h after treatment by MTT colorimetric assay.

In this assay, the yellow-colored MTT is reduced by mitochondrial dehydrogenases in living cells to a blue-colored formazan precipitate. The absorption of dissolved formazan correlates with the number of live cells.

In both cell lines, incubation concentrations up to 12.5 µM and uptake time up to 4 h did not induce dark toxicity (**Figure 2.10**).

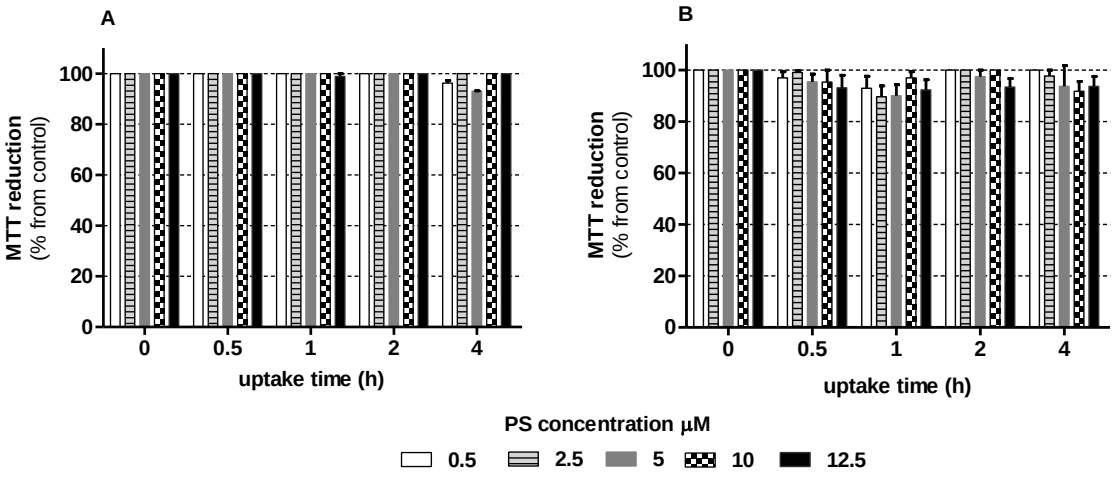

Figure 2.10. Non-dark toxicity of **PorGal$_8$** in HT-1376 (**A**) or UM-UC-3 (**B**) cells. Cells were incubated with **PorGal$_8$** at various concentrations (0.5, 2.5, 5, 10, and 12.5 µM) for increasing uptake times (0, 0.5, 1, 2, and 4 h) in dark conditions. Cytotoxicity was assessed using MTT colorimetric assay 24 h after treatment. The percentage of cytotoxicity was calculated relatively to control cells (cells incubated with PBS in darkness) at therespective uptake time. Data are the mean value ± S.D. of at least three independent experiments performed in triplicates.

The non dark toxicity of **PorGal$_8$** prompted us to perform the PDT studies. The cells were incubated with **PorGal$_8$** at the same concentrations in the dark (0.5, 2.5, 5, 10, and 12.5 µM) for 1.5 h. After **PorGal$_8$** uptake in darkness, cells were irradiated with white light at a potency of 8.4 mW.cm^{-2} for various irradiation times (5, 10, 20, and 40 min). The cell viability was assessed by MTT colorimetric assay 24 h after PDT assays. To test the effect of white light irradiation alone on cell viability, control experiments using irradiated cells (previously incubated with PBS for 1.5 h in the dark) were performed. These conditions did not induce toxicity in both cell lines. However, when cells were pre-incubated with **PorGal$_8$** and then irradiated, there was an increase of the phototoxicity in a concentration- and irradiation time-dependent manner (**Figure 2.11**). Incubation with 10 µM of **PorGal$_8$** and irradiation for 40 min induced a percentage of phototoxicity of 33.20 ± 1.84 and 55.45 ± 4.96 for the cell line HT-1376 and UM-UC-3, respectively.

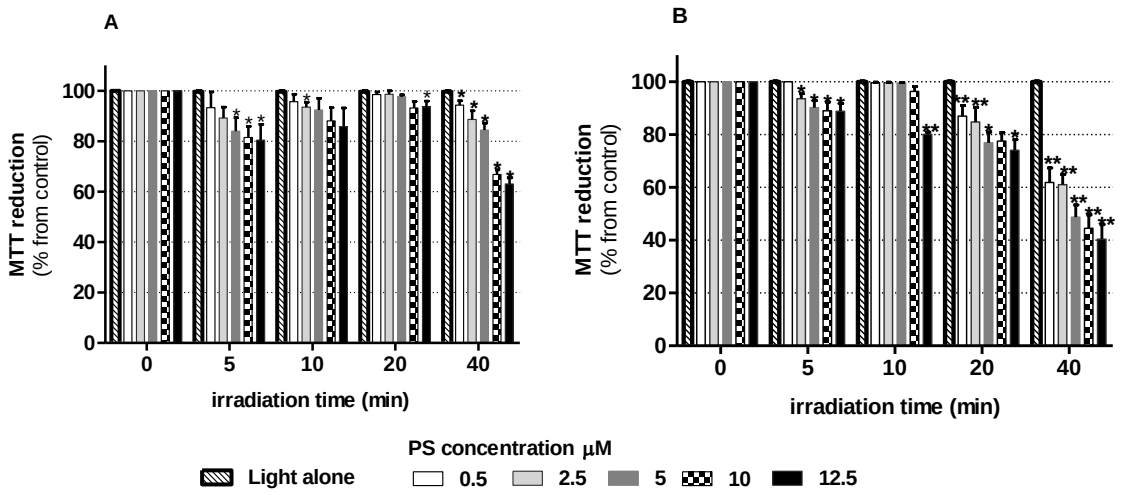

Figure 2.11. Photocytotoxic effects of PDT with **PorGal$_8$** in HT-1376 (**A**) and UM-UC-3 (**B**) cells. Cells were incubated in the dark with **PorGal$_8$** at various concentrations (0.5, 2.5, 5, 10, and 12.5 μM) for 1.5 h and irradiated with white light at a fluence rate of 8.4 mW.cm^{-2} for various times (5, 10, 20, and 40 min). Cytotoxicity was assessed 24 h after PDT using the MTT assay. The percentage of photocytotoxicity was calculated relatively to control cells (cells incubated with PBS for 1.5 h and then irradiated) at the respective irradiation time. Data are the mean value ± S.D. of at least three independent experiments performed in triplicates. *($p<0.05$).and **($p<0.001$) significantly different from control cells (incubated with PBS for 1.5 h) at the same irradiation time

Theoretically, in the MTT assay, the color intensity of the formazan dye is correlated to the number of viable cells. However, this assay is dependent of the cell metabolism to reduce MTT in formazan. To confirm the results obtained using the MTT assay, additionally studies using the trypan blue staining assay were performed. The trypan blue is excluded by live cells with intact cell membranes and it is retained in dead cells (for more detail about these two methods, see chapter IV).

MTT and trypan blue exclusion assays were performed 48 h and 72 h after **PorGal$_8$**-PDT, in order to evaluate whether cells could recover for a time superior to 24 h after PDT. A significant reduction of mitochondrial activity in HT-1376 cells was still found 48 h after PDT for the concentrations 0.5, 2.5, and 5 μM (**Figure 2.12 A**) when compared with the respective concentrations 24 h after treatment. For the concentrations 2.5, 10, and 12.5 μM the HT-1376 cells recover, at least in part their mitochondrial metabolic function 72 h after treatment. An increase of mitochondrial activity was also observed 72 h after PDT for UM-UC-3 cells, when **PorGal$_8$** was used at concentrations of 0.5 μM or 5 μM (**Figure 2.12 B**). No significant differences were seen in the proportion of membrane-damaged cells 48 h and 72 h after PDT with respect to 24 h after PDT, for both cells lines (**Figure**

2.12 C and D). Both MTT and trypan blue exclusion demonstrated that PDT with **PorGal$_8$** is more active against UM-UC-3 cells than HT-1376 cells (**Table 2.3**). Based on these results, as well as in the uptake results, the next experiments were performed by incubation of the cells with 10 µM of **PorGal$_8$** for 1.5 h in darkness and irradiating for 40 min.

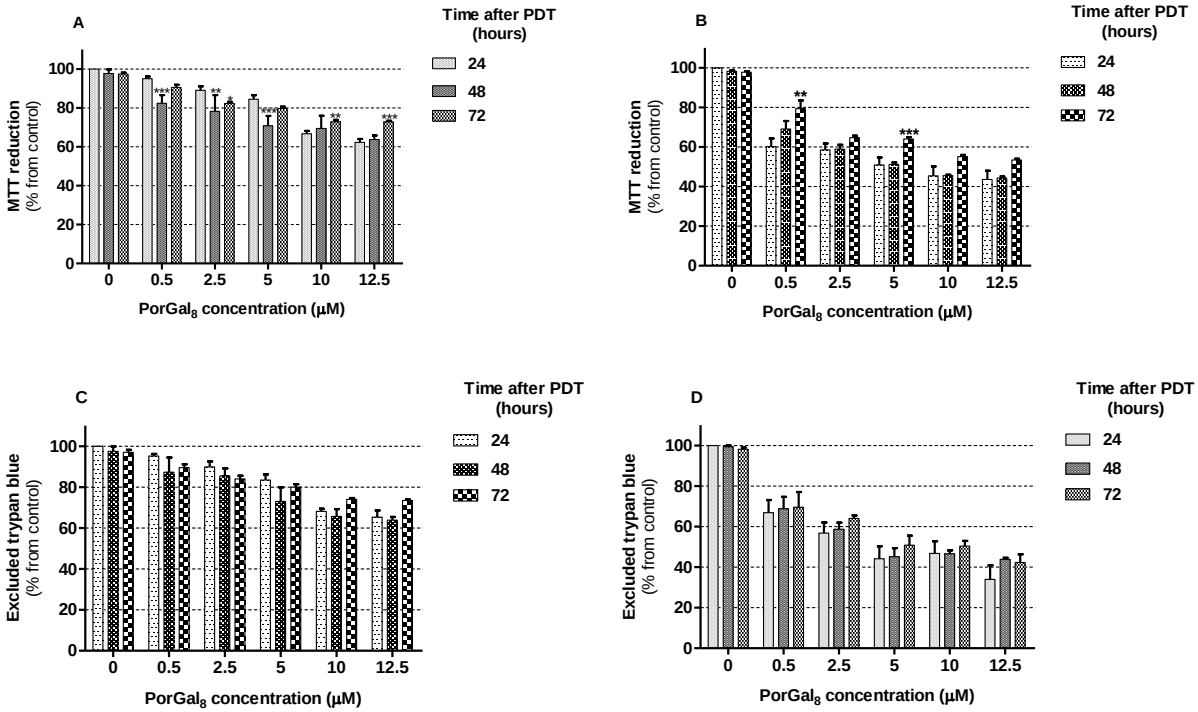

Figure 2.12. Photocytotoxic effects of **PorGal$_8$** in HT-1376 (**A** and **C**) and UM-UC-3 (**B** and **D**) cells as function of the **PorGal$_8$** concentration. Cytotoxicity was assessed 24, 48, and 72 h after **PorGal$_8$**-PDT using the MTT (**A** and **B**) and the trypan blue exclusion (**C** and **D**) assays. The percentage of cytotoxicity was calculated relatively to control cells (cells incubated with PBS and then irradiated) at the respective time after PDT. Data are the mean value ± S.D. of at least three independent experiments performed in triplicates. The symbols *($p<0.05$), **($p<0.001$), *($p<0.0001$) represent significant differences in phototoxicity comparing with MTT reduction (%) or excluded trypan blue (%) of **PorGal$_8$**-24 h after PDT for the respective concentration.

Table 2.3. Percentage values of cell toxicity after treat human bladder cancer cell lines, HT-1376 and UM-UC-3, with **PorGal$_8$** at 10 µM for 1.5 h and irradiate for 40 min. The results were obtained 24, 48, and 72 h after **PorGal$_8$**-PDT using the MTT and trypan blue exclusion assays. The symbol * represents significant ($p<0.05$) differences in cell toxicity comparing with HT-1376 cells at the respective time after PDT.

		HT-1376 cell line			UM-UC-3 cell line		
Hours after PDT		24	48	72	24	48	72
Cell toxicity (% mean ± S.D.)	**MTT assay**	33.30 ± 1.47	30.54 ± 1.88	27.19 ± 1.07	54.57 ± 4.71*	54.47 ± 0.48*	44.87 ± 0.83*
	Trypan blue exclusion	31.83 ± 1.30	34.33 ± 1.47	26 ± 0.68	53.24 ± 6.04*	53.50 ± 1.73*	49.67 ± 2.64*

2.5. Galectin inhibition studies in HT-1376 and UM-UC-3 bladder cancer cells

To clarify the role of galectins in the uptake of **PorGal$_8$**, the binding sites of galectin to galactose, in UM-UC-3 and HT-1376 cells, were "blocked" with a pre-incubation of 50 nM galactose for 1.5 h before incubation with 10 µM of **PorGal$_8$** for 1.5 h.

The pre-incubation with galactose did not completely inhibit the uptake of **PorGal$_8$** in both bladder cancer cells (**Figure 2.13 A**). In fact, there are no significant differences in the **PorGal$_8$** uptake when HT-1376 cells were pre-incubated with galactose. Interestingly, for the cell line UM-UC-3 (which expresses high levels of galectin-1, **Figure 2.7 C and D**) there was about 40% decrease in **PorGal$_8$** cell uptake when the cells were pre-incubated with galactose.

The PDT assays during 40 min were also performed after the galactose "blocking" assays and the cell viability was determined 24 h after treatment by MTT colorimetric assay. It was observed an increase of cell viability of about 15% and 53% in HT-1376 and UM-UC-3 cells, respectively (**Figure 2.13 B**).

These results demonstrate the involvement of galactose-binding proteins, namely galectin-1, on increased intracellular accumulation of **PorGal$_8$** in the bladder cancer cells, which after PDT leads to cytotoxicity and that was more evident for the cell line UM-UC-3.

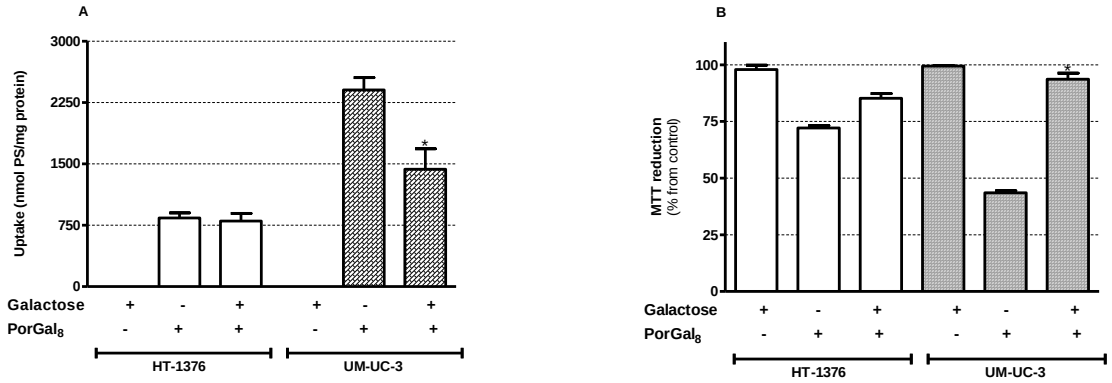

Figure 2.13. Decrease on the uptake of **PorGal$_8$** by UM-UC-3 and HT-1376 cells after pre-incubation with galactose (**A**). Photocytotoxic decrease in HT-1376 and UM-UC-3 cells after PDT in cells pre-incubated with galactose (**B**). **PorGal$_8$** uptake was determined using fluorescence spectroscopy after cells´ incubation with 50 nM of galactose for 1.5 h and then with 10 µM of **PorGal$_8$** for 1.5 h. Cytotoxicity was assessed 24 h after treatment using the MTT colorimetric assay. The percentage of cytotoxicity was calculated relatively to control cells (cells incubated with PBS) at the respective condition. Data are the mean value ± S.D. of at least three independent experiments performed in triplicates. The symbol * represents significant differences in uptake or phototoxicity comparing with uptake or MTT reduction (%) of cells without pre-incubation with galactose ($p<0.05$).

2.6. $PorGal_8$-induced reactive oxygen species after PDT in HT-1376 and UM-UC-3 bladder cancer cells

To confirm whether phototoxicity (**Figures 2.11 and 2.12**) is related with an increase of oxidative stress after **$PorGal_8$**-PDT, the generation of ROS was evaluated immediately after PDT using the probes DHE (dihydroethidium) and H_2DCFDA (2´,7´-dichlorohydrofluorescin) [18, 19]. The probe H_2DCFDA quantitatively reacts with various ROS to yield the fluorescent product DCF. DHE reacts mainly with superoxide anion being oxidized to ethidium, staining the nucleus with bright red fluorescence (for more detail about these two probes, see chapter IV).

HT-1376 and UM-UC-3 cells were incubated in darkness for 1.5 h with PBS (control) or 10 μM of **$PorGal_8$** for 1.5 h and then irradiated for 40 min. The images obtained by confocal microscopy demonstrated for both cell lines an increase of intracellular DHE and DCF fluorescence when compared to control cells (**Figure 2.14 A and B**). Additionally, quantitative analysis also demonstrated a significant increase of DHE and DCF intracellular fluorescence after **$PorGal_8$**-PDT when compared to control cells (**Figure 2.14 C and D**). The DHE fluorescence was not significantly different between cell lines (**Figure 2.14 C**) and the DCF fluorescence was about two-fold higher for UM-UC-3 than for HT-1376 cells, when 5 μM of H_2DCFDA was used (**Figure 2.14 D**).

DCF is frequently used as an overall sensor of oxidative stress in the cells, which demonstrate that the higher ROS levels observed inside the UM-UC-3 cells, can explain the higher phototoxicity in these cells than in HT-1376 cells (**Figures 2.11 and 2.12**). Moreover, it has been reported that a weaker accumulation of PSs inside the cells can enhance the antioxidant response after PDT [20]. Based on that evidence and on the fact that **$PorGal_8$** is lesser accumulated in HT-1376 cells, the possible enhancement of an antioxidant response after **$PorGal_8$**-PDT can be a plausible explanation for the lower ROS generation inside these cells, and consequently lower toxicity.

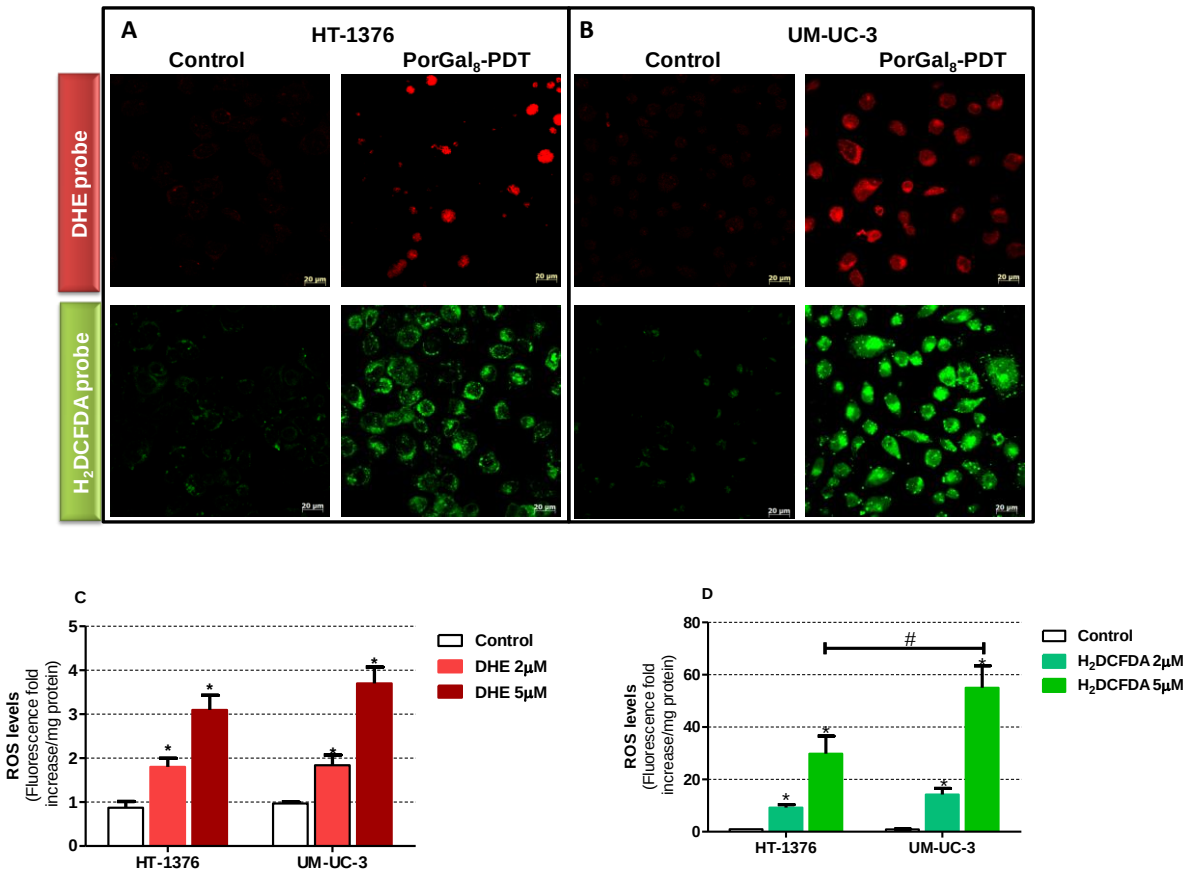

Figure 2.14. Representative fluorescence images (**A** and **B**) and quantification (**C** and **D**) of DHE and DCF fluorescence increase (as a measure of ROS production) after **PorGal$_8$**-PDT. Human bladder cancer cell lines HT-1376 and UM-UC-3 were incubated with PBS (control) or 10 µM of **PorGal$_8$** for 1.5 h in the dark. After PDT during 40 min, the images were acquired on a confocal microscope demonstrating an increase of intracellular oxidative stress in HT-1376 (**A**) and UM-UC-3 cells (**B**) when compared to control cells. The fluorescent signals of DHE (**C**) and DCF (**D**) were quantified by fluorescent spectroscopy for both cell lines. *Significantly different from irradiated-control cells (incubated with PBS for 1.5 h) and then incubated with DHE or H_2DCFDA probes ($p<0.05$). #Significantly different from treated HT-1376 cells ($p<0.05$).

To analyze the contribution of particular ROS in **PorGal$_8$**-mediated cell death, specific quenchers of $^1O_2$ (sodium azide [21] and histidine [22]) and free radical scavengers (cysteine [23]) were used. HT-1376 and UM-UC-3 cells loaded with 10 µM of **PorGal$_8$** for 1.5 h in darkness were pre-incubated with 50 nM of $^1O_2$ quenchers and ROS scavengers and were then exposed to the light. The cell viability evaluated 24 h after **PorGal$_8$**-PDT was dependent on the used scavenger and on the cell type (**Figure 2.15**). In both cell types, sodium azide, histidine and cysteine were effective as $^1O_2$ quenchers and free radical scavenger, respectively. These results demonstrate once more the involvement of several ROS-induced after PDT with **PorGal$_8$** in HT-1376 and UM-UC-3 cells.

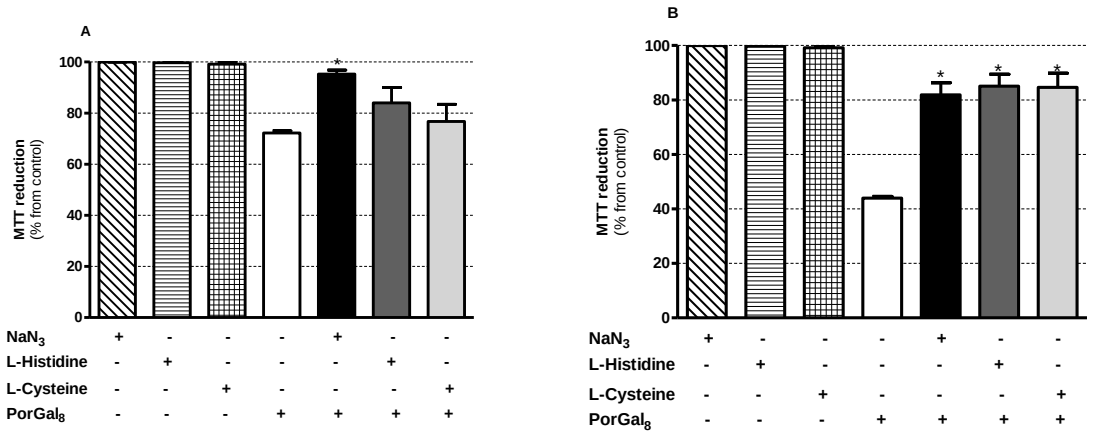

Figure 2.15. Photocytotoxicity after **PorGal$_8$**-PDT in the presence of specific quenchers of $^1O_2$ (sodium azide - NaN_3- and histidine) and free radical scavengers (cysteine) in HT-1376 (**A**) and UM-UC-3 (**B**) cells. Cytotoxicity was assessed 24 h after **PorGal$_8$**-PDT in the presence of 50 nM of ROS quenchers, using the MTT assay. The percentage of cytotoxicity was calculated relatively to control cells (untreated cells). Data are the mean value ± S.D. of at least three independent experiments performed in triplicates. The symbol * represents significant differences in phototoxicity comparing with MTT reduction (%) of **PorGal$_8$**-24 h after PDT ($p<0.05$).

2.7. The role of cancer stem cells in determination of the cell demise after PDT with **PorGal$_8$**

The results previously described demonstrated that HT-1376 cells are lesser sensible after **PorGal$_8$**-PDT than UM-UC-3 cells (**Figures 2.11 and 2.12**). Based on the putative interaction between galactose units around the Por core and cell surface galectins [24], the presence of higher galectin-1 protein levels in UM-UC-3 cells (**Figure 2.7 C and D**) may enhance the accumulation of **PorGal$_8$** inside the cells and, conquently, increase the phototoxicity. Additionally, we hypothesized that the resistance of HT-1376 cells after **PorGal$_8$**-PDT may be due to the presence of cancer stem cells (CSCs). It has been reported that bladder tumours contain a subset of cells expressing the ATP binding cassette transporter ABCG2 [25]. In fact, these cells referred as CSCs are able to survive after cancer therapy and are responsible for initiating tumour regrowth. It has been reported that porphyrins (as well as other conventional drugs used in the treatment of cancer) are not able to target CSCs, because they are substrates for ABCG2, being effluxed by these pumps [26, 27]. This idea is also supported by experiments showing that porphyrins accumulate in tissues of an ABCG2-knockout mice [28]. It has been suggested that the tetrapyrrole porphyrin structure plays an important role in interaction of protoporphyrin IX, hematoporphyrin, and pheophorbide with human ABCG2 [29]. Thus, the overexpression of ABCG2 in CSCs, which is considered to be a cancer stem cell marker [30], can protect

them from many structurally different anti-cancer compounds leading to drug resistance [31].

To assess the presence of putative CSCs in HT-1376 cell line, cells were allowed to grow in serum-free medium in anchorage-independent conditions [32]. After two or three days of cells´ culture in the aforementioned conditions, the cells started to form floating spherical colony-like structures (**Figure 2.16 A**). The sphere-forming efficiency determined by the number of colonies formed per total number of HT-1376 cells plated was of 3.2 ± 0.5% (n = 6). A second generation of spheres, designated as CSCs HT-1376, was obtained with similar sphere-forming efficiency and it was used in the experiments.

Immunofluorescence studies showed the presence of the cancer stem cell surface marker CD44 [33] in isolated CSCs HT-1376 (**Figure 2.16 B**). We investigated whether CSCs HT-1376 have increased levels of the drug efflux transporter ABCG2. Western blotting analysis revealed that ABCG2 increased approximately three-fold in CSCs HT-1376 compared to HT-1376 cells (**Figure 2.16 C**). Using the same experimental conditions, UM-UC-3 cells did not form floating spherical colony-like structures (like observed to HT-1376 cells) and their ABCG2 protein levels were negligible (**Figure 2.16 C**).

The putative lower percentage of CSCs (and lower ABCG2 protein levels) in UM-UC-3 relatively to that for HT-1376 cells can be an explanation for their higher sensitivity after **PorGal$_8$**-PDT. Moreover, it has been reported that after cancer therapy, stem cell-enriched subpopulations contain low levels of ROS and increased expression of free radical scavenging systems, when compared with the non-stem counterparts [34]. Since the photocytotoxic effects after **PorGal$_8$**-PDT result from ROS-induced cell damage, we thought that the presence of a subpopulation with stem like properties in HT-1376 cells should increase their anti-oxidative defense after **PorGal$_8$**-PDT.

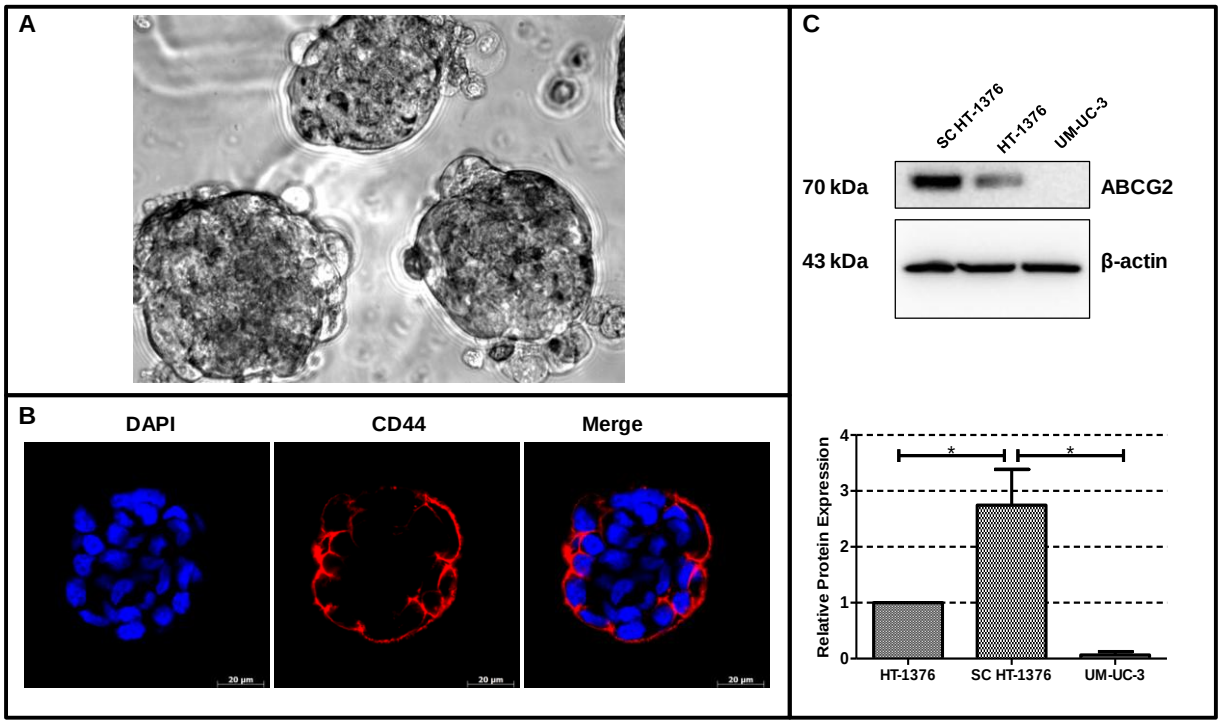

Figure 2.16. (**A**) CSCs HT-1376 derived by the sphere-formation assay with HT-1376 cells. Spherical colonies were generated from single-cell suspensions of HT-1376 cells cultured in serum-free medium supplemented with growth factors in non-adherent conditions during 7 days. Original magnification: 400x. (**B**) Representative fluorescence images of the cancer stem cell marker CD44 (red) in CSCs HT-1376, with DAPI staining the nucleus (blue). Scale bars are indicated on images. Original magnification: 400x. (**C**) Western blotting analysis of ABCG2 in HT-1376, UM-UC-3, and CSCs HT-1376. β-actin was blotted as loading control. The bellow panel shows the quantitative analysis of the ABCG2 protein (normalized to β-actin). Values are presented as mean ± S. D. of three independent experiments. The symbol * represents significant differences in ABCG2 comparing with HT-1376 or UM-UC-3 cells ($p<0.05$).

It has been described that cells expressing ABCG2 in high levels are resistant after 5-aminolevulinic acid-PDT, which demonstrates the role of ABCG2 in the efflux of the PS from those cells [35]. Next, we examined the phototoxicity after **PorGal$_8$**-PDT in isolated CSCs HT-1376 expressing ABCG2 in high levels (**Figure 2.17**). The CSCs HT-1376 were treated in darkness with several concentrations of **PorGal$_8$** (5, 10, and 12.5 μM) for 1.5 h and then irradiated for 40 min. After 24 h, cell viability assays demonstrated that CSCs HT-1376 are lesser photosensible when compared to HT-1376 cells. These results strengthen the hypothesis that the presence of high levels of ABCG2 in CSCs (in the cell line HT-1376) decreases the phototoxicity of **PorGal$_8$** in this cell line.

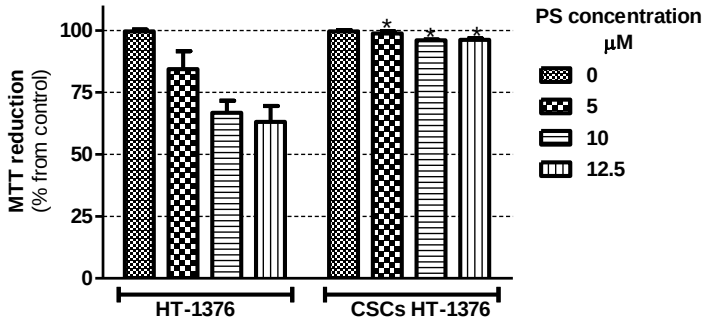

Figure 2.17. Photocytotoxic effects after **PorGal$_8$**-PDT in CSCs HT-1376 comparing with those for HT-1376 cells. Cells were incubated with **PorGal$_8$** at various concentrations (5, 10, and 12.5 µM) for 1.5 h in darkness and irradiated with white light for 40 min. Cytotoxicity was assessed 24 h after PDT using the MTT assay. The percentage of photocytotoxicity was calculated relatively to control cells (cells incubated with PBS for 1.5 h and then irradiated). Data are the mean value ± S.D. of at least one independent experiment performed in triplicates. *Significantly different from HT-1376 cells treated with **PorGal$_8$** at the same concentration ($p<0.05$).

2.8. Photo-effects of PDT with **PorGal$_8$** on actin microfilaments of HT-1376 and UM-UC-3 bladder cancer cells

The effects induced by **PorGal$_8$** after PDT, on the actin microfilaments of HT-1376 and UM-UC-3 cells were examined using a specific F-actin fluorescent probe, TRICT-phalloidin. Actin microfilaments in combination with microtubules, and intermediate filaments form the cytoskeleton systems of vertebrate cells. Cytoskeleton is a potential target in the development of new anti-cancer drugs, due to its role in cell morphology and membrane integrity. The results obtained by trypan blue exclusion assays demonstrated that the cell membrane integrity is affected after **PorGal$_8$**-PDT and it was more evident for the cell line UM-UC-3 (**Figure 2.12**). The involvement of caspases (in cell death by apoptosis) and ROS on the degradation of some cytoskeletal proteins has been reported [36]. The changes in cytoskeletal proteins provide information about the molecular mechanisms of apoptosis induced after PDT [37]. In fact, it has been reported that PDT with targeted PSs induces actin degradation (by caspases) at early stages of apoptosis [37]; while in PDT with non-targeted PSs, actin is cleaved during the later execution phase of apoptosis [38].

The HT-1376 and UM-UC-3 cells were incubated with PBS (control) or 10 µM of **PorGal$_8$** for 1.5 h in darkness and then irradiated for 40 min. In control HT-1376 cells, F-actin was found mainly in plasma membrane, exhibiting a well-organized distribution

(**Figure 2.18 A**). It was also observed a cortex-specific staining inside the HT-1376 cell colonies in the proximity of intercellular contacts. In contrast, thirty minutes after **PorGal$_8$**-PDT there was a reduction of the actin staining, which appears diffusely distributed around the nucleus of the cells (**Figure 2.18 A**). At this time point, HT-1376 cells seem to lose the contact to each other. Twenty-four hours after PDT, it was observed a reorganization of the actin filaments in HT-1376 cells with distribution similar to that observed in control cells (**Figure 2.18 A**).

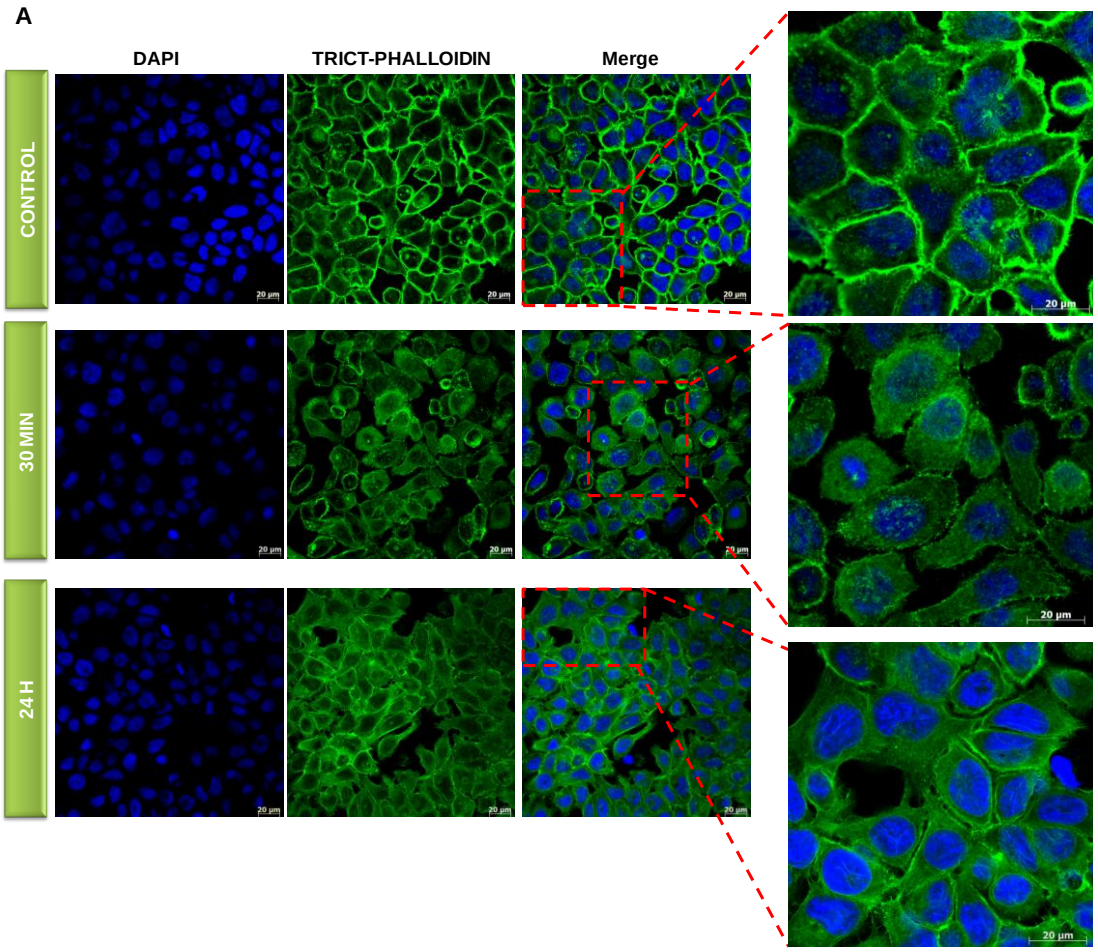

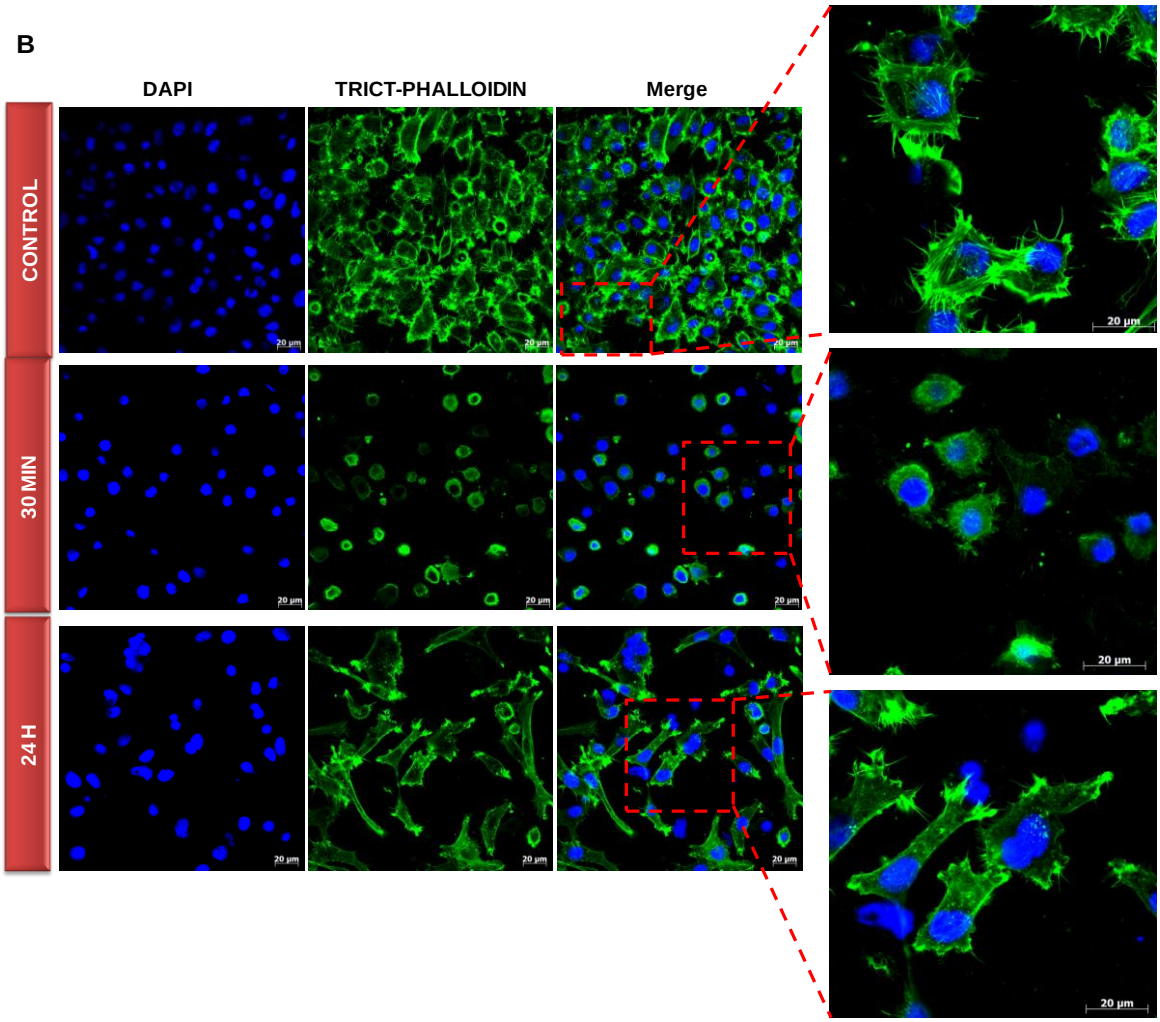

Figure 2.18. Representative fluorescence images demonstrating the changes of F-actin after **PorGal$_8$**-PDT in HT-1376 (**A**) and UM-UC-3 (**B**) cells. The cells were incubated for 1.5 h with PBS (control cells) or 10 µM of **PorGal$_8$** in darkness and then irradiated for 40 min. After treatment, the nucleus was stained with DAPI (blue) and F-actin was stained with TRICT-Phalloidin. Scale bars are indicated on images. Original magnification: 400x.

The UM-UC-3 cells do not form dense colonies as HT-1376 cells and establish intercellular contacts by cytoplasmic protrusions (**Figure 2.18 B**). In untreated UM-UC-3 cells, intracellular actin is manifested as organized stress fibres and cortex filaments localized at cell periphery (**Figure 2.18 B**). Thirty minutes after **PorGal$_8$**-PDT, the UM-UC-3 cells are retracted, the stress fibers are lost, the actin collapses and it is reorganized into a peripheral ring-like structure (**Figure 2.18 B**). Twenty-four hours after PDT, the pattern distribution of F-actin increases in the sites of cell protrusions, which indicates a reduction of cell-cell interaction. At this time point, UM-UC-3 cells are trying to establish

contact with their neighbor cells by long protrusions. The UM-UC-3 cells also contained filopodia and small actin spots (**Figure 2.18 B**).

These results demonstrated that the changes induced in actin organization after **PorGal$_8$**-PDT depend on the cell types. In HT-1376 cells, which are less photosensible after **PorGal$_8$**-PDT, the actin photodamage was transient for those cells. The actin distribution and morphology was restored 24 h after photosensitization in these cells. Thus, we hypothesize that cytoskeletal structures like F-actin can be involved in the mechanism of resistance to PDT in HT-1376 cells. In UM-UC-3 cell line, cells are completely retracted 30 min after treatment. Twenty four hours after **PorGal$_8$**-PDT the UM-UC-3 cells demonstrated an elongated shape, alteration of the actin pattern and lost stress fibers. Taking into account that ROS generated after **PorGal$_8$**-PDT can be involved on the degradation of actin microfilaments [36], the higher alteration in actin of UM-UC-3 cells can be explained by the higher accumulation of ROS inside these cells (as previously demonstrated, **Figure 2.14**).

2.9. Timing the cell death pathways in HT-1376 bladder cancer cells after PDT with **PorGal$_8$**

The evidence that the cell death mechanisms induced after PDT are dependent on the PS employed is a relevant clue in the design of new PSs. There has been a growing interest in exploiting the mechanisms of cell death at different time points after PDT, in an attempt to improve the phototoxic effects at the molecular level. In this context, we explored the temporal activation of different cell death pathways induced after **PorGal$_8$**-PDT in HT-1376 cells.

It has been reported that the proteins of the Bcl-2 family play an important role in the intrinsic pathway of apoptosis-mediated PDT where mitochondria has a central role. In Bcl-2 family, Bcl-2 and Bax are anti-apoptotic and pro-apoptotic proteins, respectively [40]. The overexpression of the anti-apoptotic protein Bcl-2 has been associated with resistance in cancer therapy by chemotherapy and radiotherapy [41]. However its role in PDT is unclear. In some studies it is demonstrated that the overexpression of Bcl-2 protects cells from photodynamic treatment [42], while in other studies the increased levels of Bcl-2 make cancer cells more sensitive to apoptosis-mediated PDT [43]. The role of the pro-apoptotic protein Bax in apoptosis-mediated PDT is being well described. In cells

suppressing or not expressing Bax that are treated with PDT, there was a complete inhibition of the release of cytochrome c from mitochondria, of the caspase activation and of the nuclear fragmentation [44].

It has been reported that PDT can target and induce changes of Bcl-2 and related anti-apoptotic proteins and activate the pro-apoptotic members of the family [45] in various cell lines and tumours. The apoptotic cell death induced by the conventional 5-aminolevulinic acid demonstrated a suppression of Bcl-2 mRNA levels and an elevation of Bax mRNA in cervical cancer cell line [46] and esophageal cancer cells [47]. *In vivo* studies also demonstrated that after 5-aminolevulinic acid-PDT there are a significant decrease in mRNA expression of Bcl-2 and an increase on the levels of Bax, in cervical cancer [48]. PDT studies with hypericin involving upregulation of Bax in human breast adenocarcinoma cell line [49] have shown that Bcl-2 levels in colorectal cancer cells were not affected [50]. Furthermore it is being plausible that ROS generated after photoactivation of the PS can trigger by itself activation of the pro-apoptotic protein Bax [43].

The HT-1376 cells were treated with PBS (control) or 10 μM of **PorGal$_8$** for 1.5 h in darkness and then irradiated for 40 min. The Bcl-2 protein levels and Bax fluorescence were then evaluated by western blotting and immunofluorescence, respectively. Western blotting results indicated that Bcl-2 did not respond significantly at several time points (0.25, 0.5, 1, 2 and 24 h) after **PorGal$_8$**-PDT (**Figure 2.19 A**). The immunofluorescence results at 30 min and 24 h after **PorGal$_8$**-PDT demonstrated an increase of the levels of Bax, when compared with control cells (**Figure 2.19 B**).

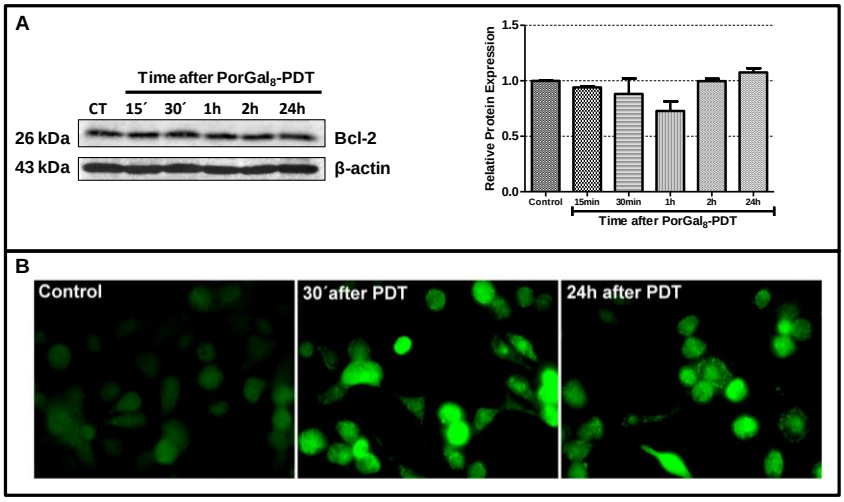

Figure 2.19. (**A**) Western blotting analysis of Bcl-2, at several time points (0.25, 0.5, 1, 2, and 24 h) after HT-1376 cells had been incubated with 10 μM of **PorGal$_8$** for 1.5 h and irradiated during 40 min. Control (CT) corresponds to irradiated cells (incubated with PBS for 1.5 h). β-actin was blotted as loading control. The graphic shows the quantitative analysis of the Bcl-2 protein (normalized to β-actin). Values are presented as mean ± S. D. of three independent experiments. (**B**) Representative fluorescence images of Bax immunofluorescence (green) in HT-1376 cells, at 0.5 h and 24 h after **PorGal$_8$**-PDT. Scale bars are indicated on images. Original magnification: 400x.

PDT is known to activate the PI3K/Akt signaling pathway in several cell lines [51, 52]. Akt/PKB is a serine/threonine kinase that plays an important role in cell survival and is activated downstream of the phosphatidylinositol-3-kinase (PI3-K) upon stimulation of numerous receptors for growth factors [53]. The phosphorylation of Akt (pAkt) in two conserved residues, Thr-308 and Ser-473 [54] activates this molecule and can provide survival cell signals those protect them from apoptotic stimuli. Numerous studies have shown that oxidative stress stimulates Akt phosphorylation and that proteins activated by phosphorylated Akt promote cell survival [55, 56]. Exposure of fibroblasts to $^1O_2$ (generated by rose bengal-mediated photosensitization) induced a strong phosphorylation of Akt [56]. Surprisingly it was reported that PS alone (Photofrin) and light alone, as well as the PDT procedure can activate the Akt signaling pathway in mouse and human breast cancer cells, as well as in mouse and human-derived breast cancer tumours growing in mice [56].

The HT-1376 cells were treated with PBS (control) or 10 μM of **PorGal$_8$** for 1.5 h and then irradiated for 40 min. The western blotting studies demonstrated immunoreactivity for pAkt in untreated cells and a significant decrease in pAkt protein levels at 15 min, 30 min and 24 h after PDT when compared to control cells (**Figure 2.20**).

Knowing that pAkt can significantly down-regulate the expression of Bax [57], the increase in immunofluorescence of Bax at 30 min and 24 h after **PorGal$_8$**-PDT (**Figure 2.19**) can be, in part, caused by dephosphorylation of Akt at these time points. In the present study, one and two hours after **PorGal$_8$**-PDT induced a significant increase in pAkt protein levels when compared to 30 min after **PorGal$_8$**-PDT (**Figure 2.20**). This seems to indicate that the increased pAkt levels can promote cell survival and block apoptosis at these time points. The total Akt band showed a similar signal density in control and treated cells. Thus, PDT with **PorGal$_8$** changed the level of phosphorylation but not the amount of Akt protein.

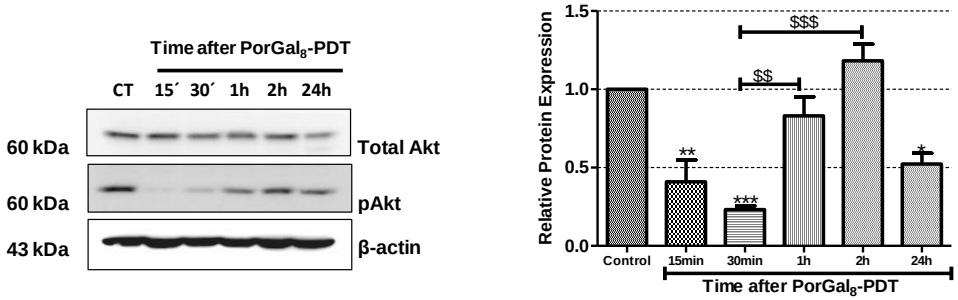

Figure 2.20. Western blotting analysis of total Akt and phosphorylated Akt (pAkt), at several time points (0.25, 0.5, 1, 2, and 24 h) after HT-1376 cells had been incubated with 10 μM of **PorGal$_8$** for 1.5 h and irradiated during 40 min. Control (CT) corresponds to irradiated cells (incubated with PBS for 1.5 h). β-actin was blotted as loading control. The graphic shows the quantitative analysis of the pAkt protein (normalized to β-actin). Values are presented as mean ± S. D. of three independent experiments. The symbols *($p<0.05$), ** and $^{\$\$}$ ($p<0.001$), *** and $^{\$\$\$}$ ($p<0.0001$) represent significant differences in pAkt protein levels comparing with control cells or treated cells at 30 min after **PorGal$_8$**-PDT, respectively.

It has been suggested that PDT can induce oxidative damage to the endoplasmic reticulum (ER), which can be further propagated to the mitochondrial cell death machinery [45, 53]. There are studies indicating that alterations in the Ca^{2+} homeostasis into the ER and alterations in the principal functions of the ER (folding, modifying and sorting newly synthetized proteins) induces ER stress and activation of the unfolded protein response (UPR) [58]. Initially, the UPR is a pro-survival process that reduces the accumulation and aggregation of unfolded or misfolded proteins and restores the ER function. However, if ER stress persists and cannot be repaired, the UPR can activate a cell death pathway, which generally converges into the caspase-activation cascade. The UPR process can lead to the translation of genes encoding for activating the transcription factor 4 (ATF4) [58]. ATF4 promotes cell survival through the induction of genes involved in restoring ER

homeostasis, but it can also induces apoptosis through the induction of the transcription factor C/EBP homologous protein (CHOP). Thus, in cases of ER stress, the CHOP induction is an important element of the switch from pro-survival to pro-death signaling in cases of ER stress [59]. Moreover, PDT-mediated apoptosis with a mitochondrial and ER-localizing porphyrin was reduced in CHOP-deficient cells, thereby confirming CHOP contribution to the induction of apoptosis in photosensitized cells [60].

In irradiated HT-1376 cells that had been previously incubated with 10 μM of **PorGal$_8$** for 1.5 h it was observed an increase in the protein levels of CHOP at 0.5, 1, 2, and 24 h after treatment (**Figure 2.21**). These results demonstrated an ER stress at these time points which can induce cell death by apoptosis.

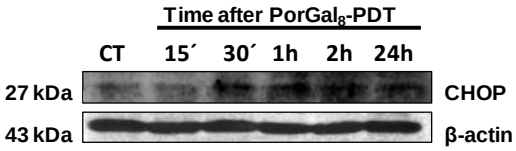

Figure 2.21. Western blotting analysis of CHOP protein, at several time points (0.25, 0.5, 1, 2, and 24 h) after HT-1376 cells had been incubated with 10 μM of **PorGal$_8$** for 1.5 h and irradiated during 40 min. Control (CT) corresponds to irradiated cells (incubated with PBS for 1.5 h). β-actin was blotted as loading control.

Apoptosis is also controlled at the ER by the pro-apoptotic protein Bax, since it has been reported that overexpression of Bax promotes Ca^{2+} mobilization from the ER to the mitochondrion during apoptosis [61]. Thus, the increase in immunofluorescence of Bax at 30 min and 24 h after PDT can be associated with the ability of ROS-induced after **PorGal$_8$**-PDT to induce ER stress. Moreover, Akt activity is important in ER stress-induced apoptosis and ER stress may induce mitochondrial-mediated apoptosis. In fact, it was reported that inactivation of PI3K-Akt induces CHOP expression in ER-stressed cells [62]. It was also reported that CHOP induces apoptosis by increasing Tribble 3 (TRB3) expression, a pseudokinase that inhibits AKT [63].

Galacto-conjugated phthalocyanine $PcGal_{16}$:
Decrease of galectin-1 protein levels and phototoxicity in bladder cancer cells
Part III

3. Galacto-conjugated phthalocyanine **$PcGal_{16}$**: decrease of galectin-1 protein levels and phototoxicity in bladder cancer cells

3.1. General overview

Phthalocyanines are PSs with remarkable photo-chemical and -physical properties [4, 8, 9]. The most important characteristics of these compounds are their ability to produce high levels of $^1O_2$ and their markedly greater absorbance of red light near of 700 nm, where the tissues are more transparent to visible radiation. As demonstrated in part I, **$PcGal_{16}$** is water soluble up to 9 µM, stable after light irradiation, efficient generator of $^1O_2$ and binds to HSA protein [9]. In this section it will be described the use of **$PcGal_{16}$** as a potential PS in PDT, looking at: uptake by cancer cells, decrease of galectin-1 after uptake, phototoxicity and ROS production after PDT in human bladder cancer cell lines HT-1376 and UM-UC-3 (**Figure 2.22**).

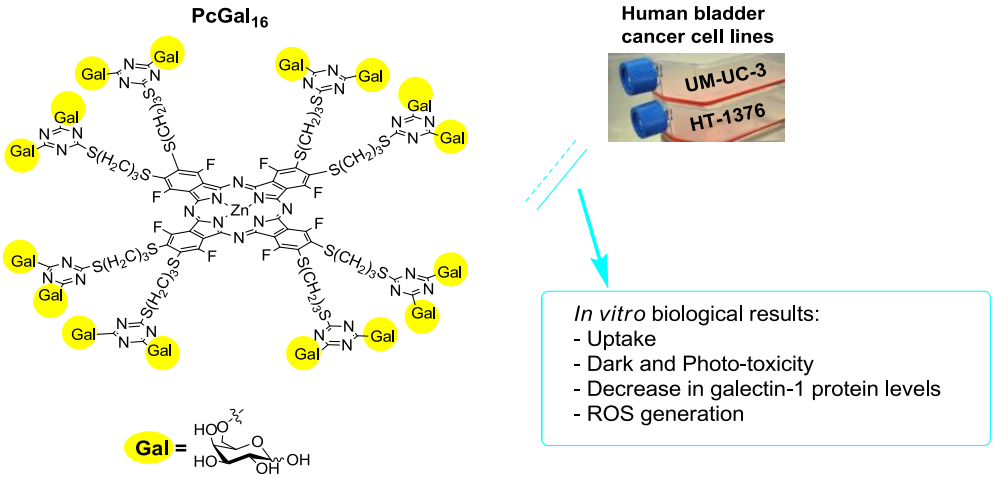

Figure 2.22. Schematic overview of this section including the *in vitro* results obtained with **$PcGal_{16}$** against the human bladder cancer cell lines UM-UC-3 and HT-1376.

3.2. Uptake of **$PcGal_{16}$** by HT-1376 and UM-UC-3 bladder cancer cells

The uptake of **$PcGal_{16}$** by cancer cells is a crucial factor for its application as a PDT agent. Bladder cancer cell lines, HT-1376 and UM-UC-3 (**Figure 2.7 A and B**), were incubated in dark conditions at various periods of time (0.5, 1, 2, and 4 h) with increasing concentrations of **$PcGal_{16}$** (0.5, 2.5, 5, and 9 µM) in PBS. The fluorescent properties of **$PcGal_{16}$** (part I, **Table 2.1**) - two emission bands in the red spectral region (734 nm and 805 nm) - allow the quantification of its intracellular concentration. The uptake of **$PcGal_{16}$**

was concentration-dependent and time-dependent, and reached a plateau after 2 h of incubation (**Figure 2.23)**. In spite of the higher levels of galectin-1 in UM-UC-3 cells when compared with HT-1376 cells (part II, **Figure 2.7 C and D**), the uptake of **$PcGal_{16}$** was similar in both cell lines. This result seems to indicate that there is not a specific recognition or an involvement of the **$PcGal_{16}$** by galectin-1 present in cell membranes.

The amphiphilic structure of **$PcGal_{16}$** allowing its localization in the hydrophobic-hydrophilic interfaces of membranes can be an explanation for the uptake of these PS by bladder cancer cells. It has been reported that a suitable combination of hydrophilic and hydrophobic substituents or structural elements improves the tumour uptake of the resulting conjugates [8].

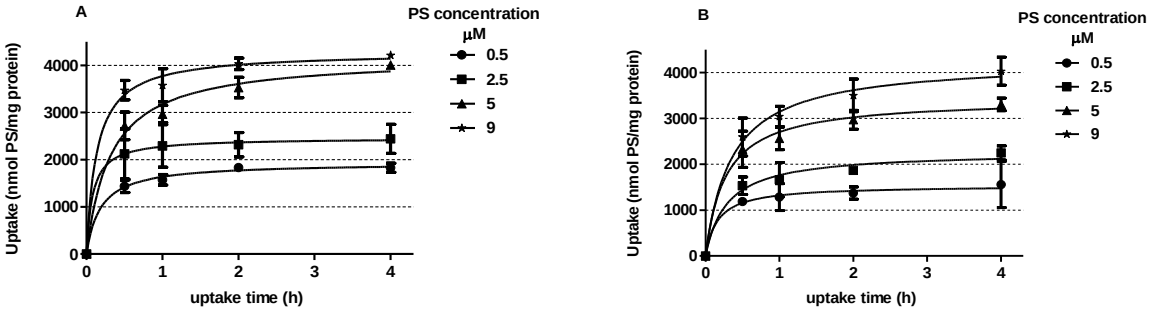

Figure 2.23. Intracellular uptake of **$PcGal_{16}$** by HT-1376 (**A**) and UM-UC-3 (**B**) cells. Cells were incubated in darkness with various concentrations of **$PcGal_{16}$** (0.5, 2.5, 5, and 9 µM) for different uptake times (0, 1, 2, 3, and 4 h). The concentration of **$PcGal_{16}$** was determined by fluorescence spectroscopy and the results were normalized to protein quantity. Data are the mean ± S.D. of at least three independent experiments performed in triplicates.

The intracellular accumulation of **$PcGal_{16}$** in bladder cancer cells was also confirmed by confocal fluorescence microscopy (**Figure 2.24**). The cells were incubated with 5 µM of **$PcGal_{16}$** for 2 h (in darkness) and nuclei were stained with DAPI. The fluorescence signal of **$PcGal_{16}$** was observed inside the cells throughout the cytoplasm.

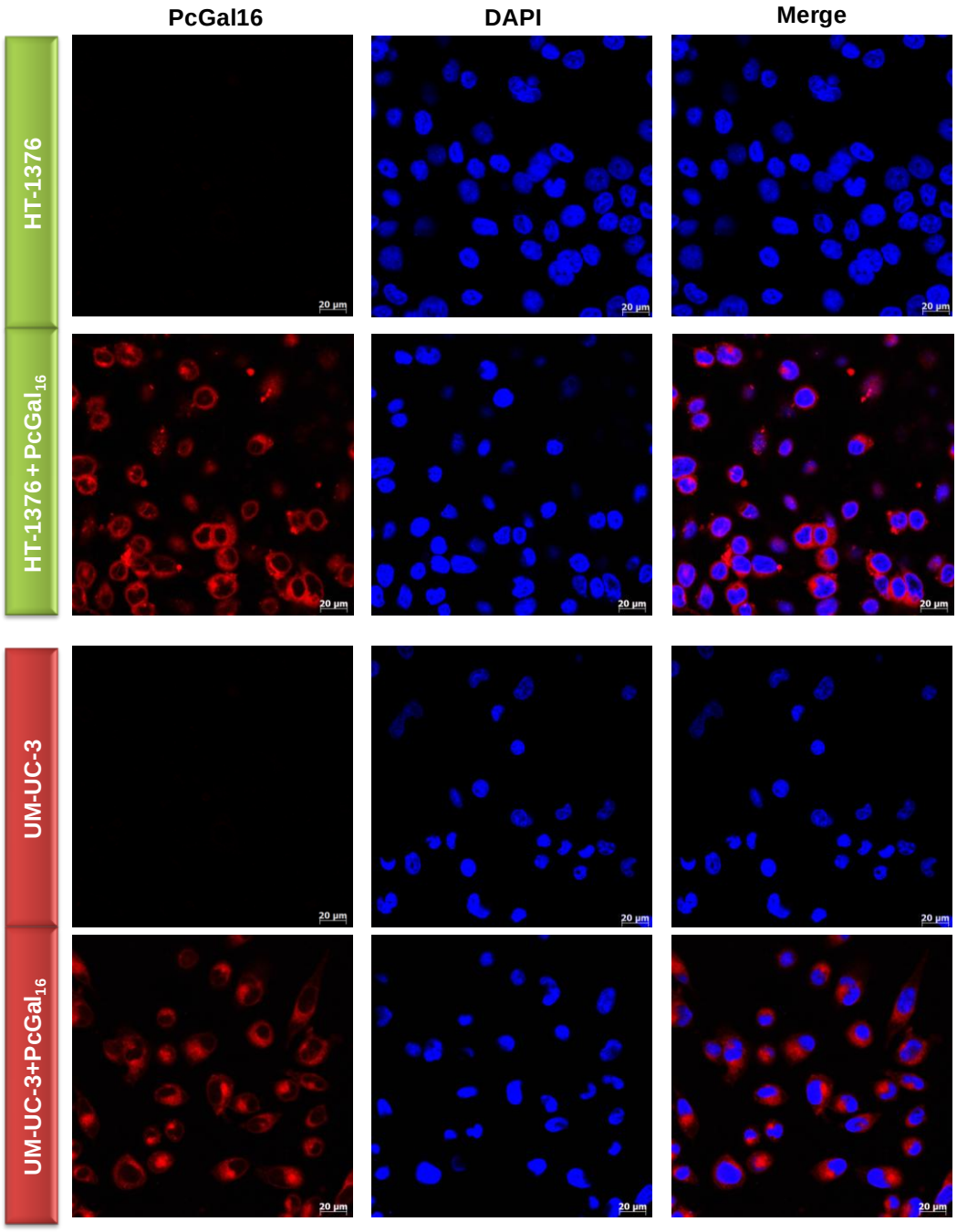

Figure 2.24. Representative fluorescence images of HT-1376 and UM-UC-3 cells incubated in darkness for 2 h with 5 µM of **$PcGal_{16}$** (red) with nucleus stained with DAPI (blue). Control fluorescence images were acquired after cells´ incubation with PBS for 2 h and staining the nucleus with DAPI (blue). Scale bars are indicated on images. Original magnification: 400x.

3.3. Galectin-1 protein levels in HT-1376 and UM-UC-3 bladder cancer cells after **$PcGal_{16}$** uptake

Immunofluorescence staining of galectin-1 was carried out on HT-1376 and UM-UC-3 cells before and after **$PcGal_{16}$** uptake (**Figure 2.25**). These studies enabled us to determine the subcellular localization of galectin-1 (that is present in higher levels in UM-UC-3 cells than in HT-1376 cells, part II **Figure 2.7 C and D**) and **$PcGal_{16}$** in bladder cancer cells, and their possible co-localization. HT-1376 and UM-UC-3 cells were incubated with 5 μM of **$PcGal_{16}$** for 2 h (in dark conditions) and immunostained with a specific antibody against galectin-1. In UM-UC-3 cells, galectin-1 is abundant in the nucleus (with some bright spots) and in HT-1376 cells it is diffusely distributed through the cytoplasm with some nuclear localization (**Figure 2.25**). The incubation of cancer cells with **$PcGal_{16}$** induces a decrease in galectin-1 immunofluorescence signal (**Figure 2.25**). For the HT-1376 cell line, it was observed co-localization of **$PcGal_{16}$** with galectin-1 in vesicular structures, mainly concentrated perinuclearly. In UM-UC-3 cells, there is also some co-localization of **$PcGal_{16}$** with galectin-1, which seems to accumulate more diffusely in vesicles located in the cytoplasm.

Although significant progress has been made in research related with the role of galectins in cancer, the information concerning the molecular mechanisms and exogenous stimuli that regulate the expression of these proteins in tumour cells is scarce. There are some reports indicating that galectin-1 expression in tumour cells can be modulated by chemotherapeutic and antimetastatic agents [64, 65]. Knowing that galectin-1 contributes to tumour progression and resistance after conventional cancer therapy [66], the ability of **$PcGal_{16}$** to reduce the levels of galectin-1 after its uptake prompted us to envisage **$PcGal_{16}$** as a potential candidate for cancer treatment.

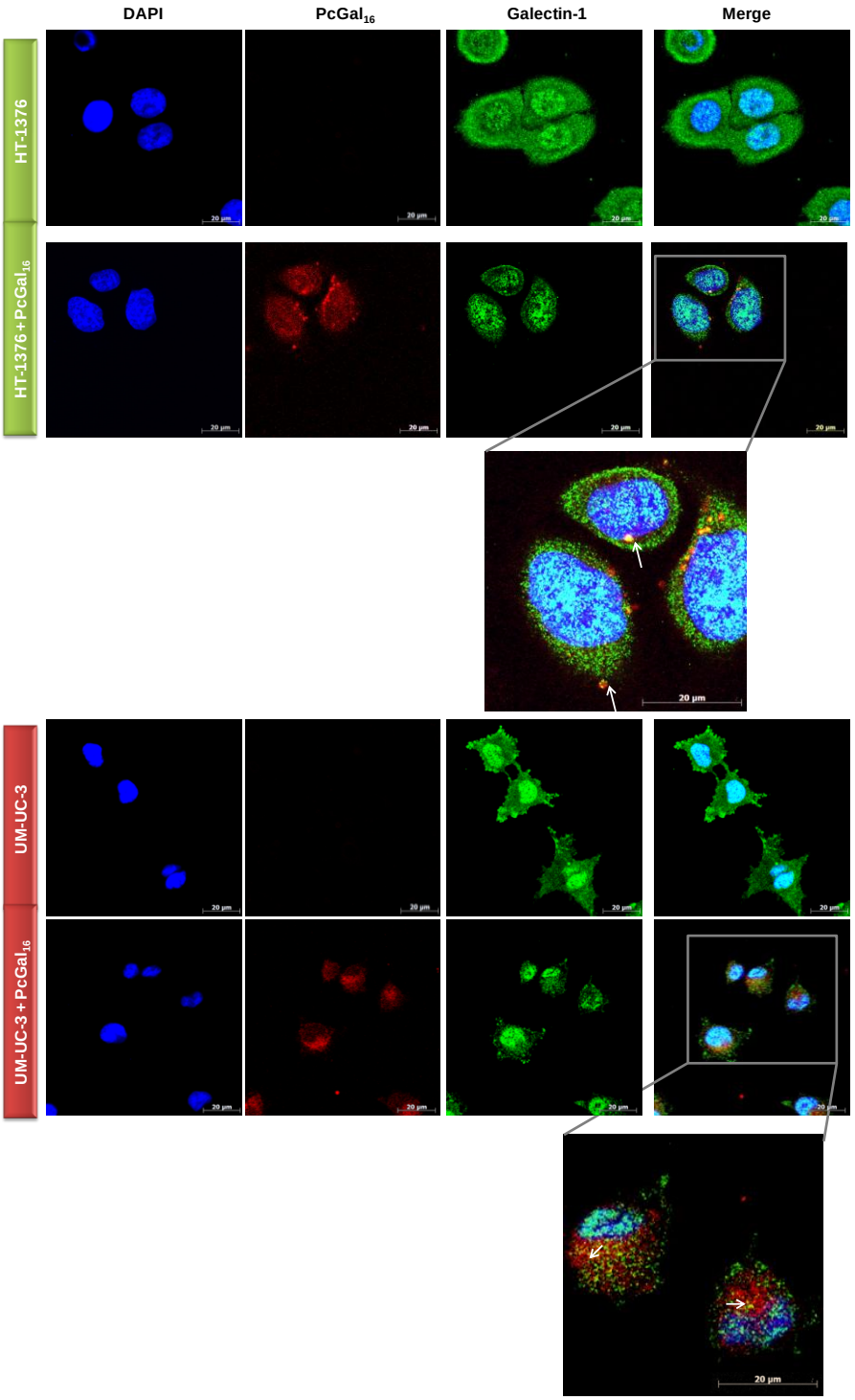

Figure 2.25. Representative fluorescence images of galectin-1 protein (green) in HT-1376 and UM-UC-3 cells before and after cells´ incubation with 5 µM of **$PcGal_{16}$** (red) for 2 h in darkness, with DAPI staining the nucleus (blue). Arrows indicate co-localization of **$PcGal_{16}$** with galectin-1. Scale bars are indicated on images. Original magnification: 400x.

3.4. Dark toxicity and phototoxicity of **$PcGal_{16}$** in HT-1376 and UM-UC-3 bladder cancer cells

After confirmation of **$PcGal_{16}$** uptake by bladder cancer cells, the cytotoxic effect of **$PcGal_{16}$** in darkness was accessed. It is of utmost importance to ensure that **$PcGal_{16}$** induces toxicity only after light activation. The dark cytotoxicity of **$PcGal_{16}$** at various periods of incubation time (0, 0.5, 1, 2, and 4 h) with increasing concentrations of **$PcGal_{16}$** (0.5, 2.5, 5, and 9 μM) on HT-1376 and UM-UC-3 cells was estimated 24 h after treatment, using the MTT assay (**Figure 2.26**). No dark toxicity was observed in untreated cells (up to 4 h) in the presence of 0.45% or less DMSO (data not shown). Moreover, **$PcGal_{16}$** showed no significant cytotoxicity at concentrations up to 9 μM, since the MTT reduction did not decrease significantly below the levels measured at the concentration zero.

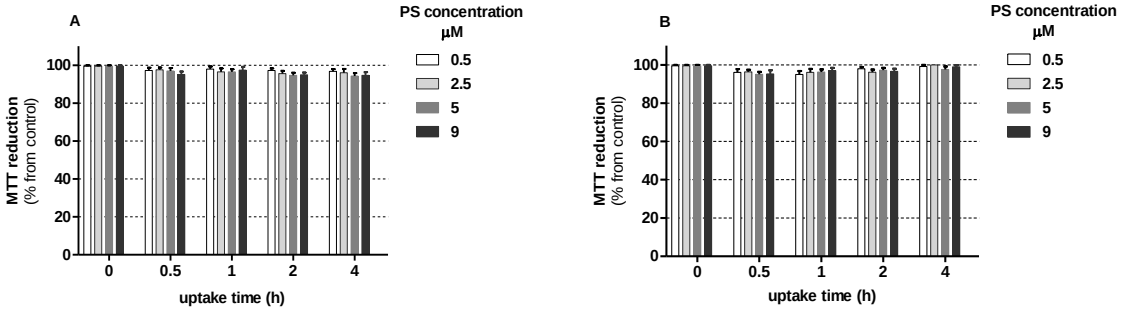

Figure 2.26. Non-dark toxicity of **$PcGal_{16}$** in HT-1376 (**A**) and UM-UC-3 (**B**) cells. Cells were incubated in darkness with **$PcGal_{16}$** at various concentrations (0.5, 2.5, 5, and 9 μM in PBS) for increasing uptake times (0, 0.5, 1, 2, and 4 h). Cytotoxicity was assessed 24 h after treatment using the MTT colorimetric assay. The percentage of cytotoxicity was calculated relatively to control cells (cells incubated with PBS in darkness) at the respective uptake time. Data are the mean value ± S.D. of at least three independent experiments performed in triplicates.

For the PDT assays, the cells were incubated with **$PcGal_{16}$** at various periods of time (0.5, 1, 2, and 4 h) with several concentrations in the dark (0.5, 2.5, 5, and 9 μM). After **$PcGal_{16}$** uptake in darkness, the cells were irradiated for 40 min and cell viability was evaluated 24 h after treatment by the MTT assay. To test the effect of light irradiation on cell viability, control experiments were performed in cells incubated with PBS and irradiated. These conditions did not induce toxicity in both cell lines. However, when cells

were incubated with **$PcGal_{16}$** and then irradiated, there was an increase of the phototoxicity in a concentration- and uptake time-dependent manner (**Figure 2.27**).

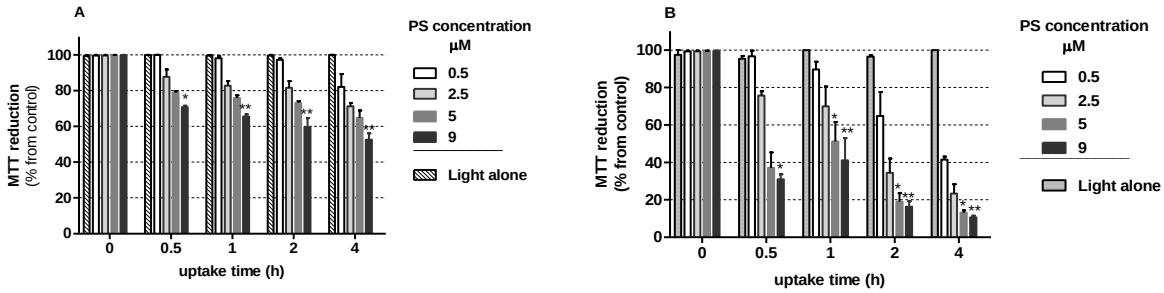

Figure 2.27. Photocytotoxic effects after **$PcGal_{16}$**-PDT in HT-1376 (**A**) and UM-UC-3 (**B**) cells. Cells were incubated in darkness with **$PcGal_{16}$** at various concentrations (0.5, 2.5, 5, and 9 µM in PBS) for 0, 0.5, 1, 2, and 4 h and irradiated with white light for 40 min. Cytotoxicity was assessed 24 h after phototreatment using the MTT assay. The percentage of photocytotoxicity was calculated relatively to control cells (cells incubated in darkness with PBS and then irradiated) at the respective uptake time. Data are the mean value ± S.D. of at least three independent experiments performed in triplicates. *($p<0.05$) and **($p<0.001$) significantly different from control cells at the same uptake time.

$PcGal_{16}$ demonstrated to be more photoactive against UM-UC-3 cells, in spite of its similar accumulation in both cell lines. Among the conditions used, 5 µM and 9 µM of **$PcGal_{16}$** and incubation times of 2 h and 4 h showed the highest phototoxicity in both cell types. For example, when 5 µM of **$PcGal_{16}$** was used for 2 h there was a percentage in toxicity of 80.97 ± 4.53 and 26.94 ± 1.08 for UM-UC-3 and HT-1376 cells, respectively. It is important to note that for the cell line UM-UC-3, low concentrations of **$PcGal_{16}$** (0.5 µM and uptake time of 4 h) were enough to achieve a percentage in toxicity of 58.54 ± 1.67.

MTT and trypan blue staining assays were performed 48 h and 72 h after **$PcGal_{16}$**-PDT, to investigate whether cells could recover for a time superior to 24 h after PDT. In both cell lines, the results obtained with the MTT colorimetric assay (cell metabolic activity) correlated well with the loss of cell membrane integrity (trypan blue staining) (**Figure 2.28**). UM-UC-3 cells were unable to recover from the photo-effects 48 h or 72 h after **$PcGal_{16}$**-PDT, for concentrations of 5 µM and 9 µM (**Figure 2.28 B**) as evaluated by MTT and trypan blue assays. For concentrations of 0.5 µM and 2.5 µM, UM-UC-3 cells were able to recover in part their metabolic activity 48 h and 72 h after PDT (**Figure 2.28 B**) as evaluated by the MTT assay. Regarding the trypan blue staining, cell membrane integrity is strongly affected 48 h and 72 h after PDT in both cell lines (**Figure 2.28 C and D**). The metabolic activity of HT-1376 cells was more affected 72 h after PDT than 24 h or 48 h (**Figure 2.28 A**). As previously described for **$PorGal_8$**, one plausible explanation for

the observed resistance of HT-1376 cells is the presence of CSCs in this cell line (part II, **Figure 2.16**). The possible ability of HT-1376 cells to produce an antioxidant adaptative response, activating antioxidant enzymes (like superoxide dismutase, catalase and glutathione peroxidase) and prosurvival mechanisms, can also explain the resistance observed 24 h after **$PcGal_{16}$-PDT**.

The concentrations of **$PcGal_{16}$** necessary to inhibit the proliferation of HT-1376 and UM-UC-3 cells in 50% can be estimated from **Figure 2.28**. These values, hereafter referred to as ''photocytotoxic concentrations'' (IC_{50}) are reported in **Table 2.4**, which also includes another photocytotoxic index, the ''intracellular phototoxic concentration'' (IPC_{50}) representing the intracellular concentration that produces a 50% decrease in cell viability.

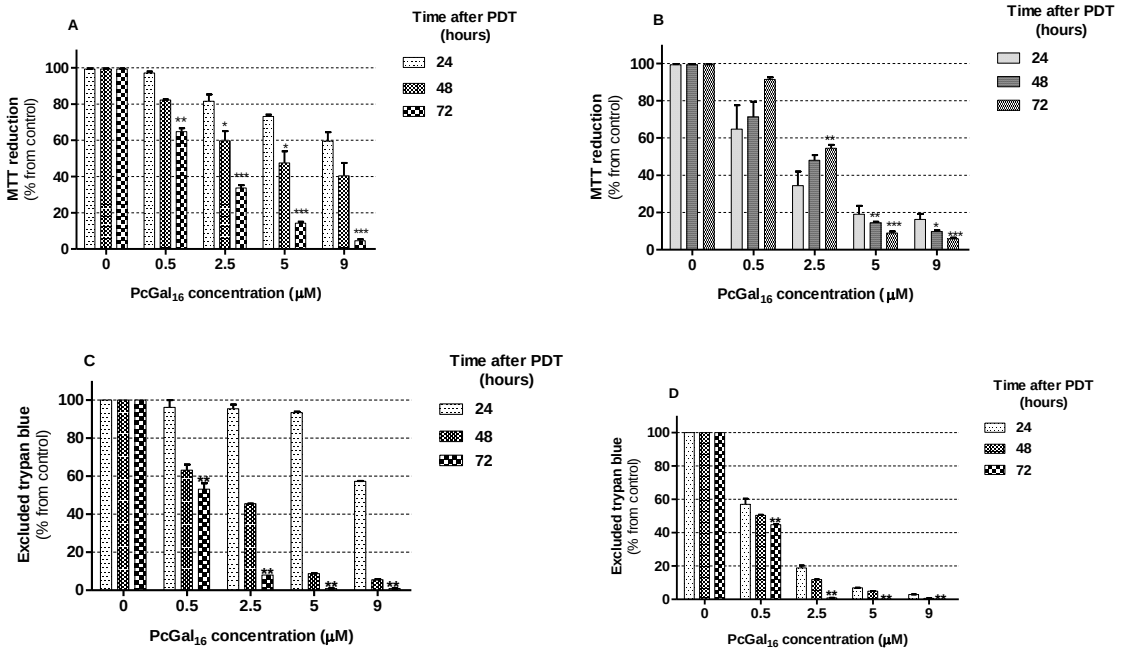

Figure 2.28. Cytotoxic effects of **$PcGal_{16}$** at various concentrations in HT-1376 (**A** and **C**) and UM-UC-3 (**B** and **D**) cells as function of the uptake time. Cytotoxicity was assessed 24, 48, and 72 h after **$PcGal_{16}$**-PDT using the MTT (**A** and **B**) and trypan blue staining (**C** and **D**) assays. The percentage of cytotoxicity was calculated relatively to control cells (cells incubated with PBS in darkness and then irradiated) at the respective uptake time. Data are the mean value ± S.D. of at least three independent experiments performed in triplicates. The symbol **($p<0.001$) represents significant differences in phototoxicity comparing with MTT reduction (%) or excluded trypan blue (%) of **$PcGal_{16}$**-24 h after PDT for the respective concentration.

Table 2.4. Values for photocytotoxic concentration (IC_{50}, μM) and intracellular phototoxic content (IP_{50}, nmol PS per mg of protein) of **$PcGal_{16}$** on human bladder cancer cell lines, HT-1376 and UM-UC-3. IC_{50} values were calculated using the MTT dose response curves (24, 48, and 72 h after PDT), obtained for cells incubated with **$PcGal_{16}$** at various concentrations for 2 h.

	HT-1376 cell line			UM-UC-3 cell line		
Hours after PDT	24	48	72	24	48	72
IC_{50} (μM), $CI_{95\%}$	-	3.3 [0.6;10.7]	2.5 [2.2;2.9]	2.1, [0.9;5.0]	2.8, [2.4; 3.2]	2.6, [2.6;2.7]
IPC_{50} (nmol PS/mg protein)	-	3450.2	3225.0	2165.9	2444.1	2373.7

IC_{50} is the incubation concentration that inhibits the proliferation of cultures in 50%, after cells´ incubation with **$PcGal_{16}$** and cells´ irradiation for 40 min
IPC_{50} is the intracellular phototoxic content corresponding to the IC_{50}
$CI_{95\%}$: 95% Confidence interval

Pcs conjugated with carbohydrates are rare, thus the photodynamic potential of this type of compounds is of great interest between PDT researchers. Recently, it was reported that Pcs conjugated with galactose units are accumulated inside HeLa carcinoma cells and produce higher toxicity in HeLa cells than in non-malignant HaCaT cells [8].

3.5. Reactive oxygen species induced by **$PcGal_{16}$** in HT-1376 and UM-UC-3 bladder cancer cells after PDT

In an attempt to correlate the observed photocytotoxicity with the ability of **$PcGal_{16}$** to generate ROS, a qualitative analysis by fluorescence microscopy and a quantitative evaluation by fluorescence spectroscopy using the H_2DCFDA probe [18], were performed (for more detail, see part II).

The PDT treatment with **$PcGal_{16}$** evidenced for the two bladder cancer cell lines, a significant increase in the DCF fluorescence (**Figure 2.29**) corresponding to ROS formation. The percentage of cells with DCF fluorescence was about 1.2-fold higher for the cell line UM-UC-3 than for the cell line HT-1376, when 5 μM of H_2DCFDA was used. The presence of CSCs (part II, **Figure 2.16**) and an adaptative antioxidant response after **$PcGal_{16}$**-PDT in HT-1376 cells can explain the less sensitivity of these cells to ROS and consequently less cell death.

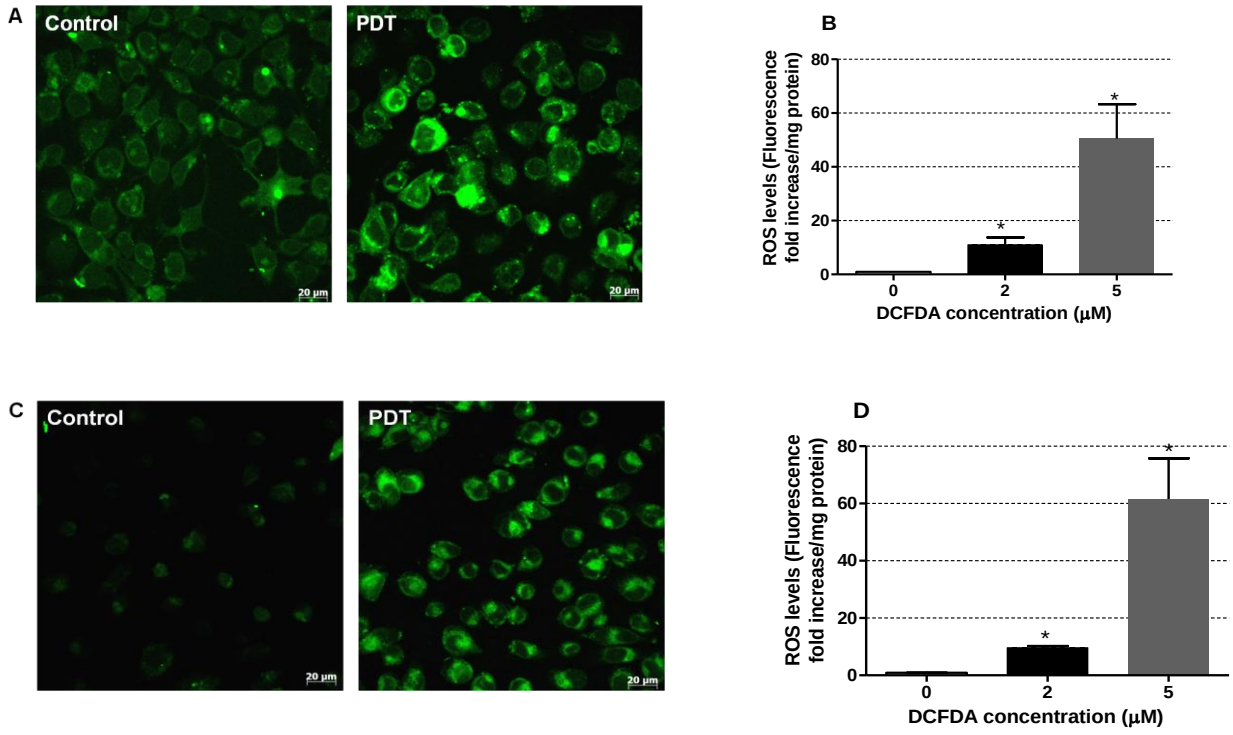

Figure 2.29. Representative fluorescence images (**A** and **C**) and quantification (**B** and **D**) of DCF fluorescence increase (as a measure of ROS production) after **PcGal$_{16}$**-PDT. Human bladder cancer cell lines, HT-1376 (**A**) and UM-UC-3 (**B**) were incubated with 5 µM of **PcGal$_{16}$** for 2 h in the dark. After PDT during 40 min, an increase in intracellular oxidative stress was detected by oxidation of the fluorescent probe H_2DCFDA. *Significantly different from irradiated-control cells ($p<0.05$).

To elucidate the role of ROS generated after **PcGal$_{16}$**-PDT in cell phototoxicity, specific quenchers of $^1O_2$ (sodium azide [21] and histidine [22]) and free radical scavengers (cysteine [23]), were added before the PDT treatment. **Figure 2.30** shows how the presence of 50 nM of NaN_3, histidine or cysteine in the solution is able to reduce the cell toxicity after **PcGal$_{16}$**-PDT. All the quenchers were non-toxic for the concentration used.

For the cell line UM-UC-3, all the quenchers were able to reduce significantly but did not totally eliminate the phototoxicity induced after **PcGal$_{16}$**-PDT. These results demonstrated that sodium azide, histidine and cysteine have a significant protection against PDT with **PcGal$_{16}$** in UM-UC-3 cells, suggesting that both $^1O_2$ and hydroxyl radical are involved in the induction of cytotoxicity after **PcGal$_{16}$**-PDT.

The free radical scavenger (cysteine) was the only one able to reduce significantly the cell toxicity in HT-1376 cells.

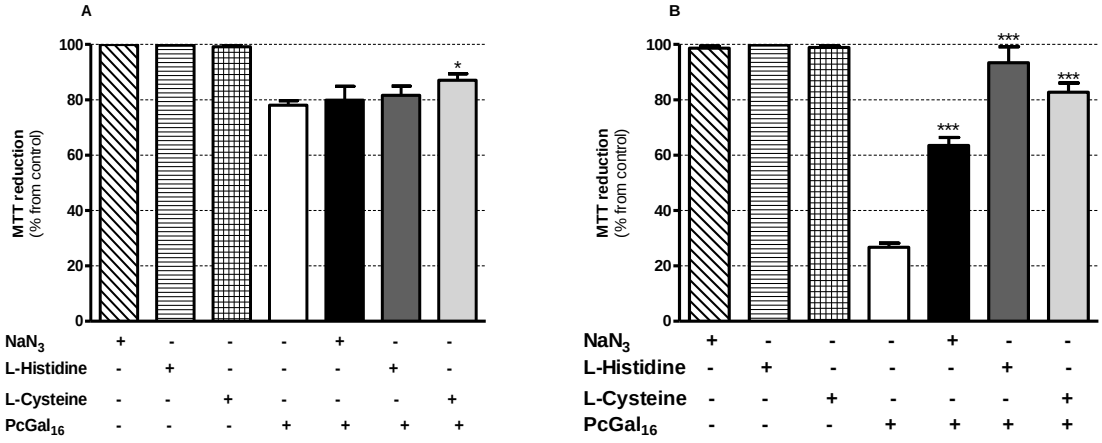

Figure 2.30. Photocytotoxicity after **$PcGal_{16}$**-PDT in the presence of specific quenchers of $^1O_2$ (sodium azide and histidine) and free radical scavengers (cysteine) in HT-1376 (**A**) and UM-UC-3 (**B**) cells. Cytotoxicity was assessed 24 h after **$PcGal_{16}$**-PDT in the presence of 50 nM of ROS quenchers, using the MTT assay. The percentage of cytotoxicity was calculated relatively to control cells (untreated cells). Data are the mean value ± S.D. of at least three independent experiments performed in triplicates. The symbol *($p<0.05$) and ***($p<0.0001$) represents significant differences in phototoxicity comparing with MTT reduction (%) after **$PcGal_{16}$**-PDT.

Por 1-albumins and Por 1-mAb anti-CD104:
Target-directed destruction of bladder cancer cells
Part IV

4. **Por 1-albumins** and **Por 1-mAb anti-CD104**: Target-directed destruction of bladder cancer cells

4.1. **Por 1-BSA** and **Por 1-HSA** bioconjugates

4.1.1. General overview

Albumins are emerging as versatile protein carriers for target-directed drugs and for improving the pharmacokinetic profile of peptide- and protein-based treatments [67]. Conjugates of porphyrins (and their derivatives) with human and bovine serum albumin (HSA and BSA, respectively) have been successfully produced and characterized [68-70]. From an experimental point of view, the PS conjugated with HSA or BSA is a model for developing bioconjugation strategies and extensive structural characterization of the conjugates. From a biological point of view, albumin can be accumulated in tumour tissues due to the EPR effect (enhanced permeability and retention of macromolecules in tumour tissues) [71]. EPR is the result of two effects: firstly, blood vessels of tumour tissues have an enhanced vascular permeability for circulating albumin and secondly, it was demonstrated that macromolecules having a molecular weight higher than 40 kDa have a reduced clearance from the tumour tissue. These properties make albumin a good candidate as a photosensitizer carrier, as well as a good model in the development of bioconjugation strategies [67].

In this section it will be described the characterization of **Por 1-BSA/HSA** bioconjugates by UV-Visible, LC-UV-MS and MALDI-TOF-MS. At the end, *in vitro* results with these conjugates against UM-UC-3 human bladder cancer cell line after PDT are reported (**Figure 2.31**).

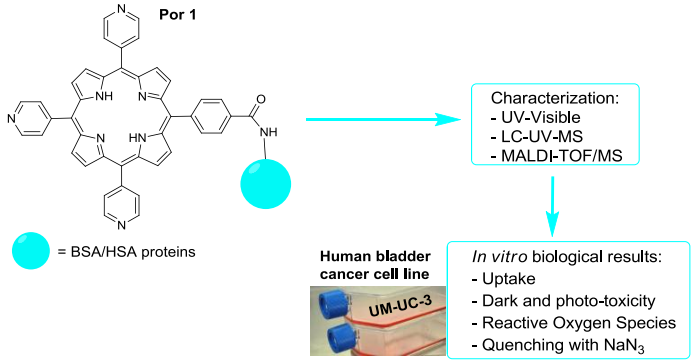

Figure 2.31. Schematic overview of this section including the characterization of **Por 1-BSA/HSA**, as well as the biological assays against UM-UC-3 bladder cancer cell line.

4.1.2. **Por 1-BSA** and **Por 1-HSA** bioconjugates characterization

4.1.2.1. UV-Visible

The synthesis of porphyrins bearing an *N*-hydroxysuccinimide (NHS) activated ester group has been well documented [72] and sets the ground for the herein reported bioconjugation strategy. With this regard, the carboxyl functionality present on **Por 1** was transformed into an NHS ester. Porphyrin was thereafter conjugated with the free amine groups of amino acids (usually lysines) of the albumins, in aqueous buffered medium with a slightly basic pH. The free amine groups of an amino acid attack the carbonyl carbon of porphyrin and initiate the ligation followed by elimination of NHS.

Conjugation of both albumins (HSA and BSA) was successfully carried out with **Por 1** and these conjugates were named as **Por 1-albumin** bioconjugates. To optimize the conjugation strategy, variable molar amounts of **Por 1** (30:1, 40:1, and 80:1 mole ratio per albumin) were used in the conjugation reaction. The degree of porphyrin labeling (DOL), after purification of the conjugates, was assessed using UV-Visible spectroscopy (**Table 2.5**).

Table 2.5. DOLs for **Por 1-albumin** bioconjugates at different initial molar ratios. DOL is the degree of labeling, i.e. moles of **Por 1** per moles of albumin after conjugates purification.

Conjugate	Initial Molar ratios	µmol after purification		DOL
		Por 1	Albumin	
Por 1-BSA	30:1	12.30	10.10	1.22
Por 1-BSA	40:1	11.50	10.40	1.11
Por 1-BSA	80:1	11.00	10.90	1.01
Por 1-HSA	30:1	10.80	5.19	2.08
Por 1-HSA	40:1	11.10	6.46	1.72
Por 1-HSA	80:1	10.80	6.39	1.69

For the conjugates obtained after reaction of **Por 1** with the albumins, it was observed that the DOL decreases with increasing initial molar ratios. These results suggest that for the ratios 40:1 and 80:1 the amount of albumin was insufficient to react with all **Por 1** made available. Also, this outcome can be a consequence of the reduced solubility of these proteins when higher concentrations of **Por 1** were employed for the higher ratios. Hence, the ratio 30:1 of **Por 1** to proteins was considered to pursuit further studies. The

DOLs obtained for **Por1-BSA** (about 1) or **Por 1-HSA** (about 2) conjugates are in agreement with the literature for a chlorin$_{e6}$-BSA [68] and a methotrexate-HSA conjugate [73].

4.1.2.2. MALDI-TOF-MS and LC-UV-MS

The conjugation of both albumins with **Por 1** was successfully achieved as documented by the MALDI-TOF-MS spectra (**Figure 2.32**), obtained for both the non-conjugated BSA or HSA (native proteins) and for the **Por 1-albumin** bioconjugates. The spectra displayed in **Figure 2.32** are characterized by three main peaks: the molecular ion m/z $[M-H]^+$ (M = BSA, HSA, **Por 1-BSA** or **Por 1-HSA**), the doubled charged molecular ion m/2z $[M-H]^{2+}$ with half the m/z of the molecular ion, and the triply charged molecular ion m/3z ($[M-H]^{3+}$) with 1/3 of the molecular ion m/z value.

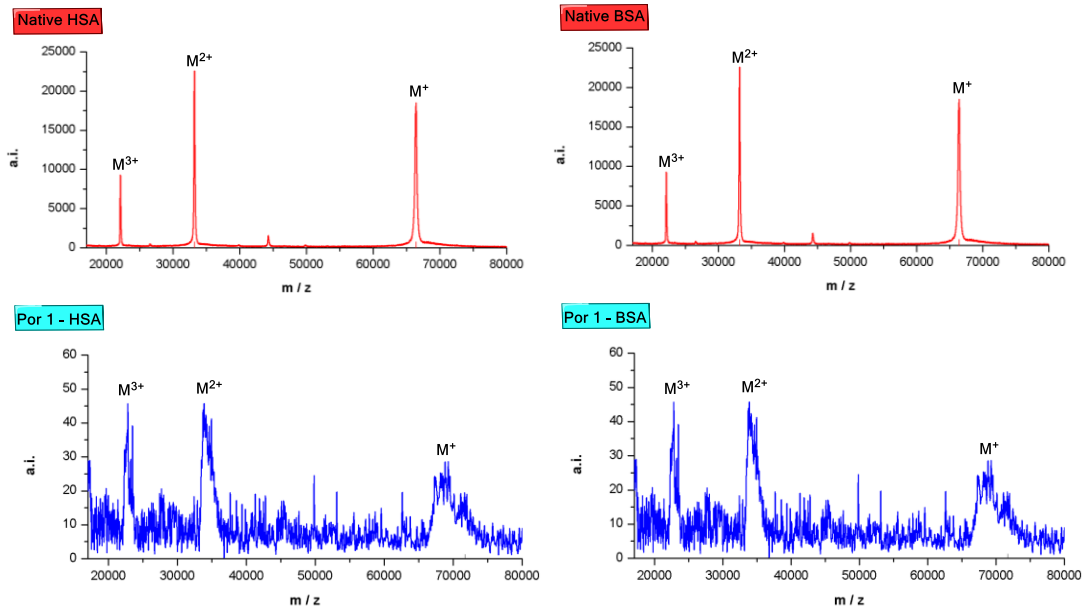

Figure 2.32. MALDI-TOF-MS spectra of native albumins (non-conjugated proteins) and of **Por 1-albumin** bioconjugates.

The characterization of **Por 1-albumin** bioconjugates was also accomplished by LC-UV-MS and some chromatograms are depicted in **Figure 2.33**, using the **Por 1-HSA** conjugate as an example. Chromatographic fractions monitored at 280 nm (wavelength of albumin´s maximum absorbance) and at 415 nm (wavelength corresponding to Soret band of **Por 1**) showed a single peak of the bioconjugate. The peak of the HSA native protein

elutes at 17.8 min whereas the bioconjugate elutes slightly later, at 21.2 min. The mass spectra of these peaks eluting at 17.8 min and 21.2 min were obtained and reconstructed using the Bayesian Protein Reconstruction add-in feature from Analyst™ software (**Figure 2.34**). In **Figure 2.33** (right-hand side) the presence of non-conjugated HSA in the sample was also detected at about 20.8 min elution time and the mass spectra of this peak was also obtained and reconstructed (**Figure 2.34**).

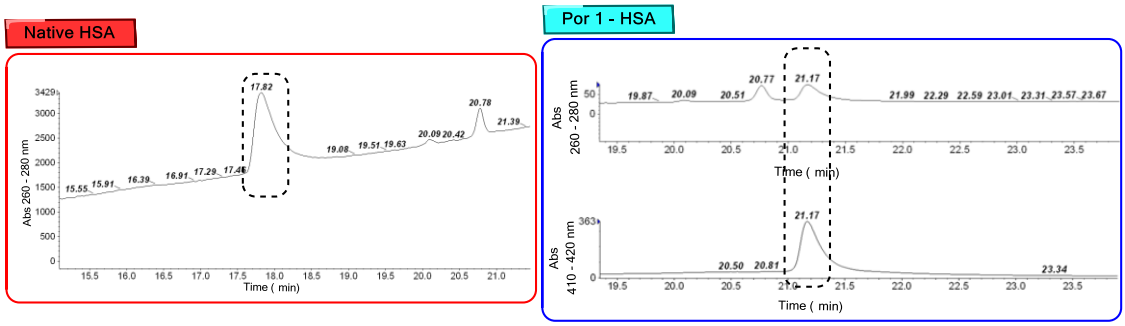

Figure 2.33. Chromatograms of non-conjugated HSA and **Por 1-HSA** conjugate. The chromatograms were obtained for the HSA absorption wavelengths range between 260 nm to 280 nm and for the **Por 1** maximum absorption range between 410 nm to 420 nm.

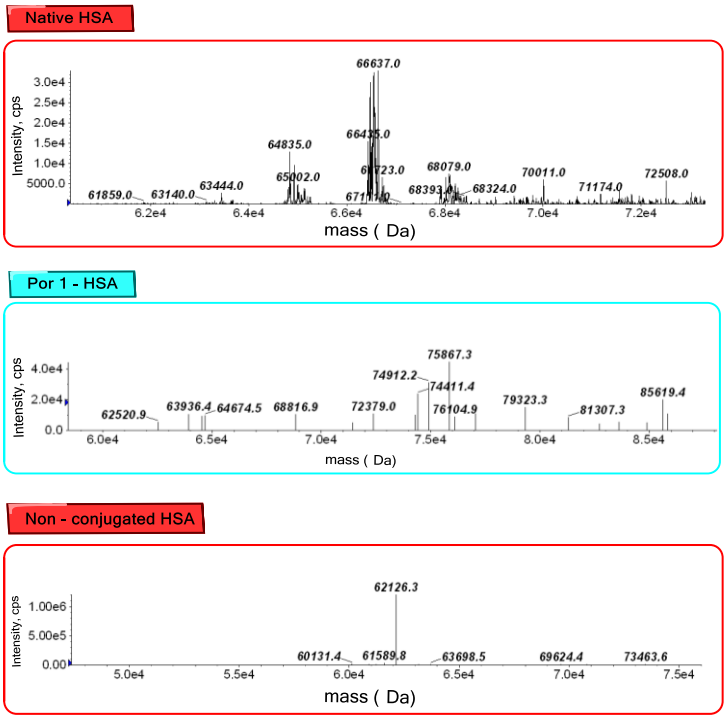

Figure 2.34. Reconstructed masses of native HSA, **Por 1-HSA** bioconjugate and non-conjugated HSA after Bayesian Protein Reconstruction.

4.1.3. Biological *in vitro* assays with **Por 1-albumin** bioconjugates against UM-UC-3 bladder cancer cells

4.1.3.1. Uptake of **Por 1-albumin** bioconjugates by UM-UC-3 bladder cancer cells

The ability of **Por 1-albumin** bioconjugates to be accumulated inside the cancer cells was evaluated using the human bladder cancer cell line UM-UC-3 (**Figure 2.7 B**). The structure of **Por 1** generates a fluorescence signal, which allows the uptake determination of **Por 1-albumin** by fluorimetry. UM-UC-3 cells were incubated in darkness with 5 µM of bioconjugates in PBS buffer for 0.5, 1, 2, and 4 h (**Figure 2.35**).

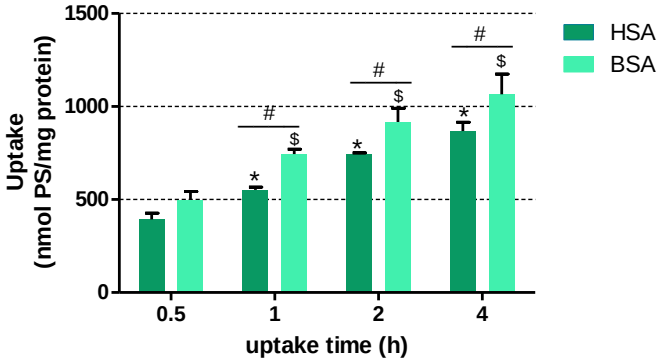

Figure 2.35. Cellular uptake of **Por 1-albumin** bioconjugates by UM-UC-3 bladder cancer cells. Conjugates containing 5 µM of **Por 1** were incubated in the dark for 0.5, 1, 2, and 4 h in PBS with UM-UC-3 cells. The results are expressed as **Por 1** concentration (nmol) per mg of intracellular protein against uptake time (h). Values are presented as mean ± S. D. of three independent experiments performed in triplicates. *Significantly different from **Por 1-HSA** at uptake time of 0.5 h ($p<0.05$). $^{\$}$Significantly different from **Por 1-BSA** at uptake time of 0.5 h ($p<0.05$). The symbol $^{\#}$ represents significant differences between **Por 1-HSA** and **Por 1-BSA** at the same uptake time ($p<0.05$).

The uptake of **Por 1-albumin** bioconjugates was significantly increased for the uptake times of 1, 2, and 4 h when compared with the uptake value of the respective conjugate at 0.5 h. The uptake kinetics was statistically different between the **Por 1-albumin** bioconjugates (when using the same uptake time) for the uptake times of 1, 2, and 4 h (**Figure 2.35**). Due to the high homology between HSA and BSA [74], it is expected that the BSA conjugate is processed likewise the HSA conjugate. The uptake of **Por 1-albumin** bioconjugates increased as a function of the incubation time. Four hours after incubation, the cellular uptake values were 868.7 ± 23.54 nmol per mg of protein, for the **Por 1-HSA** conjugate and 1066.0 ± 54.23 nmol per mg of protein for the **Por 1-BSA** one. The four hours uptake time was, therefore, selected for subsequent experiments.

It is expected that the albumin is accumulated in cells as a source of amino acids and energy under conditions of cellular stress, as observed in cancer cells [75]. It was demonstrated that albumin is accumulated through albumin-mediated endocytosis into the lysosomal compartment of cancer cells, where it is degraded [75]. It was also shown that the uptake of a methotrexate-HSA bioconjugate in cancer cells occurs by endocytosis [73], thus we also hypothesize the same for our bioconjugates. The membrane receptor responsible for the uptake of albumin inside the cancer cells, and whether the endocytosis process is dependent or not of a specific receptor is not clear [76].

4.1.3.2. Dark toxicity and phototoxicity of **Por 1-albumin** bioconjugates in UM-UC-3 bladder cancer cells

To prove whether **Por 1-albumin** bioconjugates are toxic just after light activation, their cytotoxicity in darkness was evaluated. **Por 1-albumin** bioconjugates at various concentrations (0.5, 1, 5, and 10 μM in PBS) were incubated with UM-UC-3 cells for 4 h. The control experiments were performed by incubation of the cells in the dark with PBS for 4 h. The toxicity was estimated 24 h after treatment using the MTT colorimetric assay. No cytotoxicity was observed in the control cells. Moreover, the two **Por 1-albumin** bioconjugates did not exhibit dark cytotoxicity at incubation concentrations up to 10 μM, as the MTT reduction did not decrease significantly below the control levels, i.e. when 0 μM of the conjugates is used (**Figure 2.36 A**).

For the PDT assays, the cells were irradiated using white light for 40 min after incubation of the cells with the **Por 1-albumin** bioconjugates at 0.5, 1, 5, and 10 μM for 4 h. As shown in **Figure 2.36 B**, an MTT gradual reduction was observed for both conjugates in a concentration dependent manner.

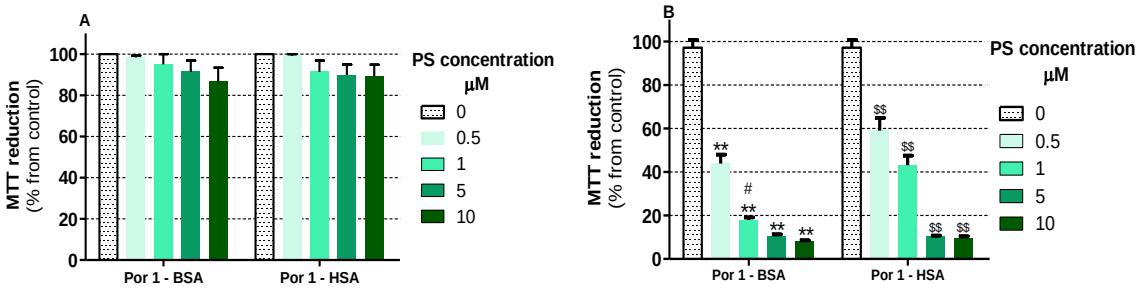

Figure 2.36. **Por 1- albumin** bioconjugates' toxicity, after UM-UC-3 cells had been incubated in the dark with different concentrations of the conjugates (0.5, 1, 5, and 10 μM) for 4 h (**A**) and then irradiated for 40 min (**B**). The cell survival fractions were determined 24 h after treatment by the MTT colorimetric assay. Values are presented as mean ± S. D. of three independent experiments performed in triplicates, using the respective controls (cells incubated with PBS and (**A**) non-irradiated or (**B**) irradiated) as reference value for cellular viability (100%). **($p<0.001$) significantly different from 0 μM of **Por 1-BSA**. $^{\$\$}$($p<0.001$) significantly different from 0 μM of **Por 1-HSA**, $^{\#}$significantly different from **Por 1-HSA** at the same concentration ($p<0.05$).

The MTT reduction was statistically different between **Por 1-BSA** and **Por 1-HSA** conjugates for the concentration of 1 μM. The best results were obtained when the cells were incubated with 5 μM and 10 μM solutions of the bioconjugates. **Por 1-BSA** and **Por 1-HSA** at 5 μM resulted in cell toxicity percentages of 89.48 ± 1.98 and 90.02 ± 1.16, respectively. Combining the uptake results with the phototoxicicity outcome, further experiments were performed using 5 μM of **Por 1-albumin** bioconjugates and uptake time of 4 h.

Accounting to other reported studies [73], we hypothesize that the accumulation and phototoxicity of **Por 1-albumin** bioconjugates will be succeeded *in vivo* because of the enhanced microvascular permeability, as well as specific cellular uptake mechanisms. As aforementioned, albumin conjugates can be accumulated inside the cancer cells due to the EPR effect [67]. The vasculature of the tumour tissue is permeable for macromolecules due to the leaky defective blood vessels, whereas in healthy tissues only small molecules can pass through the blood vessels.

4.1.3.3. Reactive oxygen species induced by **Por 1-albumin** bioconjugates in UM-UC-3 bladder cancer cells after PDT

To ensure that the bioconjugation did not influence the ability of **Por 1** to produce ROS after photoactivation and also to determine whether or not the phototoxicity observed in **Figure 2.36 B** is related to ROS production after PDT, the intracellular levels of ROS were measured using the probes H_2DCFDA [77] and DHE [19] (for more detail, see part II).

The ROS measurements are displayed in **Figure 2.37**. For both tested **Por 1-albumin** bioconjugates, the ROS levels were significantly increased in comparison to cells without PS. The differences between the conjugates using the same probe, were statistically different for DHE probe.

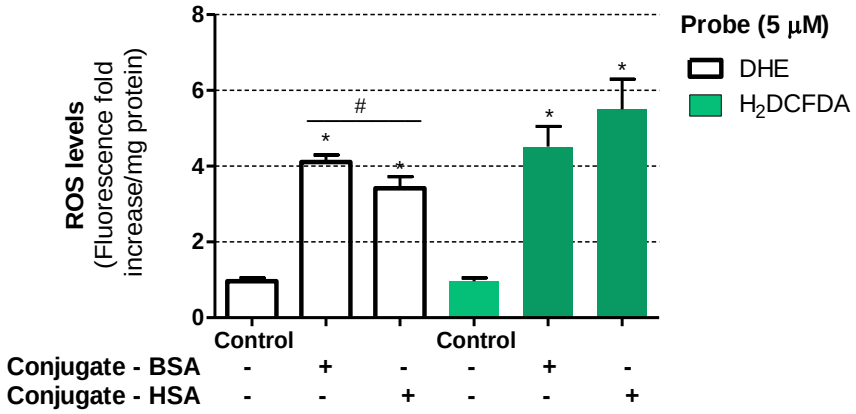

Figure 2.37. ROS production inside the UM-UC-3 cells after cells´ incubation in darkness with 5 µM of **Por 1-albumin** bioconjugates for 4 h and irradiation with white light for 40 min. The intracellular ROS levels were determined after PDT treatment, by DHE and H_2DCFA staining. Values are presented as the mean ± S. D. of three independent experiments performed in triplicates. *significantly different when compared with control cells (cells without conjugate, incubated with DHE or H_2DCFDA) ($p<0.05$); #statistical differences between **Por 1-HSA** and **Por 1-BSA** using the DHE probe ($p<0.05$).

The production of ROS after albumin bioconjugates-PDT demonstrates that the conjugation of **Por 1** to BSA or HSA is not able to quench the porphyrin excited states by amino acid residues on the protein. Thus, the phototoxicity observed with the conjugates is related with their ability to generate ROS.

To correlate the $^1O_2$ production by **Por 1-albumin** bioconjugates with their phototoxicity, after PDT, the $^1O_2$ quencher - sodium azide (NaN_3) - was used [21]. UM-UC-3 cells were incubated with 5 μM of **Por 1-albumin** bioconjugates for 4 h in darkness and then with a non-toxic concentration of NaN_3 (50 nM) before the PDT treatment. **Figure 2.38** shows how the presence of NaN_3 is able to reduce the cell toxicity. The effectiveness of the conjugates is not completely reversed with NaN_3, which suggests that $^1O_2$ generation is a minor part of the phototoxic effect.

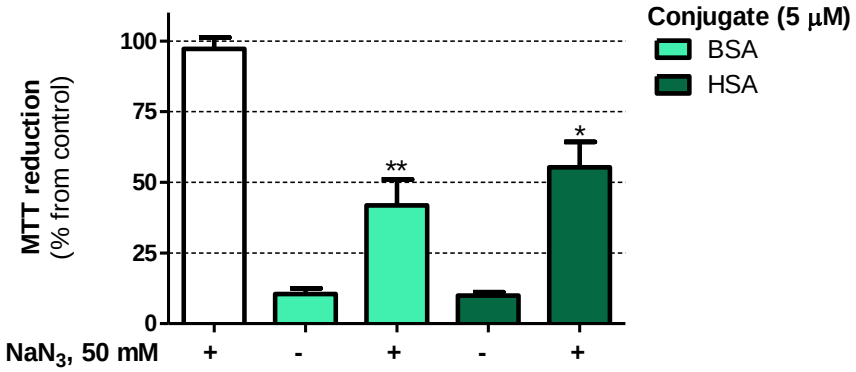

Figure 2.38. Inhibition of cell phototoxicity induced by **Por 1-albumin** bioconjugates after PDT, using sodium azide (NaN_3) as the quencher. After conjugates uptake at 5 μM for 4 h in darkness, the cells were incubated with 50 nM of NaN_3 and irradiated with white light for 40 min. The cell viability was evaluated 24 h after treatment by the MTT colorimetric assay. Values are presented as the relative mean ± S. D. of three independent experiments performed in triplicates. *($p<0.05$) and **($p<0.001$) significantly different when compared with the respective conjugate (without quencher), after PDT.

4.2. **Por 1-mAb anti-Caf** and **Por 1-mAb anti-CD104** immunoconjugates

4.2.1. General overview

The conjugation of PSs with specific antibodies allows the direct targeting of the PS to the correct cell type [72]. The mAb anti-CD104 recognizes the human antigen CD104, also known as integrin beta 4. The role of CD104 in tumourigenicity is well established and its overexpression in colorectal and bladder carcinomas has been reported [78, 79]. There are two reports about the synthesis and photodynamic activity of cationic isothiocyanato diphenyl porphyrins conjugated with mAb anti-CD104 [80, 81].

Since limited quantities of mAb anti-CD104 were available, the mAb anti-Caf was used as a model for the optimization of our bioconjugation strategy.

In this section it will be described the characterization of **Por 1-mAb anti-Caf** and **Por 1-mAb anti-CD104** by UV-Visible and the immunoreactivity of the conjugate **Por 1-mAb anti-Caf** by ELISA assay. At the end, PDT *in vitro* results obtained with **Por 1-mAb anti-CD104** against UM-UC-3 human bladder cancer cell line are reported (**Figure 2.39**).

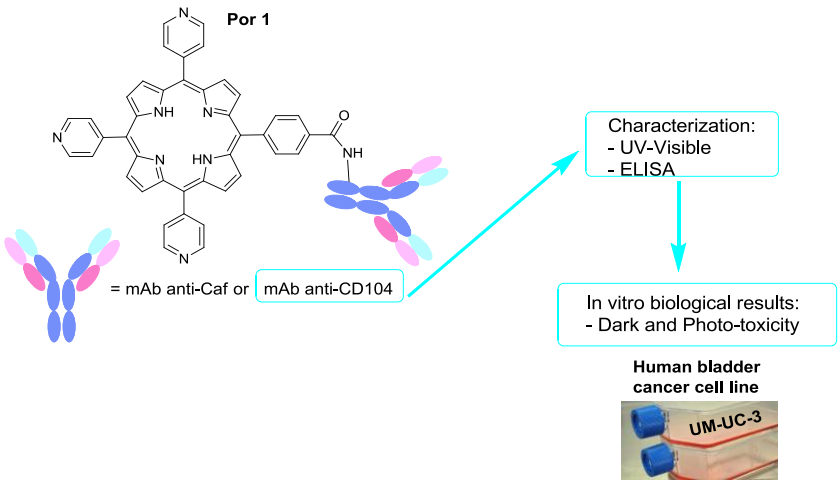

Figure 2.39. Schematic overview of this section including the characterization of **Por 1-mAb anti-Caf** and **Por 1-mAb anti-CD104** conjugates, as well as the biological assays with **Por 1-mAb anti-CD104** against UM-UC-3 bladder cancer cells.

4.2.2. **Por 1-mAb anti-Caf** and **Por 1-mAb anti-CD104** immunoconjugates characterization

4.2.2.1. UV-Visible and ELISA

The efficient conjugation of **Por 1** with albumins and the successful biological results obtained with these bioconjugates suggest that the adopted experimental procedure has general applicability. Thus, the conjugation of **Por 1-mAb anti-Caf** was performed using the same methodology.

The DOL for the **Por 1-mAb anti-Caf**, i.e. moles of **Por 1** per mole of mAb anti-Caf, was calculated from two independent experiments, using initial molar ratios of 30:1 and 80:1 (**Table 2.6**). It was observed that the DOL decreases with increasing initial molar ratios, like had been obtained for the conjugates **Por 1-albumin** bioconjugates (**Table 2.5**), an effect reported elsewhere for other photosensitizer-antibody conjugates [82]. Consequently, the conjugation of **Por 1** with the mAb anti-CD104 was also performed using an initial molar ratio of 30:1, based on the obtained data with the albumins conjugates. For the **Por 1-mAb anti-CD104** a DOL of 0.803 was obtained (**Table 2.6**), that is in accordance with the ratio described in the literature for cationic isothiocyanato diphenyl porphyrins conjugated with the same mAb anti-CD104 [80].

Table 2.6. DOLs of **Por 1-mAb anti-Caf** and **Por 1-mAb anti-CD104** immunoconjugates at different initial molar ratios. DOL is the degree of labeling (i. e. moles of **Por 1** per moles of antibody after conjugate purification).

Immunoconjugate	**Initial Molar ratios**	**nmol after purification**		**DOL**
		Por 1	mAb	
Por 1-mAb anti-Caf	30:1	0.165	0.204	0.809
Por 1-mAb anti-Caf	80:1	0.919	2.750	0.334
Por 1-mAb anti-CD104	30:1	0.191	0.238	0.803

The conjugate **Por 1-mAb anti-Caf** was used in an attempt to confirm that the antibody binding specificity is not affected after conjugation, since it has been described that conjugated porphyrins can interfere with the antigen recognition by the antibody [83]. Thus, the immunoreactivity of **Por 1-mAb anti-Caf** was checked by ELISA assay (data

not shown). ELISA demonstrated that the immunespecificity of mAb anti-Caf is unaffected after conjugation with **Por 1**.

4.2.3. Biological *in vitro* assays with **Por 1-mAb anti-CD104** immunoconjugate against UM-UC-3 bladder cancer cells

The dark toxicity of **Por 1** (control) and **Por 1-mAb anti-CD104** on the UM-UC-3 cell line was examined 24 h after treatment by the MTT colorimetric assay (**Figure 2.40**). Because of the reactive nature of the ester group, **Por 1** containing a carboxylic group was used. The cells were incubated for 4 h in darkness with **Por 1-mAb anti-CD104** immunoconjugate at 0.0025, 0.005, 0.05, 0.5, and 1 µM for 4 h. Non-conjugated **Por 1** was used as control, tested for concentrations between 0.0025 µM to 10 µM. The non conjugated **Por 1** and **Por 1-mAb anti-CD104** were not toxic to cells in the absence of light.

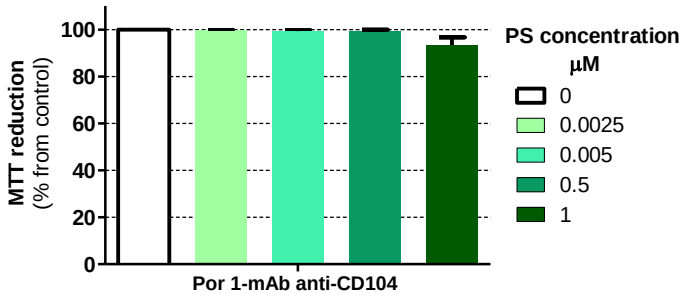

Figure 2.40. Non-dark toxicity of **Por 1-mAb anti-CD104** immunoconjugate, after UM-UC-3 cells had been incubated in the dark with different concentrations of the immunoconjugate (0.0025, 0.005, 0.5, and 1 µM) for 4 h. The cell survival fractions were determined 24 h after treatment by the MTT colorimetric assay. Values are presented as mean ± S. D. of three independent experiments performed in triplicates, using the control (cells incubated with PBS for 4 h) as reference value for cellular viability (100%).

For the PDT assays, the cells were incubated with **Por 1-mAb anti-CD104** at various concentrations (0.0025, 0.005, 0.05, 0.5, and 1 µM) for 4 h in darkness and then irradiated for 40 min. The cell toxicity obtained with **Por 1-mAb anti-CD104** was statistically different for all studied concentrations in relation to untreated cells (**Figure 2.41**). The IC_{50} values (concentration of porphyrin needed to kill 50% of UM-UC-3 cells after PDT) were 0.09, 0.14, and 0.53 µM for **Por 1-mAb anti-CD104**, **Por 1-BSA** and **Por 1-HSA**, respectively. The immunoconjugate IC_{50} was lower when compared with that for reported photosensitizers conjugated with mAb anti-CD104 antibody against human colon

adenocarcinoma cell line LoVo and human caucasian lung large cell carcinoma CORL23 [81]. These results show that the immunoconjugate is a potential target-directed photosensitizer. Knowing that anti-CD104 binds to a 205-kDa glycoprotein (integrin beta 4) involved in cell-cell adhesion that is up-regulated in bladder carcinomas, future *in vivo* studies with higher quantities of the **Por 1-mAb anti-CD104** are needed to validate the putative potential of this immunoconjugate against bladder tumours.

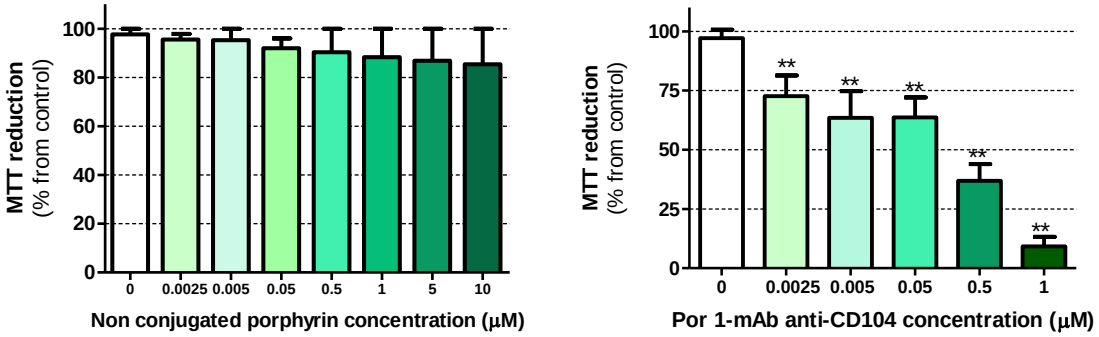

Figure 2.41. Phototoxicity of non conjugated porphyrin and **Por 1-mAb anti-CD104** immunoconjugate. UM-UC-3 cells were incubated in the dark with compounds at different concentrations for 4 h and irradiated with white light for 40 min. The cell survival fractions were determined 24 h after treatment by the MTT colorimetric assay. Values are presented as mean ± S. D. of three independent experiments performed in triplicates, in relation to the control (concentration equal to zero), expressed in percentage. **($p<0.001$) significantly different from **Por 1-mAb anti-CD104** immunoconjugate at 0 µM.

References

1. Novakova, V.; Kobak, R. Z.; Kucera, R.; Kopecky, K.; Miletin, M.; Krepsova, V.; Ivincova, J. and Zimcik, P. *The effect of the number of carbohydrate moieties on the azaphthalocyanine properties*. Dalton Trans, **2012**, 41(35), p. 10596-10604.
2. Lyubimtsev, A.; Iqbal, Z.; Crucius, G.; Syrbu, S.; Taraymovich, E. S.; Ziegler, T. and Hanack, M. *Aggregation behavior and UV-vis spectra of tetra- and octaglycosylated zinc phthalocyanines*. J Porphyrins and Phthalocyanines, **2011**, 15(1), p. 39-46.
3. Iqbal, Z.; Lyubimtsev, A.; Herrmann, T.; Hanack, M. and Ziegler, T. *Synthesis of Octaglycosylated Zinc(II) Phthalocyanines*. Synthesis-Stuttgart, **2010**, (18), p. 3097-3104.
4. Zorlu, Y.; Dumoulin, F.; Bouchu, D.; Ahsen, V. and Lafont, D. *Monoglycoconjugated water-soluble phthalocyanines. Design and synthesis of potential selectively targeting PDT photosensitisers*. Tetrahedron Lett, **2010**, 51(50), p. 6615-6618.
5. Soares, A. R.; Tome, J. P.; Neves, M. G.; Tome, A. C.; Cavaleiro, J. A. and Torres, T. *Synthesis of water-soluble phthalocyanines bearing four or eight D-galactose units*. Carbohydr Res, **2009**, 344(4), p. 507-510.
6. Choi, C. F.; Huang, J. D.; Lo, P. C.; Fong, W. P. and Ng, D. K. *Glycosylated zinc(II) phthalocyanines as efficient photosensitisers for photodynamic therapy. Synthesis, photophysical properties and in vitro photodynamic activity*. Orgm Biomol Chem, **2008**, 6(12), p. 2173-2181.
7. Ribeiro, A. O.; Tome, J. P. C.; Neves, M. G. P. M. S.; Tome, A. C.; Cavaleiro, J. A. S.; Iamamoto, Y. and Torres, T. *[1,2,3,4-tetrakis(alpha/beta-D-galactopyranos-6-yl)-phthalocyaninato]zinc(II): a water-soluble phthalocyanine*. Tetrahedron Lett, **2006**, 47(52), p. 9177-9180.
8. Soares, A. R. M.; Neves, M. G. P. M. S.; Tome, A. C.; Iglesias-de la Cruz, M. C.; Zamarron, A.; Carrasco, E.; Gonzalez, S.; Cavaleiro, J. A. S.; Torres, T.; Guldi, D. M. and Juarranz, A. *Glycophthalocyanines as Photosensitizers for Triggering Mitotic: Catastrophe and Apoptosis On Cancer Cells*. Chem Res Toxicol, **2012**, 25(4), p. 940-951.
9. Silva, S.; Pereira, P. M.; Silva, P.; Paz, F. A.; Faustino, M. A.; Cavaleiro, J. A. and Tome, J. P. *Porphyrin and phthalocyanine glycodendritic conjugates: synthesis, photophysical and photo-chemical properties*. Chem Commun, **2012**, 48(30), p. 3608-3610.
10. Seybold, P. G. and Gouterma.M. *Porphyrins .13. Fluorescence Spectra and Quantum Yields*. J Mol Spectrosc, **1969**, 31(1), p. 1.
11. Silva, E. M. P.; Ramos, C. I. V.; Pereira, P. M. R.; Giuntini, F.; Faustino, M. A. F.; Tome, J. P. C.; Tome, A. C.; Silva, A. M. S.; Santana-Marques, M. G.; Neves, M. G. P. M. S. and Cavaleiro, J. A. S. *Cationic beta-vinyl substituted meso-*

tetraphenylporphyrins: synthesis and non-covalent interactions with a short poly(dGdC) duplex. J Porphyrins and Phthalocyanines, **2012**, 16(1), p. 101-113.

12. Williams, A. T. R.; Winfield, S. A. and Miller, J. N. *Relative Fluorescence Quantum Yields Using a Computer-Controlled Luminescence Spectrometer*. Analyst, **1983**, 108(1290), p. 1067-1071.
13. Ascoli, G. A.; Domenici, E. and Bertucci, C. *Drug binding to human serum albumin: Abridged review of results obtained with high-performance liquid chromatography and circular dichroism*. Chirality, **2006**, 18(9), p. 667-679.
14. Zhang, Y. Z.; Zhou, B.; Zhang, X. P.; Huang, P.; Li, C. H. and Liu, Y. *Interaction of malachite green with bovine serum albumin: determination of the binding mechanism and binding site by spectroscopic methods*. J Hazard Mater, **2009**, 163(2-3), p. 1345-1352.
15. Cindolo, L.; Benvenuto, G.; Salvatore, P.; Pero, R.; Salvatore, G.; Mirone, V.; Prezioso, D.; Altieri, V.; Bruni, C. B. and Chiariotti, L. *Galectin-1 and galectin-3 expression in human bladder transitional-cell carcinomas*. Int Cancer, **1999**, 84(1), p. 39-43.
16. Baumgart, E.; Cohen, M.S.; Silva, Neto B.; Jacobs, M.A.; Wotkowicz, C.; Rieger-Christ, K.M.; Biolo, A.; Zeheb, R.;, Loda, M.; Libertino, J.A. and Summerhayes, I.C. *Identification and prognostic significance of an epithelial-mesenchymal transition expression profile in human bladder tumors.* Clin Cancer Res, **2007**, 13(6), p. 1685-1694.
17. Chiariotti, L.; Berlingieri, M.T.; De Rosa, P.; Battaglia, C.; Berger, N.; Bruni, C.B. and Fusco, A. *Increased expression of the negative growth factor, galactoside-binding protein, gene in transformed thyroid cells and in human thyroid carcinomas.* Oncogene, **1992**,7(12), p. 2507-2511.
18. Chandel, N. S.; Maltepe, E.; Goldwasser, E.; Mathieu, C. E.; Simon, M. C. and Schumacker, P. T. *Mitochondrial reactive oxygen species trigger hypoxia-induced transcription*. Proc Natl Acad Sci U S A, **1998**, 95(20), p. 11715-11720.
19. Fernandes, R.; Hosoya, K. and Pereira, P. *Reactive oxygen species downregulate glucose transport system in retinal endothelial cells*. Am J Physiol - Cell Physiology, **2011**, 300(4), p. 927-936.
20. Saczko, J.; Kulbacka, J.; Chwilkowsa, A.; Pola, A.; Lugowski, M.; Marcinkowska, A.; Malarska, A. and Banas, T. *Cytosolic superoxide dismutase activity after photodynamic therapy, intracellular distribution of Photofrin II and hypericin, and P-glycoprotein localization in human colon adenocarcinoma*. Folia Histochem Cytobiol, **2007**, 45(2), p. 93-98.
21. Bancirova, M. *Sodium azide as a specific quencher of singlet oxygen during chemiluminescent detection by luminol and Cypridina luciferin analogues*. J Lumin, **2011**, 26(6), p. 685-688.
22. Hara, K.; Holland, S. and Woo, J. *Effects of Exogenous Reactive Oxygen Species Scavengers on the Survival of Escherichia coli B23 during Exposure to UV-A radiation*. J Exper Microbiol Immunol, **2004**, 12, p. 62-66.

23. Aruoma, O. I.; Halliwell, B.; Hoey, B. M. and Butler, J. *The antioxidant action of N-acetylcysteine: its reaction with hydrogen peroxide, hydroxyl radical, superoxide, and hypochlorous acid*. Free Radic Biol Med, **1989**, 6(6), p. 593-597.
24. D'Auria, S.; Petrova, L.; John, C.; Russev, G.; Varriale, A. and Bogoeva, V. *Tumour-specific protein human galectin-1 interacts with anticancer agents*. Mol BioSyst, **2009**, 5(11), p. 1331-1336.
25. She, J. J.; Zhang, P. G.; Wang, Z. M.; Gan, W. M. and Che, X. M. *Identification of side population cells from bladder cancer cells by dyecycle violet staining*. Cancer Biol Ther, **2008**, 7(10), p. 1663-1668.
26. Dean, M.; Fojo, T. and Bates, S. *Tumour stem cells and drug resistance*. Nature Rev Cancer, **2005**, 5(4), p. 275-284.
27. Robey, R. W.; Steadman, K.; Polgar, O. and Bates, S. E. *ABCG2-mediated transport of photosensitizers: potential impact on photodynamic therapy*. Cancer Biol Ther, **2005**, 4(2), p. 187-194.
28. Jonker, J. W.; Buitelaar, M.; Wagenaar, E.; Van Der Valk, M. A.; Scheffer, G. L.; Scheper, R. J.; Plosch, T.; Kuipers, F.; Elferink, R. P.; Rosing, H.; Beijnen, J. H. and Schinkel, A. H. *The breast cancer resistance protein protects against a major chlorophyll-derived dietary phototoxin and protoporphyria*. Proc Natl Acad Sci U S A, **2002**, 99(24), p. 15649-15654.
29. Saito, H.; Hirano, H.; Nakagawa, H.; Fukami, T.; Oosumi, K.; Murakami, K.; Kimura, H.; Kouchi, T.; Konomi, M.; Tao, E.; Tsujikawa, N.; Tarui, S.; Nagakura, M.; Osumi, M. and Ishikawa, T. *A new strategy of high-speed screening and quantitative structure-activity relationship analysis to evaluate human ATP-binding cassette transporter ABCG2-drug interactions*. J Pharmacol Exp Ther, **2006**, 317(3), p. 1114-1124.
30. Patrawala, L.; Calhoun, T.; Schneider-Broussard, R.; Zhou, J. J.; Claypool, K. and Tang, D. G. *Side population is enriched in tumourigenic, stem-like cancer cells, whereas ABCG2(+) and ABCG2(-) cancer cells are similarly tumourigenic*. Cancer Res, **2005**, 65(14), p. 6207-6219.
31. Glavinas, H.; Krajcsi, P.; Cserepes, J. and Sarkadi, B. *The role of ABC transporters in drug resistance, metabolism and toxicity*. Curr Drug Deliv, **2004**, 1(1), p. 27-42.
32. Martins-Neves, S. R.; Lopes, A. O.; do Carmo, A.; Paiva, A. A.; Simoes, P. C.; Abrunhosa, A. J. and Gomes, C. M. F. *Therapeutic implications of an enriched cancer stem-like cell population in a human osteosarcoma cell line*. BMC Cancer, **2012**, 12.
33. Jaggupilli, A. and Elkord, E. *Significance of CD44 and CD24 as Cancer Stem Cell Markers: An Enduring Ambiguity*. Clin Develop Immunol, **2012**, p. 1-11.
34. Diehn, M.; Cho, R. W.; Lobo, N. A.; Kalisky, T.; Dorie, M. J.; Kulp, A. N.; Qian, D.; Lam, J. S.; Ailles, L. E.; Wong, M.; Joshua, B.; Kaplan, M. J.; Wapnir, I.; Dirbas, F. M.; Somlo, G.; Garberoglio, C.; Paz, B.; Shen, J.; Lau, S. K.; Quake, S. R.; Brown, J. M.; Weissman, I. L. and Clarke, M. F. *Association of reactive oxygen species levels and radioresistance in cancer stem cells*. Nature, **2009**, 458(7239), p. 780-783.

35. Hagiya, Y.; Endo, Y.; Yonemura, Y.; Takahashi, K.; Ishizuka, M.; Abe, F.; Tanaka, T.; Okura, I.; Nakajima, M.; Ishikawa, T. and Ogura, S. *Pivotal roles of peptide transporter PEPT1 and ATP-binding cassette (ABC) transporter ABCG2 in 5-aminolevulinic acid (ALA)-based photocytotoxicity of gastric cancer cells in vitro*. Photodiagnosis Photodyn Ther, **2012**, 9(3), p. 204-214.
36. Lavastre, V.; Roberge, C. J.; Pelletier, M.; Gauthier, M. and Girard, D. *Toxaphene, but not beryllium, induces human neutrophil chemotaxis and apoptosis via reactive oxygen species (ROS): Involvement of caspases and ROS in the degradation of cytoskeletal proteins*. Clin Immunol, **2002**, 104(1), p. 40-48.
37. Liu, T.; Wu, L. Y. and Berkman, C. E. *Prostate-specific membrane antigen-targeted photodynamic therapy induces rapid cytoskeletal disruption*. Cancer Lett, **2010**, 296(1), p. 106-112.
38. Mashima, T.; Naito, M. and Tsuruo, T. *Caspase-mediated cleavage of cytoskeletal actin plays a positive role in the process of morphological apoptosis*. Oncogene, **1999**, 18(15), p. 2423-2430.
39. Ndozangue-Touriguine, O.; Hamelin, J. and Breard, J. *Cytoskeleton and apoptosis*. Biochem Pharmacol, **2008**, 76(1), p. 11-18.
40. Cory, S. and Adams, J. M. *The BCL2 family: Regulators of the cellular life-or-death switch*. Nature Rev Cancer, **2002**, 2(9), p. 647-656.
41. Adams, J. M. and Cory, S. *The Bcl-2 apoptotic switch in cancer development and therapy*. Oncogene, **2007**, 26(9), p. 1324-1337.
42. He, J.; Agarwal, M. L.; Larkin, H. E.; Friedman, L. R.; Xue, L. Y. and Oleinick, N. L. *The induction of partial resistance to photodynamic therapy by the protooncogene BCL-2*. Photochem Photobiol, **1996**, 64(5), p. 845-852.
43. Kim, H. R.; Luo, Y.; Li, G. and Kessel, D. *Enhanced apoptotic response to photodynamic therapy after bcl-2 transfection*. Cancer Res, **1999**, 59(14), p. 3429-3432.
44. Chiu, S. M.; Xue, L. Y.; Usuda, J.; Azizuddin, K. and Oleinick, N. L. *Bax is essential for mitochondrion-mediated apoptosis but not for cell death caused by photodynamic therapy*. Br J Cancer, **2003**, 89(8), p. 1590-1597.
45. Oleinick, N. L.; Morris, R. L. and Belichenko, I. *The role of apoptosis in response to photodynamic therapy: what, where, why, and how*. Photochem Photobiol Sci, **2002**, 1(1), p. 1-21.
46. He, G. F.; Bian, M. L.; Zhao, Y. W.; Xiang, Q.; Li, H. Y. and Xiao, C. *A study on the mechanism of 5-aminolevulinic acid photodynamic therapy in vitro and in vivo in cervical cancer*. Oncol Rep, **2009**, 21(4), p. 861-868.
47. Chen, X.; Zhao, P.; Chen, F.; Li, L. and Luo, R. *Effect and mechanism of 5-aminolevulinic acid-mediated photodynamic therapy in esophageal cancer*. Lasers Med Sci, **2011**, 26(1), p. 69-78.
48. He, G. F.; Bian, M. L.; Zhao, Y. W.; Xiang, Q.; Li, H. Y. and Xiao, C. *Effects of 5-aminolevulinic acid photodynamic therapy on cervical cancer: in vivo experiment with nude mice*. Zhonghua Yi Xue Za Zhi, **2008**, 88(9), p. 635-640.

49. Koval, J.; Mikes, J.; Jendzelovsky, R.; Kello, M.; Solar, P. and Fedorocko, P. *Degradation of HER2 Receptor Through Hypericin-mediated Photodynamic Therapy*. Photochem Photobiol, **2010**, 86(1), p. 200-205.
50. Mikes, J.; Koval, J.; Jendzelovsky, R.; Sackova, V.; Uhrinova, I.; Kello, M.; Kulikova, L. and Fedorocko, P. *The role of p53 in the efficiency of photodynamic therapy with hypericin and subsequent long-term survival of colon cancer cells*. Photochem Photobiol Sci, **2009**, 8(11), p. 1558-1567.
51. Espada, J.; Galaz, S.; Sanz-Rodriguez, F.; Blazquez-Castro, A.; Stockert, J. C.; Bagazgoitia, L.; Jaen, P.; Gonzalez, S.; Cano, A. and Juarranz, A. *Oncogenic H-Ras and PI3K Signaling can Inhibit E-Cadherin-Dependent Apoptosis and Promote Cell Survival After Photodynamic Therapy in Mouse Keratinocytes*. J Cell Physiol, **2009**, 219(1), p. 84-93.
52. Bozkulak, O.; Wong, S.; Luna, M.; Ferrario, A.; Rucker, N.; Gulsoy, M. and Gomer, C. J. *Multiple components of photodynamic therapy can phosphorylate akt*. Photochem Photobiol, **2007**, 83(5), p. 1029-1033.
53. Almeida, R. D.; Manadas, B. J.; Carvalho, A. P. and Duarte, C. B. *Intracellular signaling mechanisms in photodynamic therapy*. Biochim Biophys Acta, **2004**, 1704(2), p. 59-86.
54. Vivanco, I. and Sawyers, C. L. *The phosphatidylinositol 3-kinase-AKT pathway in human cancer*. Nature Rev Cancer, **2002**, 2(7), p. 489-501.
55. Yang, P.; Peairs, J. J.; Tano, R. and Jaffe, G. J. *Oxidant-mediated akt activation in human RPE cells*. Invest Ophthalmol Vis Sci, **2006**, 47(10), p. 4598-4606.
56. Zhuang, S. and Kochevar, I. E. *Singlet Oxygen–induced Activation of Akt/Protein Kinase B is Independent of Growth Factor Receptors*¶. Photochem Photobiol, **2003**, 78(4), p. 361-371.
57. Han, Z.; Hong, L.; Han, Y.; Wu, K.; Han, S.; Shen, H.; Li, C.; Yao, L.; Qiao, T. and Fan, D. *Phospho akt mediates multidrug resistance of gastric cancer cells through regulation of P-gp, Bcl-2 and Bax*. J Exp Clin Cancer Res, **2007**, 26(2), p. 261-268.
58. Buytaert, E.; Dewaele, M. and Agostinis, P. *Molecular effectors of multiple cell death pathways initiated by photodynamic therapy*. Biochim Biophys Acta, **2007**, 1776(1), p. 86-107.
59. Szegezdi, E.; Logue, S. E.; Gorman, A. M. and Samali, A. *Mediators of endoplasmic reticulum stress-induced apoptosis*. EMBO Rep, **2006**, 7(9), p. 880-885.
60. Wong, S.; Luna, M.; Ferrario, A. and Gomer, C. J. *CHOP activation by photodynamic therapy increases treatment induced photosensitization*. Lasers Surg Med, **2004**, 35(5), p. 336-341.
61. Nutt, L. K.; Pataer, A.; Pahler, J.; Fang, B.; Roth, J.; McConkey, D. J. and Swisher, S. G. *Bax and Bak promote apoptosis by modulating endoplasmic reticular and mitochondrial Ca2+ stores*. J Biol Chem, **2002**, 277(11), p. 9219-9225.
62. Hyoda, K.; Hosoi, T.; Horie, N.; Okuma, Y.; Ozawa, K. and Nomura, Y. *PI3K-Akt inactivation induced CHOP expression in endoplasmic reticulum-stressed cells*. Biochem Biophys Res Commun, **2006**, 340(1), p. 286-290.

63. Ohoka, N.; Yoshii, S.; Hattori, T.; Onozaki, K. and Hayashi, H. *TRB3, a novel ER stress-inducible gene, is induced via ATF4-CHOP pathway and is involved in cell death*. Embo Journal, **2005**, 24(6), p. 1243-1255.
64. Daroqui, C. M.; Ilarregui, J. M.; Rubinstein, N.; Salatino, M.; Toscano, M. A.; Vazquez, P.; Bakin, A.; Puricelli, L.; Joffe, E. B. D. and Rabinovich, G. A. *Regulation of galectin-1 expression by transforming growth factor beta 1 in metastatic mammary adenocarcinoma cells: implications for tumour-immune escape*. Cancer Immunol Immunother, **2007**, 56(4), p. 491-499.
65. Lu, Y.; Lotan, D. and Lotan, R. *Differential regulation of constitutive and retinoic acid-induced galectin-1 gene transcription in murine embryonal carcinoma and myoblastic cells*. BBA-Gene Structure and Expression, **2000**, 1491(1-3), p. 13-19.
66. Rabinovich, G. A. *Galectin-1 as a potential cancer target*. Br J Cancer, **2005**, 92(7), p. 1188-1192.
67. Kratz, F. *Albumin as a drug carrier: design of prodrugs, drug conjugates and nanoparticles*. J Controlled Release, **2008**, 132(3), p. 171-183.
68. Hamblin, M. R.; Miller, J. L. and Ortel, B. *Scavenger-receptor targeted photodynamic therapy*. Photochem Photobiol, **2000**, 72(4), p. 533-540.
69. Hamblin, M. R. and Newman, E. L. *Photosensitizer targeting in photodynamic therapy. I. Conjugates of haematoporphyrin with albumin and transferrin*. Journal of Photochem Photobiol B-Biology, **1994**, 26(1), p. 45-56.
70. Sutton, J. M.; Clarke, O. J.; Fernandez, N. and Boyle, R. W. *Porphyrin, chlorin, and bacteriochlorin isothiocyanates: useful reagents for the synthesis of photoactive bioconjugates*. Bioconjugate Chem, **2002**, 13(2), p. 249-263.
71. Maeda, H.; Wu, J.; Sawa, T.; Matsumura, Y. and Hori, K. *Tumour vascular permeability and the EPR effect in macromolecular therapeutics: a review*. J Controlled Release, **2000**, 65(1-2), p. 271-284.
72. Bullous, A. J.; Alonso, C. M. and Boyle, R. W. *Photosensitiser-antibody conjugates for photodynamic therapy*. Photo Photobiol Sci, **2011**, 10(5), p. 721-750.
73. Wosikowski, K.; Biedermann, E.; Rattel, B.; Breiter, N.; Jank, P.; Loser, R.; Jansen, G. and Peters, G. J. *In vitro and in vivo antitumour activity of methotrexate conjugated to human serum albumin in human cancer cells*. Clin Cancer Res, **2003**, 9(5), p. 1917-1926.
74. Huang, B. X.; Kim, H. Y. and Dass, C. *Probing three-dimensional structure of bovine serum albumin by chemical cross-linking and mass spectrometry*. J Am Soc Mass Spectrom, **2004**, 15(8), p. 1237-1247.
75. Stehle, G.; Sinn, H.; Wunder, A.; Schrenk, H. H.; Stewart, J. C.; Hartung, G.; Maier-Borst, W. and Heene, D. L. *Plasma protein (albumin) catabolism by the tumour itself--implications for tumour metabolism and the genesis of cachexia*. Crit Rev Oncol Hematol, **1997**, 26(2), p. 77-100.
76. Frei, E. *Albumin binding ligands and albumin conjugate uptake by cancer cells*. Diabetol Metab Syndr, **2011**, 3(1), p. 3-11.

77. Kolarova, H.; Bajgar, R.; Tomankova, K.; Krestyn, E.; Dolezal, L. and Halek, J. *In vitro study of reactive oxygen species production during photodynamic therapy in ultrasound-pretreated cancer cells*. Physiol Res, **2007**, 56, p. 27-32.
78. Simon-Assmann, P.; Leberquier, C.; Molto, N.; Uezato, T.; Bouziges, F. and Kedinger, M. *Adhesive properties and integrin expression profiles of two colonic cancer populations differing by their spreading on laminin*. J Cell Sci, **1994**, 107 (Pt 3), p. 577-587.
79. Falcioni, R.; Sacchi, A.; Resau, J. and Kennel, S. J. *Monoclonal-Antibody to Human Carcinoma-Associated Protein Complex - Quantitation in Normal and Tumour-Tissue*. Cancer Res, **1988**, 48(4), p. 816-821.
80. Malatesti, N.; Smith, K.; Savoie, H.; Greenman, J. and Boyle, R. W. *Synthesis and in vitro investigation of cationic 5,15-diphenyl porphyrin-monoclonal antibody conjugates as targeted photodynamic sensitisers*. Int J Oncol, **2006**, 28(6), p. 1561-1569.
81. Smith, K.; Malatesti, N.; Cauchon, N.; Hunting, D.; Lecomte, R.; van Lier, J. E.; Greenman, J. and Boyle, R. W. *Mono- and tri-cationic porphyrin-monoclonal antibody conjugates: photodynamic activity and mechanism of action*. Immunology, **2011**, 132(2), p. 256-265.
82. Hudson, R.; Carcenac, M.; Smith, K.; Madden, L.; Clarke, O. J.; Pelegrin, A.; Greenman, J. and Boyle, R. W. *The development and characterisation of porphyrin isothiocyanate-monoclonal antibody conjugates for photoimmunotherapy*. Br J Cancer, **2005**, 92(8), p. 1442-1449.
83. Milgrom, L. R. and Oneill, F. *Towards Synthetic-Porphyrin Monoclonal-Antibody Conjugates*. Tetrahedron, **1995**, 51(7), p. 2137-2144.

CONCLUSIONS AND FUTURE PERPECTIVES

CHAPTER 3

Conclusions and future perspectives

In the present study we intended to assess the photo-activity of three types of bioconjugates: PSs conjugated with galactose units, albumin proteins and mAb anti-CD104. Although structurally different, all of these bioconjugates have a common purpose – molecular targeted photodynamic therapy of bladder cancer cells. **PorGal$_8$** and **PcGal$_{16}$** are decorated with eight and sixteen galactose molecules, respectively, which can be recognized by galectins (galactose-binding proteins), overexpressed in bladder tumours. **Por 1-albumin bioconjugates** correspond to porphyrin conjugated with human and bovine serum albumin, which can be selectively accumulated in cancer cells, since the vasculature of the tumour tissue is permeable to macromolecules due to the leaky blood vessels, whereas in healthy tissues only small molecules can pass through the blood vessels. **Por 1-mAb anti-CD104** could have specificity to bladder cancer cells, since mAb anti-CD104 binds to a 205-kDa glycoprotein (integrin beta 4) involved in cell-cell adhesion that is up-regulated in bladder carcinomas.

The photophysical and -chemical characterization of the two new galacto-conjugates, **PorGal$_8$** and **PcGal$_{16}$**, demonstrated that the presence of galactose units in the periphery of Por and Pc improves their hydrophilicity. The interaction of these galacto-conjugates with HSA and their high singlet oxygen production demonstrated high capacity for their use as PDT agents.

For the *in vitro* photodynamic assays two human bladder cancer cell lines, HT-1376 and UM-UC-3, were used. UM-UC-3 cells correspond to a more invasive phenotype, while HT-1376 cells have an epithelial morphology associated with a non-invasive phenotype. The promising results obtained *in vitro*, encourages the move on to the next step: *in vivo* tests with all bioconjugates in tumour masses.

The uptake of **PorGal$_8$** was higher in UM-UC-3 cells than in HT-1376 cells and it can be somehow related to the higher protein levels of galectin-1 in UM-UC-3 cell line, which may serve as docking sites for **PorGal$_8$** on the cell membrane and probably, facilitating entry of **PorGal$_8$**. Moreover, the pre-incubation of cells with galactose decreased the uptake and phototoxicity of **PorGal$_8$**. Specific inhibition of galectin-1

expression by RNAi (interference) will be an approach to be used in future works, in an attempt to investigate the involvement of this lectin in the uptake of **PorGal$_8$** by bladder cancer cells.

In both cell lines, **PorGal$_8$** was inert until activation by light. The phototoxicity after **PorGal$_8$**-PDT was higher for the cell line UM-UC-3 than for the cell line HT-1376, being mediated by ROS production. Using the sphere formation assay, the presence of CSCs expressing ABCG2 (multi-drug resistance pump) protein in HT-1376 cells was detected. Thus, it is possible that CSCs in HT-1376 offer some resistance after **PorGal$_8$**-PDT. The presence of CSCs in HT-1376 cell line can be validated, in future works, by flow cytometry approaches using for example violet-excited Dye Cycle Violet (a cell permeable DNA binding dye) that is effluxed via ABCG2 pump-dependent mechanism.

PDT with **PorGal$_8$** induced transient changes in actin organization in HT-1376 cells. Therefore, it is plausible that cytoskeletal structures like F-actin can be involved in the mechanism of resistance to PDT in HT-1376 cells. For these cells, PDT with **PorGal$_8$** increased the expression of the pro-apoptotic protein Bax and ER-stress associated protein CHOP. To determine whether the mechanisms of action of the PDT agent **PorGal$_8$** are different between the two cell lines, we intend to evaluate (in future works) in both cell lines the expression of proteins associated to cell death at different time points after PDT.

The uptake of **PcGal$_{16}$** was similar in both cell lines and fluorescence microscopy demonstrated its accumulation inside the cells throughout the cytoplasm. In dark conditions, **PcGal$_{16}$** was non toxic and induced a decrease in galectin-1 protein levels. Western blotting studies are needed to quantify the galectin-1 protein levels before and after cellular uptake of PcGal$_{l6}$. For the HT-1376 cell line, it was observed co-localization of **PcGal$_{16}$** with galectin-1 in vesicular structures often concentrated perinuclearly. For the UM-UC-3 cell line, it was also observed dispersed co-localization of **PcGal$_{16}$** with galectin-1 in the cytoplasm. After **PcGal$_{16}$**-PDT, HT-1376 cell line was relatively resistant 24 h and 48 h after PDT with **PcGal$_{16}$**. However, 72 h after PDT there is a massive cell death. For the cell line UM-UC-3 there was a strong phototoxicity twenty-four hours after PDT without cell recovery until 72 h after PDT. The PDT treatment with **PcGal$_{16}$** evidenced, for the two bladder cancer cell lines, a significant increase in ROS formation and it was higher for the cell line UM-UC-3 than for the cell line HT-1376. Determination

of the activity of antioxidant enzymes in UM-UC-3 and HT-1376 cells, like superoxide dismutase, catalase and glutathione peroxidase before and after **$PcGal_{16}$**-PDT may be an attractive approach to investigate the involvement of these antioxidant enzymes in detoxification of ROS-induced by **$PcGal_{16}$**. This approach is planned to take place in a near future in our laboratory. Regarding the phototoxicity and generation of ROS in the two bladder cancer cell lines, it is expected that the activity of antioxidant enzymes is higher in HT-1376 cells than in UM-UC-3 cells.

The conjugation of human and bovine albumin, and mAb anti-CD104 with porphyrin 1 was successfully achieved. The biological potential of these conjugates was evaluated against the human bladder cancer cell line UM-UC-3. No photodynamic effect was detected when the non-conjugated porphyrin was used. Yet, when it was coupled covalently with the mAb anti-CD104, BSA and HSA, the resulting conjugates demonstrated high efficacy in destroying the cancer cells, with the mAb anti-CD104 efficacy overruling the albumin ones.

The porphyrin used in the synthesis of these bioconjugates has the longest-wave absorption band around 600 nm, thus the *in vivo* biological effects will occur only to a tissue depth of about 5 mm. Considering the limitations of **Por 1-mAb anti-CD104** for *in vivo* studies, we intend to conjugate the mAb anti-CD104 with phthalocyanines whose may be particularly effective in treating deeply seated tumours due to their markedly greater absorbance of red light near of 650 nm.

METHODS AND MATERIALS

CHAPTER 4

Photo -Physical and -Chemical assays of galacto-conjugates

Part I

1.1. Equipment and reagents

1.1.1. General instrumentation

1.1.1.1. Equipment and material for the UV-Visible absorbance and fluorescent measurements

The fluorescence assays were performed on a computer controlled by FluoroMax-3 spectrofluorimeter from Horiba Jobin Yvon. The data acquisition and post processing/analysis were performed using its software DataMax.

The UV-visible assays were performed on the UVIKON 922 spectrophotometer from Biotek Instruments.

1.1.1.2. Equipment for irradiation assays

The illumination system used to determine the photostability and $^1O_2$ generation of PSs was the Light Source Model Lc-122 from Lumacare, equipped with a halogen/quartz 250 W lamp coupled to one optic fiber probe (400-800 nm). The fluence rates were determined with the energy meter Coherent FieldMaxII-Top with a Coherent PowerSens PS19Q energy sensor.

1.1.2. Reagents, chemical products and buffers

PorGal$_8$, **PcGal$_{16}$**, TPP and ZnPc were synthesized by Doctor Sandrina Silva in the Porphyrins and Phthalocyanines Materials Research Group, Department of Chemistry, University of Aveiro, Portugal.

Dimethylsulfoxide (DMSO), dimethylformamide (DMF), 1,3-diphenylisobenzofuran (DPBF) were obtained from Sigma-Aldrich. Phosphate buffered saline (PBS) buffer was prepared in Milli-Q water at pH 7.60: 10 mM NaH_2PO_4, 70 mM Na_2HPO_4 and 145 mM NaCl.

The Human Serum Albumin (HSA) lyophilized powder, essentially protease free; ≥96% (agarose gel electrophoresis) was purchased from Sigma-Aldrich (Ref. A4327).

1.1.3. Softwares

Microsoft Excel was used for the displayed graphs and ChemDraw Ultra 12.00 from CambridgeSoft was the software used to draw the chemical structures.

1.2. Protocols

1.2.1. Aggregation assays

Principle

The aggregation behaviour of **PorGal$_8$** and **PcGal$_{16}$** in PBS buffer is studied at different concentrations by Lambert-Beer´s law plots, where the relation of absorbance and concentration is linear:

$$A = \varepsilon \times b \times c$$

where A is the absorbance, ε is the molar absorptivity of the compound (L.mol^{-1}.cm^{-1}), b is the length of the light path (cm) and c is the concentration of the compound in solution (mol.L^{-1}) [1].

Protocol

Stock solutions of the galacto-conjugates at a concentration of 20 mM were prepared in DMSO and stored in the dark at room temperature (RT). The working solutions were freshly prepared prior to use, by diluting the stock solutions in PBS buffer with the concentration of DMSO being always inferior to 1% (v/v).

Two milliliters of working solutions (without air bubbles) was placed into quartz cuvettes and the absorbance was scanned for wavelengths between 300 to 800 nm for **PcGal$_{16}$** and 300 to 700 nm for **PorGal$_8$**.[1] The wavelengths of maximum absorption were determined and the molar absorptivity of the compounds was calculated by plotting the absorbance against the respective concentration, by Lambert-Beer´s law.[2]

1.2.2. Fluorescence assays

Principle

The fluorescence quantum yields (Φ_F) of **PorGal$_8$** and **PcGal$_{16}$** can be calculated in DMF by comparison of the area below the corrected emission spectra (between 620 nm to 850 nm) using 5,10,15,20-tetraphenylporphyrin (TPP) as standard ($\lambda_{excitation}$ at 601 nm, Φ_f = 0.11 in DMF) [2]. For that, the following equation is used:

$$\Phi_f^{sample} = \Phi_f^{standard} \frac{AUC^{sample}(1 - 10^{-Abs_{standard}})}{AUC^{standard}(1 - 10^{-Abs_{sample}})}$$

[1] The maximum absorbance was always inferior to 1.0, in all working solutions.
[2] It was considered that the length of the light path (b) is equal to 1 cm.

where *AUC* is the integrated area under the fluorescence curves for each sample and standard, and *Abs* is the absorbance of the samples and the standard at the excitation wavelength ($\lambda_{excitation}$ at 601 nm) [3].

Protocol

$PorGal_8$, **$PcGal_{16}$** and TPP working solutions were freshly prepared in DMF to give absorbance near of 0.03[3] at 601 nm. The fluorescence emission spectra of **$PorGal_8$**, **$PcGal_{16}$** and TPP were measured between 620 to 850 nm, after excitation at 601 nm. The excitation and emission slits width were set at 2.0 nm. Using the DataMax software, the emission spectra were corrected and the area under the fluorescence emission curves was calculated.

1.2.3. Photostability assays

Principle

The photostability of **$PorGal_8$** and **$PcGal_{16}$** can be studied by monitoring, respectively, the decrease of the absorbance of Soret and Q bands, after different times of irradiation with white light (400-800 nm) delivered by an illumination system.

Protocol

Solutions of **$PorGal_8$** at 19 µM and **$PcGal_{16}$** at 9 µM were freshly prepared in PBS buffer (0.5% v/v DMSO) and kept in the dark at RT. The irradiation experiments were performed in magnetically stirred cuvette solutions (with 2 mL of sample) in a dark room, over a period of 30 min with white light (400-800 nm) at a fluence rate of 150 mW.cm^{-2}. The absorbance at 415 nm or 722 nm[4] for **$PorGal_8$** or **$PcGal_{16}$**, respectively, was determined before irradiation and at 1, 3, 4, 5, 10, 15, 20, 25, and 30 min periods of time after irradiation. The results were expressed as follows: $Photostability\,(\%) = \frac{Abs\ at\ a\ given\ time\ of\ irradiation}{Abs\ before\ irradiation}$.

[3] This condition minimizes reabsorption of radiation by the ground-state species.

[4] The wavelengths 415 nm and 722 nm correspond to the maximum absorbance of $PorGal_8$ and $PcGal_{16}$, respectively.

1.2.4. Singlet oxygen assays

Principle

Singlet oxygen ($^1O_2$) can be determined by a chemical method using 1,3-diphenylisobenzofuran (DPBF) as $^1O_2$ scavenger [4]. The yellow-colored DPBF reacts specifically with $^1O_2$ in a [4+2] cycloaddition reaction, being oxidized to the colorless o-dibenzoylbenzene (**Figure 4.1**). DPBF has an absorption maximum at 415 nm, thus it is possible to follow the ability of the **PorGal$_8$** and **PcGal$_{16}$** to generate $^1O_2$ by measuring the DPBF absorption decay, at this wavelength.

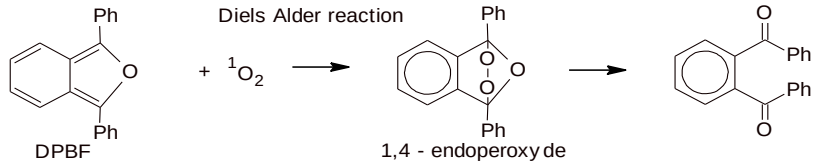

Figure 4.1. Reaction of DPBF with $^1O_2$ by a Diels Alder reaction.

Protocol

Freshly prepared stock solutions of 50 µM DPBF, 10 µM of galacto-conjugates (DMF:H_2O; 9:1, by volume) were maintained in the dark at RT until use. Solutions containing DPBF (16.15 µM) with or without **PorGal$_8$** or TPP at 0.67 µM; **PcGal$_{16}$** or ZnPc at 0.1615 µM were prepared in DMF:H_2O (9:1, by volume) in a quartz cuvette. The solutions were irradiated at RT and under gentle magnetic stirring, with filtered[5] white light (500 to nm 800 nm) at a fluence rate of 4.5 mW.cm^{-2}. The breakdown of DPBF was monitored by measuring the decrease in absorbance at 415 nm at pre-established irradiation intervals. The results were expressed by plotting the DPBF depletion against the irradiation time. The depletion of DPBF was calculated as follows: $DPBF\ depletion = \frac{Abs_t}{Abs_0}$.

Abs_0 and Abs_t are the absorbance values at 415 nm before and after irradiation, respectively.

1.2.5. Human Serum Albumin interaction assays

Principle

The interaction of the galacto-conjugates with HSA protein can be determined by measuring the intrinsic fluorescence quenching of tryptophan residues (excited at 280 nm)

[5] The white light was filtered through a cut-off filter for wavelengths inferior to 550 nm.

on HSA protein. If occurs interaction between conjugates and HSA, the binding constant (K_a) and the number of binding sites (n) can be determined by the following equation:

$$\frac{F_0 - F}{F} = K_a \times n \times log[Q]$$

F_0 and F are the tryptophan fluorescence intensities in the absence and presence of the quencher (Q) [5].

Protocol

Stock solutions of the galacto-conjugates at a concentration of 20 mM were prepared in DMSO and kept in dark conditions at RT. HSA was freshly prepared at a concentration of 2 μM in PBS buffer at RT. Two mL of HSA solution was titrated with increasing concentrations of galacto-conjugates, keeping always the final concentration of DMSO to no more than 0.15% (v/v).[6] The final concentrations of the conjugates were 0, 0.5, 1.0, 1.5, 2.0, 3.0, 4.0, 6.0, 8.0, 10.0, 15.0, 20.0, and 30.0 μM.

The fluorescence emission spectra of the HSA´s tryptophan residues were acquired for the wavelength range between 300 nm to 450 nm upon excitation at 280 nm. The excitation and emission slits width were set at 2.0 nm. The fluorescence quenching curves were obtained by plotting the tryptophan residues quenching (in percentage) against conjugates concentration. The tryptophan residues quenching (in percentage) was calculated, as follows:

$$Trypthophan\ residues\ quenching\ (\%) = \frac{(F_0 - F)}{F_0} \times 100$$

K_a and n values were determined by plotting the $log((F_0\text{-}F)/F)$ against log(**PorGal$_8$** or **PcGal$_{16}$** concentration), giving a linear plot, where $log(K_a)$ and $log(n)$ are the ordinate at the origin and slope, respectively.

[6] Over a concentration range of 0-0.5% (v/v), DMSO did not quench HSA fluorescence.

Synthesis and characterization of bioconjugates and immunoconjugates

Part II

2.1. Equipment and common materials

2.1.1. General equipment

The plate shaker was a Titramax 101 from Heidolph. The plate washer was an automatic 96-channel plate washer, ELx405 Select™ from BioTek Instruments.

2.1.1.1. Equipment for the UV-visible absorbance and fluorescence measurements

The microplate spectrophotometer used was a SpectraMax Plus384 from Molecular Devices controlled by SoftMax Pro software (v.5.3, Molecular Devices).

2.1.1.2. Liquid Chromatography (LC) coupled to Ultraviolet-Visible (UV) and Mass Spectrometric (MS) detection, LC-UV-MS

The LC-UV-MS used for the **Por 1-albumin** bioconjugates characterization, was an Agilent 1100 liquid chromatography system from Agilent Technologies and an API 4000 triple-quadrupole mass spectrometer from Applied Biosystems. Both instruments were controlled by Analyst TM software (v.1.4.2, Applied Biosystems).

2.1.1.3. Matrix-Assisted Laser Desorption/Ionization-Time Of Flight-Mass Spectrometry, MALDI-TOF-MS)

MALDI-TOF mass spectra of **Por 1-albumin** bioconjugates were acquired using a Bruker Reflex III MALDI mass spectrometer from Bruker-Daltonik, operated with a nitrogen laser and at 20 kV acceleration voltage.

2.1.2. Materials

The PD-10 Desalting Columns containing Sephadex G-25 Medium used for the purification of the immunoconjugates were from GE HealthCare.

The MaxiSorp^{TM} transparent microtiter plates with 96 flat-bottom polystyrene wells (plates used for the ELISA) possessing high protein-binding capacity were purchased from Nunc. The UV-Star^{TM} transparent microtiter plates with 96 wells, with an optical window down to 230 nm, were from Greiner Bio-One.

The Vivaspin 500 filters with a cut off 3 kDa used to concentrate the **Por 1-albumin** bioconjugates were supplied by Sartorius.

The HPLC column used in the LC-UV-MS assays was a protein reversed-phase column, Prot RP 18S, UltraSep ESD 300, 125 mm x 3 mm, from SepServ.

2.1.3. Reagents, antibodies and chemical products

Bovine Serum Albumin (BSA), the lyophilised albumin fraction V (min. 99%, receptor grade) used for preparing the conjugates, was purchased from Serva Electrophoresis (Ref. 11924). Human serum albumin (HSA), essentially fatty acid free, used for preparing the conjugates, was obtained from Sigma-Aldrich (Ref. A1887).

The mouse monoclonal antibody against caffeine (mAb anti-Caf) was purchased from USBiological (Ref. C0110-06) at a concentration of 1.0 $mg.mL^{-1}$. The mouse monoclonal antibody against human CD104 (mAb anti-CD104), was obtained from AbD Serotec (Ref. MCA1456). The secondary antibody used in the ELISA was the polyclonal antibody anti-mouse IgG (whole molecule)-Peroxidase, produced in goat, provided as a solution from Sigma-Aldrich (Ref. A4416). The caffeine-BSA conjugate was synthesized and directly provided by the PhD student Julia Grandke in the Immunoanalytics Division, Analytical Chemistry; Reference Materials, BAM, Berlin.

The porphyrin 1 (**Por 1**) containing an reactive ester group was synthesized and directly provided by Doctor Sandrina Silva of the Porphyrins and Phthalocyanines Materials Research Group, Department of Chemistry, University of Aveiro, Portugal.

Hydrogen peroxide (H_2O_2) 30% Trace Select and tetrabutylammonium borohydride (TBAB) were obtained from Fluka. 3,3`,5,5´-tetramethylbenzidine (TMB) and sulphuric acid (H_2SO_4) were from Baker, Tween™ 20 was purchased from Serva. Trifluoroacetic acid was purchased from Merck. Ultrapure Sinapic matrix for MALDI was supplied by Protea Biosciences. All other reagents were from Sigma.

2.1.4. Buffers and solutions

Table 4.1. Buffers used in the synthesis and characterization of bioconjugates (**Por 1-albumins**) and immunoconjugates (**Por 1-mAb anti-Caf** and **Por 1-mAb anti-CD104**).

Buffer/Solution name	Composition	pH
Sodium bicarbonate ($NaHCO_3$) buffer	0.1 M $NaHCO_3$ Prepared in Milli-Q water	9.3
Phosphate buffered saline (PBS) buffer	10 mM NaH_2PO_4 70 mM Na_2HPO_4 145 mM NaCl Prepared in Milli-Q water	7.60
Washing buffer	0.05% (v/v) Tween 20 Prepared in PBS buffer	7.60
Substrate buffer	220 mM Potassium dihydrogen citrate 0.5 mM Sorbic acid potassium salt Prepared in Milli-Q water	4.00
3,3',5,5'-Tetramethylbenzidine (TMB) solution	40 mM TMB 8 mM TBAB Prepared in N,N-dimethylacetamide	___
Peroxidase substrate	2.45% (v/v) TMB solution 3 mM H_2O_2 Prepared in substrate buffer	___

2.1.5. Softwares

Origin^{TM} 8.0 software from OriginLab was used for most of the displayed graphs. ChemDraw Ultra 12.00 from CambridgeSoft was the software used to draw the chemical structures.

2.2. Protocols

2.2.1. Bioconjugation of Porphyrin 1 (**Por 1**) with BSA, HSA, mAb anti-Caf and mAb anti-CD104

Principle

The conjugation of porphyrins with monoclonal antibodies (mAbs) or proteins (like albumin) can be carried out via activated ester derivatives [6]. A porphyrin bearing a *N*-hydroxysuccinimide (NHS) activated ester (**Por 1**) [7] reacts with the amine groups of the albumin or mAb in aqueous medium and slightly basic pH, provoking the elimination of the NHS (**Figure 4.2**):

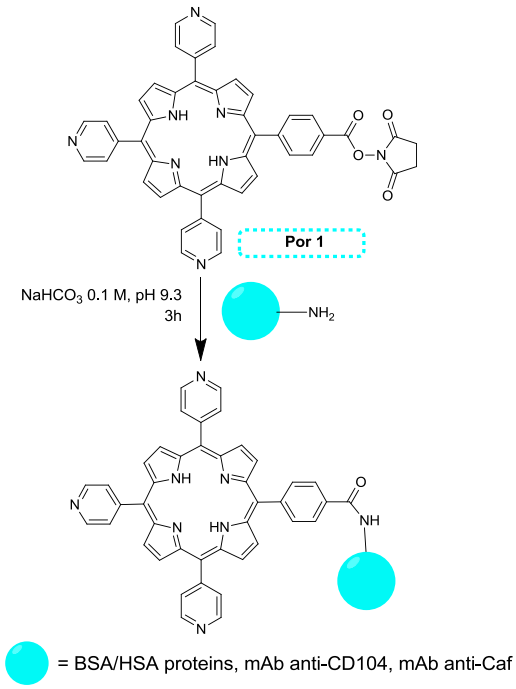

Figure 4.2. Por 1-albumin and **Por 1-mAbs** synthesis. The amine-reactive ester of the porphyrin is coupled to the amine groups of the albumins or mAbs in aqueous medium and basic pH.

Protocol: Preparation of Por 1 and BSA/HSA proteins for bioconjugation

A stock solution of **Por 1** at a concentration of 237 µM was prepared in anhydrous DMSO.[7] Stock solutions of BSA and HSA at a concentration of 6.85 µM were prepared in 0.1 M $NaHCO_3$, pH 9.3. The **Por 1-albumin** bioconjugates were prepared by mixing 30,

[7] **Por 1** contains an amine-reactive NHS-ester, which is susceptible to hydrolysis when water is present. Thus, stock solutions of this porphyrin were prepared in anhydrous DMSO and under a nitrogen atmosphere.

60, or 80 moles of **Por 1** with 1 mol of albumins, in a reaction volume of 2 mL in $NaHCO_3$ buffer (**Table 4.2**):[8]

Table 4.2. Molar reaction ratios used in the bioconjugation of **Por 1** with the albumins.

Molar reaction ratio (Por 1:Albumin)	Por 1 concentration (µM)	Albumin concentration (µM)	Reaction volume (mL)
30:1	206	6.87	2
40:1	206	3.43	2
80:1	206	2.57	2

Protocol: Preparation of Por 1, mAb anti-Caf and mAb anti-CD104 for bioconjugation

As a first approach, conjugation of **Por 1** with the mAb anti-Caf was performed. For that, a stock solution of **Por 1** at 237 µM was prepared in anhydrous DMSO.[7] The mAb anti-Caf was supplied at a concentration of 1 $mg.mL^{-1}$.[9] The **Por 1-mAb anti-Caf** conjugate was prepared by mixing 30 moles or 80 moles of **Por 1** with 1 mol of the mAb anti-Caf in a total reaction volume of 100 µL in $NaHCO_3$ buffer (**Table 4.3**):[8]

Table 4.3. Molar reaction ratios used for bioconjugation of **Por 1** with mAb anti-Caf.

Molar reaction ratio (Por 1:mAb anti-Caf)	Por 1 concentration (µM)	mAb anti-Caf concentration (µM)	Reaction Volume (µL)
30:1	66.36	2.21	100
80:1	66.36	0.83	100

For the **Por 1-mAb anti-CD104** bioconjugation, a stock solution of **Por 1** at a concentration of 660 µM was prepared in anhydrous DMSO.[7] The mAb anti-CD104 was supplied at a concentration of 1 $mg.mL^{-1}$.[10] The **Por 1-mAb anti-CD104** reaction ratio was

[8] The solutions were prepared before use under a nitrogen atmosphere, in microtubes sealed with parafilm.

[9] Considering the molecular weight of mAb Caf (whole antibody) equal to 150 kDa, the concentration of the stock solution was 6.67 µM.

[10] Considering the molecular weight of the mAb anti-CD104 (whole antibody) equal to 166 kDa, the concentration of the stock solution was 6.02 µM.

prepared using 30 moles of **Por 1** per 1 mol of mAb anti-CD104 in 50 µL of $NaHCO_3$ buffer (**Table 4.4**):[8]

Table 4.4. Molar reaction ratios used in the bioconjugation of **Por 1** with the mAb anti-CD104.

Molar reaction ratio (Por 1:mAb anti-CD104)	Por 1 concentration (µM)	mAb anti-CD104 concentration (µM)	Reaction Volume (µL)
30:1	180.60	6.02	50

Protocol: Bioconjugation and purification

The mixtures were gently agitated at RT for 3 h protected from light. The bioconjugates were then purified from remaining free **Por 1** or free albumin/mAb over a gel permeation chromatography (GPC) and kept in $NaHCO_3$ buffer. Four drops (about 100 µL) were collected in each well of a microtitre 96-wells plate. The eluted fractions were monitored at 418 nm (**Por 1** absorption at the wavelength of Soret band) and at 280 nm (albumin/mAb absorption wavelength), showing a single peak containing both the porphyrin and the albumin/mAb (i.e. the bioconjugate). The volumes of the wells with highest absorbance were pooled and stored at 4 ºC in darkness (**Figure 4.3**):

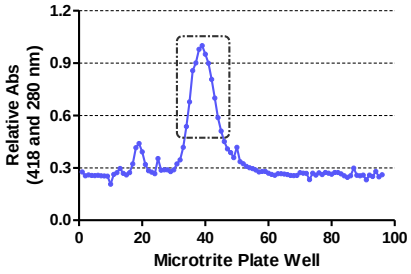

Figure 4.3. Bioconjugate recovery (**Por 1-mAb anti-CD104**) after clean-up on a Sephadex PD-10 column. The microtitre plate was read at 280 nm and 418 nm and the top fractions were combined.

Protocol: Characterization, degree of labeling

The degree of labeling (number of moles of **Por 1** per mole of conjugated albumin/mAb, DOL) was calculated using spectroscopic methods. The concentration of the albumins was determined considering the molar coefficient extinction (at 280 nm)

approximately equal to 47,000 $cm^{-1}.M^{-1}$. As for the antibodies, the concentration was determined as: $mAb\ concentration\ (mg.mL^{-1}) = \frac{Abs\ 280\ nm}{1.3}$.

The concentration of **Por 1** was determined photometrically at 418 nm using **Por 1** dilutions to set up the calibration curve. The DOL was derived for each conjugate at all the initial molar ratios employed as follows: $Degree\ of\ labelling\ (DOL) = \frac{Moles\ of\ Por\ 1}{Moles\ of\ Albumin/mAb}$.

2.2.2. Enzyme-Linked Immunosorbent Assays

Principle

The presence of the immunoconjugate **Por 1-mAb anti-Caf** in the sample collected after purification can be confirmed by an indirect ELISA [8]. Moreover, ELISA can be used to investigate whether the conjugation affects the immunoreactivity of the mAb anti-Caf. Firstly, the **Por 1** conjugated with the monoclonal antibody against caffeine is immobilized in a solid support. For that purpose, the solid support needs to be coated with a conjugate BSA-caffeine (**Figure 4.4**, Step 1). The BSA-caffeine conjugate has two functions: the BSA will be coated to the solid support and the caffeine will be recognized by the mAb anti-Caf, which, in turn, is conjugated with **Por 1** (**Figure 4.4**, Step 2). Next, a specific antibody (secondary antibody) linked to an enzyme (peroxidase) is applied over the surface, recognizing the mAb anti-Caf (**Figure 4.4**, Step 3). In the final step, a solution containing the enzyme´s substrate is added producing a detectable signal at 450 nm (**Figure 4.4**, Step 4).

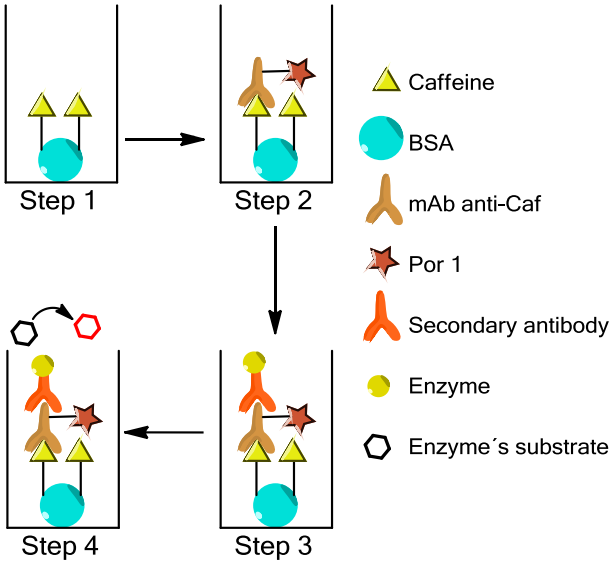

Figure 4.4. Illustration of the competitive indirect ELISA, used in this thesis. The reservoir (squared-like shape) represents the wells of a microtitre plate well.

Protocol

Conjugate BSA-caffeine and secondary antibody dilutions (in PBS buffer previously equilibrated at RT) were optimized in order to provide an acceptable absorbance signal (between 0.5 and 1 at the wavelength of 450 nm after ELISA). A 1,000-fold dilution for the conjugate BSA-caffeine and a 10,000-fold dilution for the secondary antibody originated the optimal absorbance values. The transparent high-binding microtitre 96-wells plates were coated directly with the conjugate BSA-caffeine (100 µL per well) diluted 1,000-fold in PBS buffer, covered with parafilm and incubated overnight (about 16 h at RT) on a microtiter plate shaker at 750 rpm. The plates were then washed once with washing buffer (PBS containing 0.05% (v/v) Tween 20). After addition of 100 µL per well of the bioconjugate PS-mAb anti-Caf diluted in PBS buffer (1,000-fold or 10,000-fold), the plates were covered with parafilm to avoid evaporation and incubated for 3 h with shaking. Thereafter, the plates were washed once again with the washing buffer. The secondary antibody diluted in PBS 1:10,000 was added to the plate (100 µL per well) and incubated for 1 h on the plate shaker at RT. After washing out the calibration standards, samples and unbound secondary antibody, 100 µL of peroxidase substrate (prepared prior to use) was added into the wells and incubated for 16 min with shaking, protected from light at RT.[11]

[11] In the presence of peroxidase substrate, the solution becomes blue and after H_2SO_4 addition, it becomes yellow.

The reaction was stopped using 50 µL of 1 M H_2SO_4, per well. The optical density was measured at 450 nm using 650 nm as the reference wavelength.

2.2.3. Matrix-Assisted Laser Desorption/Ionization-Time Of Flight-Mass Spectrometry assay, MALDI-TOF-MS

Principle

The **Por 1-albumin** bioconjugates can be characterized by mass spectrometry based techniques such as MALDI/TOF-MS [9].

In this technique, the sample is mixed with a chemical matrix which contains an organic molecule with a cromophore. After spot the mixture into a small plate it is allowed to dry, forming a crystal lattice into which the protein to be characterized is mixed. The plate is then placed into the source which has a laser that emits a beam of light to the sample. The organic molecule in the matrix absorbs energy at the wavelength of the laser radiation and transfers this energy to the protein in the matrix. With this energy, the protein is ejected from the target surface (without undergoing thermal degradation) to the gas phase and accepts a proton (gas-phase proton-transfer reactions), producing ions.

Then, the TOF analyzer measures the time it takes for the ions to fly from one end of the analyzer to the other and strike the detector. The speed by which the ions fly down the analyzer tube is proportional to their mass-to-charge (m/z) ratios.

In such way, with the MALDI interface it is possible the detection of the "full" molecule, since the process causes little or no fragmentation of the protein or protein conjugated with **Por 1**, allowing the detection of the molecular ion. The native and conjugated protein masses can be directly obtained from the spectra.

Protocol

The **Por 1-albumin** bioconjugates purified by GPC, were concentrated by ultrafiltration (diafiltration) using filters with a cut-off of 3 kDa (Vivaspin 500 µL).[12] For that, 100 µL of the conjugate was placed in the concentrator of the Vivaspin. The assembled concentrator was centrifuged at 15,000 *x g* at 20 ºC for 5 min. After emptying

[12] In this process it is important to remove salts and buffers (that will compete with the molecular ion peaks, affecting negatively MS analysis) and to concentrate the sample.

the filtrate container, the concentrate was refilled with 100 µL of Milli-Q water and the sample was centrifuged once more. The last step was repeated and the samples were kept at 4 ºC.

The albumin´s solutions were freshly prepared at a concentration of 2 $mg.mL^{-1}$ in Milli-Q water.

Sinapic acid MALDI matrix was freshly prepared in aqueous solution at a concentration of 10 $g.L^{-1}$ containing 50% (v/v) acetonitrile and 0.1% (v/v) trifluoroacetic acid. The concentrated sample was mixed up with the matrix 1:2 (by volume), added onto the plate[13] and air-dried for at least 1 h. The data were assessed using Origin 8.0 software and the resulting mass spectra data were fitted by a Lorentzian function, assigning the centres of the resulting peaks to unconjugated albumins and **Por 1-albumin** bioconjugates masses (the m/z values).

2.2.4. Liquid Chromatography (LC) coupled to Ultraviolet-Visible (UV) and Mass Spectrometric (MS) detection, LC-UV-MS assays

Principle

The **Por 1-albumin** bioconjugates can also be characterized by LC-UV-MS [10]. The LC-UV-MS encloses three interfaces: High Performance Liquid Chromatography (HPLC), Ultraviolet-Visible spectroscopy (UV) and Mass Spectrometry (MS). The HPLC separates the components present in the sample by reverse phase chromatography. The conjugate is detected first via a photodiode array (PDA), taking into account the absorbance of albumin and **Por 1** at 280 nm and 418 nm, respectively. Then, on the mass spectrometer, the metabolites are ionized (by electrospray ionization, ESI) and the mass detector separates all ions that have different masses producing a high full resolution spectrum. The spectra obtained are then reconstructed, using the Bayesian Protein Reconstruction add-in feature from the Analyst™ software and the conjugate mass range can be determined.

[13] This steep needs to be performed quickly, since the mixture can dry before its application in the sample plate.

Protocol

After concentrating the samples, as aforementioned for the MALDI/TOF-MS, the **Por 1-albumin** bioconjugates characterization by LC-UV-MS was performed. The separation was performed on a reverse-phased protein column with a binary gradient consisting of eluent A (0.1% trifluoroacetic acid in Milli-Q water) and eluent B (0.1% trifluoroacetic acid in methanol), at a flow rate of 450 μL.min^{-1}. The column oven temperature was set at 30 ± 2°C. The injection volume was 10 μL. The gradient profile is provided in **Table 4.5**.

Table 4.5. Gradient profile used in LC-UV-MS assays for the **Por 1-albumin** bioconjugates characterization.

t (min)	% B
0	60
3	60
12	90
25	90
25.1	60
35	60

For the diode array detection (DAD) the wavelength range 190 to 900 nm was chosen with a step width of 2.0 nm. The settings shown in **Table 4.6** were used for the LC-UV-MS measurements.

Table 4.6. MS profile used in LC-UV-MS assays for the **Por 1-albumin** bioconjugates characterization.

Ionization	ESI in the positive ion mode
Acquisition mode	Scan from 200.0-3000.0 a.m.u
Dwell time	2 sec
Curtain gas	30 psi (207 KPa)
Ion source gas #1	50 psi (345 kPa)
Ion source gas #2	50 psi (345 kPa)
Source temperature	500°C
Entrance potential	10 V
Declustering potential	70 V
Ion spray voltage	5.0 kV

The conjugates were identified after extracting the chromatograms at the wavelengths 280 nm (for the albumins) and at 418 nm (for **Por 1**). The m/z range was extracted between 1,000 to 3,000 and the Bayesian Protein Reconstruction was applied, using the Bio tools extension of Analyst TM software (starting mass: 20,000 Da; stop mass: 70,000 Da; step mass: 1 Da; S/N threshold: 20; 20 iterations).

In vitro biological assays

Part III

3.1. Equipment and common materials

3.1.1. General instrumentation

3.1.1.1. General equipment

The centrifuge used was a SIGMA 2-16 and the microcentrifuge was a VWR MiniFuge Galaxy MiniStar C1413. The vortex was from VWR. The liquid aspirator system used was the Vacusip from Integra. The shaker used was a standard analog shaker from VWR.

3.1.1.2. Equipment for the UV-visible absorbance and fluorescence measurements

The UV-visible absorbance measurements were performed on a microplate reader Synergy™ HT (Biotek Instruments) controlled by BioTek's Gen5™ Data Analysis Software. For the porphyrin based photosensitizers, the fluorescence measurements were also performed on this equipment. For the phthalocyanine based photosensitizers, the fluorescence measurements were determined using the IVIS Lumina XR system (Caliper Life Sciences) in combination with its Living Image Software.

3.1.1.3. Equipment for the cells irradiation

A LED array was prepared by Mr. Cândido Casqueira, electromechanic technician of the Departement of Chemistry of the University of Abeiro, and it was used in the irradiation assays. It is composed of a matrix of 24 x 16 LEDs which makes a total of 384 light sources, emitting white light with two emission peaks at $\lambda = 450 \pm 20$ and $\lambda = 550 \pm 50$ nm (**Figure 4.5)**. The regulated Plug-in adaptor with LED indicator 800 mA was purchased from MW.

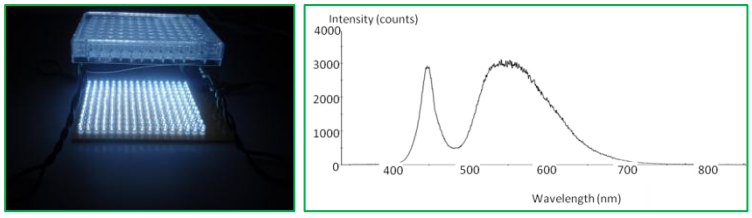

Figure 4.5. (Left) Image of the LED array used in the photodynamic experiments. (Right) Emission spectra of the LED array system.

3.1.1.4. Equipment for the Western Blotting

The Mini Protean electrophoresis system and the Mini Trans-Blot system were from Bio-Rad Laboratories. The tube roller SRT6D was from Stuart. The chemiluminescence detection system used was the Chemi Doc^{TM} XRS from Bio-Rad controlled by the software Quantity One.

3.1.1.5. Microscopes

The fluorescence microscope was purchased from Leica Microsystems (Model DFC350) and the confocal microscope was from Zeiss (LSM 710, Carl Zeiss).

3.1.2. Materials

Canted neck cell culture flasks 75 cm^2 with 0.2 µM vent cap were purchased from Corning. CyroPure tubes were purchased from SARSTEDT. The tissue culture testplates and the conical tubes of 15 mL or 50 mL were from Orange Scientific. Rubber spatulas, cell scrappers were purchased from Greiner Bio-One. The Coverslip Glasses with diameters of 5 mm were purchased from Warner Instruments. The Neubauer chamber was from VWR. The Immun-Blot PVDF membranes were purchased from Bio-Rad. The plates used were transparent (Orange Scientific) and black (Greiner Bio-One) 96-wells microtiter plates for the absorbance and fluorescence studies, respectively.

3.1.3. Cell culture and trypsins

UM-UC-3 (ATCC Number: CRL-1749^{TM}) and HT-1376 (ATCC Number: CRL-1472^{TM}), human bladder transitional cell carcinoma cell lines, have been isolated from urinary bladder of a male and a female Caucasian aged 58 years, respectively, with a grade 3 bladder carcinoma.

EMEM medium: ATCC-formulated Eagle´s Minimum Essential Medium (EMEM) from ATCC (Ref. 30-2003) with Earle´s Balanced Salt Solution, Nonessential Amino Acids, Sodium pyruvate, 10% (v/v) heat-inactivated Fetal Bovine Serum (FBS) from Gibco (Ref. 10270-106) and 1% (v/v) antibiotic/antimicotic containing penicillin, streptomycin and amphotericin B from Sigma-Aldrich (Ref. 15240-062).

N2 medium with 1% (m/v) of methylcellulose: Serum-free Dulbecco´s Modified Eagle Medium/Nutrient Mixture F-12 Ham (DMEM/F12 was purchased from Sigma-

Aldrich (Ref. D2906) with 1% (m/v) of methylcellulose (Sigma-Aldrich, Ref. M0387) supplemented with 1% (v/v) antibiotic/antimicotic containing penicillin, streptomycin and amphotericin B from Sigma-Aldrich (Ref. 15240-062), 20 nM progesterone (Sigma-Aldrich, Ref. P7556), 100 µM putrescine (Sigma-Aldrich, P5780), 1% (v/v) of the supplement insulin(20 $\mu g.mL^{-1}$)-transferrin(25 $\mu g.mL^{-1}$)-selenium(30 nM) (Gibco Invitrogen Life Technologies), 10 $ng.mL^{-1}$ human basic fibroblast growth factor (bFGF, Peprotech EC) and 10 $ng.mL^{-1}$ human recombinant epidermal growth factor (EGF, Sigma-Aldrich, Ref. E9644).

Trypsin-EDTA 0.25% (w/v) and Trypsin Tryple Express were purchased from Gibco (Refs. 25200-072 and 12605-010, respectively). Accutase™ was purchased from Sigma-Aldrich (Ref. A 6964).

3.1.4. Proteins, molecular weight marker and antibodies

Bovine Serum Albumin (BSA), the lyophilized albumin fraction V was purchased from Biochemical (Ref. 441554Y).

The protein standard for the western blotting assays was the Precision Plus Protein™ Dual Color standard, containing ten protein bands (10, 15, 20, 25, 37, 50, 75, 100, 150, and 250 kDa) from Bio-Rad (Ref. #161-0374).

Table 4.7. Primary antibodies used in the western blotting and immunofluorescence assays.

Antibody	Antigen Molecular Weight (kDa)	Dilution		Supplier
		Western Blotting	Immunofluorescence	
Mouse Monoclonal Antibody against CD44 antigen (PGp-1)	90	___	1:50	Santa Cruz Biotechnology
Rabbit Monoclonal Antibody against Galectin-1 antigen	14	1:1000	1:100	Abcam
Mouse Monoclonal Antibody Against CHOP antigen	27	1:1000	___	Cell Signaling
Mouse Monoclonal Antibody against Bcl-2 antigen	26	1:200	___	Santa Cruz Biotechnology
Rabbit Monoclonal Antibody against Phospho-Akt antigen	60	1:2000	___	Cell Signaling
Rabbit Monoclonal Antibody against Akt antigen	60	1:1000	___	Cell Signaling
Rabbit Polyclonal Antibody against Bax antigen	20	___	1:50	Santa Cruz Biotechnology
Mouse Monoclonal Antibody against β-actin antigen	43	1:20000	___	Sigma-Aldrich
Mouse Monoclonal Antibody against ABCG2 (BCRP) antigen	70	1:500	___	Millipore

The horseradish peroxidase-conjugated secondary anti-rabbit (GAR-HRP) or anti-mouse (GAM-HRP) antibodies, used in the western blotting assays, were purchased from Bio-Rad.

The secondary anti-rabbit or anti-mouse antibodies, used in the immunofluorescence assays, were the Alexa Fluor 488 Goat Anti-Rabbit and Alexa Fluor 568 Goat Anti-Mouse, purchased from Molecular Probes.

3.1.5. KITS and probes

The Immun-Star^{TM} WesternC^{TM} Chemiluminescent Kit (containing the chemiluminescent substrate: luminol/enhancer and peroxide solution) used in the western blotting assays was from Bio-Rad.

The Pierce BCA Protein Assay Kit-Reducing Agent Compatible (containing the BCA Protein Assay Reagent and BSA standards at 2 $mg.mL^{-1}$) was purchased from Thermo Scientific.

The 4′,6-Diamidino-2-phenylindole (DAPI) was purchased from Enzo Life Sciences.

The 2´,7´-dichlorohydrofluorescin (H_2DCFDA) and dihydroethidium (DHE) were purchased from Life Sciences. TRITC (tetramethylrhodamine isothiocyanate)-conjugated phalloidin was purchased from Sigma.

3.1.6. Buffers, reagents and chemical products

$PorGal_8$ and **$PcGal_{16}$** were synthesized by Doctor Sandrina Silva in the Porphyrins and Phthalocyanines Materials Research Group, Department of Chemistry, University of Aveiro, Portugal. **Por 1-albumin** bioconjugates and **Por 1-mAb anti-CD104** were synthesized as described in Part II.

Sodium Chloride (NaCl), Triton X-100, formaldehyde (PFA) and sodium azide (NaN_3) extra pure were from Merck. Tris Base ULTROL Grade was from CalbioChem. Protease inhibitor cocktail tablets were purchased from Complete Mini.

Glycerol electrophoresis reagent, DL-dithiothreitol 99%, bromophenol blue salt solution, sodium dodecyl sulfate (SDS), ethylene glycol tetraacetic acid (EGTA), iodoacetamide (IAD), phenylmethanesulfonyl fluoride (PMSF), sodium deoxycholate (DOC), Tween 20, DMSO Hybri-Max™, 3-[4,5-dimethylthiazol-2-yl]-2,5-diphenyl-tetrazolium bromide (MTT), ammonium persulfate, TEMED electrophoresis reagent, glycine, D(+)Galactose, L-histidine, L-cysteine, poly(2-hydroxyethyl methacrylate) poly-HEMA and agarose were purchased from Sigma-Aldrich.

The trypan blue stain 0.4% was from BioWhittaker Reagents, Lonza. The 2-propanol was from J.T.Baker BAKER ANALYZED™ A.C.S reagents. The methanol (MeOH) was from EMSURE, Merck. The hydrochloric acid (HCl) 37% was from Panreac.

The acrylamide/Bis 20% solution was from BIO-RAD. The ECL reagent was from Amersham Biosciences.

The Glycergel was purchased from DAKO. The VectaSHIELD mounting medium with DAPI was purchased from VECTOR.

Table 4.8. Buffers used in the biological studies. All buffers were prepared in Milli-Q water unless other solvent is mentioned.

	Buffer name	Composition	pH
	PBS buffer	137 mM NaCl, 27 mM KCl, 81 mM Na_2HPO_4, 15 mM KH_2PO_4	7.30
	1% SDS lysis buffer	1% (v/v) SDS , Prepared in PBS buffer	7.00
	RIPA buffer	150 mM NaCl, 50 mM Tris base, 5 mM EGTA, 1% (v/v) Triton X-100, 0.5% (m/v) DOC, 0.1% (m/v) SDS, 2 mM PMSF, 2 mM IAD, 1 tablet of protease inhibitor cocktail	7.50
	6x Laemmli buffer	350 mM Tris-HCl, pH 6.8, 30% (m/v) glycerol, 10% (m/v) SDS, 600 mM DTT, 0.012% (m/v) bromophenol blue	6.80
	1.5 M Tris-HCl buffer	1.5 M Tris base	8.80
	0.5 M Tris-HCl buffer	0.5 M Tris base	6.80
	Fixation buffer	4% (v/v) PFA, Prepared in PBS buffer	7.30
Western Blot	Running buffer	25 mM Tris base, 192 mM Glicyine, 0.1% (m/v) SDS	8.80-8.50
	Transfer buffer	25 mM Tris base, 192 mM Glycine, 20% (v/v) MeOH, 0.005% (m/v) SDS	8.00-8.50
	Tris Buffer Saline Tween20 (TBST) buffer	20 mM Tris base, 150 mM NaCl, 0.1% (v/v) Tween 20	7.60
	Blocking buffer	5% (v/v) non-fat milk or 3% (v/v) BSA, Prepared in TBST buffer	7.60
Immunofluorescence	Blocking buffer	5% (v/v) BSA or 1:10 (by volume) goat serum, Prepared in PBS buffer	
	Permeabilization buffer	1% (v/v) Triton X-100, 0.02% (m/v) BSA, 0.02% (m/v) NaN_3, Prepared in PBS	7.30
	PBS Triton X-100 (PBST) buffer	0.25% (v/v) Triton X-100, 1% (m/v) BSA, 0.02% (m/v) NaN_3, Prepared in PBS	7.3
	Washing buffer	0.02% (m/v) BSA, 0.02% (m/v) NaN_3, Prepared in PBS	7.3

3.1.7. Softwares

Paint Shop Pro™ (v.6.00, Jasc Software) was used for the treatment of the images obtained in microscopy.

ImageJ 1.42n (Wayne Rasband, National Institutes of Health, USA) was used for the quantification of the proteins expression on western blotting assays.

GraphPad Prism (v.5.00, GraphPad Software) was used for most of the displayed graphs, as well as for the statistical analysis.

3.1.8. Statistical Analysis

The results are presented as mean ± standard deviation (S.D.) with n indicating the number of experiments. Statistical significance among two conditions was assessed using the nonparametric Mann-Whitney test. Statistical significance among three conditions was assessed by the nonparametric Kruskal-Wallis test. Statistical significance among several conditions was assessed with the Friedman test. P-value was considered at the 5% level of significance to deduce inference of the significance of the data.

3.2. Protocols

3.2.1. Maintenance of UM-UC-3 and HT-1376 bladder cancer cell lines

Principle

Animal cell lines, obtained from certain cancer cells and from genetic engineering, under the appropriate nutrients and strict aseptic conditions grow and replicate in culture [11].

Protocol: Defrosting Cells

The human bladder carcinoma cell lines were frozen in 1 mL vials in liquid nitrogen. The vial content was thawed, as fast as possible, in 37 ºC water bath and transferred to 5 mL of prewarmed EMEM medium. After centrifugation at 1,000 *x g* during 5 min, appropriate aliquots of cell suspension were added to new 25 cm^2 or 75 cm^2 cell culture flasks. Cells grown in monolayer at 37 ºC in a humidified incubator gassed with 5% carbon dioxide (CO_2) and 95% air.

Protocol: Subculturing

After 1 week or 3 days, respectively, HT-1376 and UM-UC-3 cell layers were normally confluent, and subculturing was necessary. The EMEM medium was removed

from culture flasks by aspiration and discarded. The cell layers were rinsed with 5 mL of warm sterile PBS, in order to remove traces of serum which would inhibit the action of the trypsin. UM-UC-3 and HT-1376 cells were treated with 0.033 $mL.cm^{-2}$ of trypsin Tryple Express or 0.040 $mL.cm^{-2}$ of trypsin-EDTA, respectively. The trypsinization progress was monitored under an inverted microscope. Flasks were incubated at 37 ºC until the cells rounded up and the cell layer begun being dispersed: 5 min or 8 min to 10 min for the cell line UM-UC-3 and HT-1376, respectively. EMEM medium (0.1 $mL.cm^{-2}$) was added to inhibit further tryptic activity and the cells were dispersed by repeated pippeting over the surface bearing the monolayer. The cells suspensions were then centrifuged at 1,000 *x g* for 5 min. The supernatant was removed, the cells were re-suspended in EMEM medium and appropriate aliquots of cells were added to new 25 cm^2 or 75 cm^2 culture flasks. Cells were examined carefully every day by eye on an inverted microscope, for signs of contamination and the EMEM medium was changed two or three times per week.[14] UM-UC-3 and HT-1376 cells were subcultivated at a ratio of 1:4 to 1:10 or 1:2 to 1:6, respectively, in the conditions described above.

Protocol: Freezing Cells

UM-UC-3 and HT-1376 cells were stored frozen as stocks in liquid nitrogen using EMEM medium containing 10% (v/v) DMSO at a density of 2-4 x 10^6 $cells.mL^{-1}$. Cells were also frozen at -80 ºC for short times. Cells were harvested in the same manner used for routine subculture. The cell pellet was re-suspended in EMEM medium to give a final concentration of about 3 x 10^6 $cells.mL^{-1}$ and 900 µL were aliquot into each sterile vial containing 100 µL of sterile DMSO. The cells were frozen in a -80 ºC freezer prior to transfer to liquid nitrogen.

3.2.2. HT-1376 sphere-formation assay

Principle

Cancer stem-like cells (CSCs) can be isolated from the HT-1376 cell line using the sphere-formation assay in ultra-low attachment surfaces. The general idea of the sphere-formation assay is that each sphere derived from a single cell is clonal. For that assay, HT-

[14] The cells HT-1376 were growing slowly and only half the medium was removed and replaced.

1376 cells are trypsinized and single cells are plated in non-adherent conditions in serum-free supplemented with epidermal growth factor (EGF) and basic fibroblast growth factor (bFGF). A small population of cells will began to divide, forming spheres of proliferating cells. To show self-renewal, the formed spheres are dissociated and cultured again in the presence of EGF and bFGF, with a subset forming secondary spheres.

The spheres obtained with this method were designated CSCs HT-1376.

Protocol: Coating cell culture plates

The 6-wells or 96-wells cell culture plates were coated with 50 µL per cm^2 of 10% (m/v) poly-HEMA solution prepared in 95% ethanol or 1% (m/v) of agarose prepared in Milli-Q autoclaved water. The plates were dried at RT overnight and sterilized under UV light for at least 2 h. The plates were then rinsed with sterile warm PBS.

Protocol: Culturing HT-1376 cells as spheres

Adherent HT-1376 cells growing in EMEM medium[15] were detached with trypsin and plated in N2 medium with 1% (m/v) methylcellulose, at a density of 4,200 cells.cm^{-2} in 6-wells or 96-wells coated cell culture plates (according to the experiment). Spheres were formed in suspension at 37 ºC in a humidified incubator gassed with 5% carbon dioxide (CO_2) and 95% air. The EGF and bFGF growth factors 10 ng.mL^{-1} were added twice a week.[16] After 5 to 7 days in culture, the first generation spheres were expanded. For that, they were removed from the 6-wells cell culture plates and centrifuged at 1,000 *x g* for 5 min. After washing with warm PBS, the supernatant was removed and the cells were re-suspended in N2 medium (without methylcellulose) containing 2% (v/v) FBS. The cells were allowed to attach to adherent 25 cm^2 flask surfaces as described above (Part III, 3.2.1). After reaching 60% to 80% confluence (10-12 days), the expanded cells were re-seeded in stressful growth conditions for the formation of secondary generation spheres. For that, the cells were detached with trypsin and plated in N2 medium with 1% (m/v)

[15] The cells should have about 80% of confluence and only cells with viability above 90% were used in all experiments. For these experiments, the tryptic digestion was inhibited with 1 mL of EMEM medium (with low FBS concentration, 0.02% v/v) because the addition of the serum results in cells differentiation and their growth as an adherent layer.

[16] The cells were evaluated daily to follow sphere formation, to ensure that they were derived from single cells and that they did not become confluent and adherent during the experiment.

methylcellulose, at a density of 4,200 cells.cm^{-2} in 6-wells coated cell culture plates (2 mL per well).

Protocol: Counting the spherical colonies

The total number of spherical colonies obtained at each passage was determined by platting the cells in N2 medium with 1% of methylcellulose, at a density of 4,200 cells.cm^{-2} in 96-wells coated cell culture plates (100 µL per well). After 5-7 days in culture, the spheres were counted using a light microscope. The results were expressed as follows: $Sphere\ formation\ efficiency\ (\%) = \frac{Number\ of\ spheres\ formed}{Total\ number\ of\ cells\ seeded} \times 100.$

3.2.3. Preparation and treatment of UM-UC-3, HT-1376 and CSCs HT-1376 cells with photosensitizers

Principle

UM-UC-3, HT-1376 and CSCs HT-1376 cells in exponential growth (in conventional monolayer culture) are treated with working sterile solutions of PSs.

Protocol: Preparing PSs working solutions

Stock solutions of the PSs at a concentration of 2 mM were prepared in DMSO and stored at 0-4 ºC in dark conditions. Freshly working solutions were prepared from the respective stock solution in sterile PBS, accounting their water solubility range. The concentration of DMSO was always lower than 0.45% (v/v), in all working solutions.

Protocol: Preparing UM-UC-3 and HT-1376 bladder cancer cell lines, and CSCs HT-1376

UM-UC-3 and HT-1376 adherent cells were detached with trypsin as described before (Part III, 3.2.1).

HT-1376 second generation spheres were dissociated with accutase during 3 min. EMEM medium was then added to inhibit accutase/trypsin activity and cells were dispersed by repeated pippeting up and down for 4 min. The cells suspensions were then centrifuged at 1,000 *x g* for 5 min.

The cells were re-suspended in EMEM medium and seeded into cell culture plates (plates of 6, 12, 24, or 96-wells according to the experiment) at a density of 9.4 x 10^4

cells.cm^{-2} [17] and incubated overnight in an incubator at 37 ºC with 5% CO_2 and 95% air to promote cell adhesion.

Protocol: Treatment of UM-UC-3 and HT-1376 bladder cancer cell lines, and CSCs HT-1376 with photosensitizers

After seeding the cells overnight, the EMEM medium was removed and the cells were washed with PBS.[18] The cells were incubated in dark conditions at various periods of time with increasing concentrations of PSs in sterile PBS.

3.2.4. Determination of intracellular photosensitizer concentration by fluorimetry

Principle

Taking into account the fluorescence properties of the porphyrin and phthalocyanine PSs, their concentration inside the cancer cells can be determined by fluorimetry (after cell lysis) and normalized to total protein quantity.

The concentration of proteins in a sample can be measured spectrophotometrically using the Bicinchoninic Acid Assay (BCA assay), also known as the Smith assay [12]. The procedure involves two steps. The first is the biuret reaction, whose faint blue color results from the reduction of cupric ion (Cu^{2+}) to cuprous ion (Cu^{+}) by peptide bonds in protein, in an alkaline environment. Therefore, the amount of reduced Cu^{2+} is proportional to the amount of protein present in the solution. The second is the chelation of two molecules of BCA with one cuprous ion, resulting in an intense purple-colored product that strongly absorbs light at the wavelength of 562 nm. The BCA-copper complex exhibits a strong linear absorbance at 562 nm with increasing concentration of protein. The purple color can be measured at any wavelength between 550 nm and 570 nm with minimal loss of signal.

[17] The concentration of viable cells per milliliter of cell supession was calculated using the Trypan Blue Staining (described on the Part III, 3.2.7.2). Only cells with viability above 90% were used in all experiments.

[18] This washing step allows the elimination of serum proteins that are able to interact with the PSs.

Protocol: Determination of intracellular photosensitizer fluorescence by fluorimetry

UM-UC-3, HT-1376 and CSCs HT-1376 cells were seeded into 96-wells cell culture plates at a density of 3 x 10^4 cells per well (final volume of 100 µL per well) and incubated overnight in an incubator at 37 ºC with 5% CO_2 and 95% air. On the following day, immediately after PSs incubation (as described in Part III, 3.2.3), cells were washed twice with PBS. Cells were mechanically scrapped in 130 µL of 1% (m/v) SDS solution in PBS (pH 7.0) and the plate was stirred on an automatic plate shaker in the dark at RT. One hundred µL of this cell suspension was transferred to 96-wells black plates and the intracellular fluorescence of the PSs was determined by fluorometric measurement, using standard PSs solutions for calibration. For the porphyrin based PSs, the intracellular fluorescence was determined using the plate reader fluorometer in combination with its software. For these PSs, the excitation and emission filters used were 360/40 nm and 645/40 nm, respectively. For the phthalocyanine based PSs, the intracellular fluorescence was determined using the IVIS Lumina XR equipment. For these PSs, the excitation and emission filters used were 675 nm and 695-770 nm, respectively. The PS concentration in the samples was directly obtained by plotting the average of the fluorescence for each PS standard in function of its concentration (µM).

Protocol: Determination of total protein

In a 96-wells plate, the following solutions were pipetted into each well:

- 25 µL of sample buffer: 1% (m/v) SDS in PBS (pH 7.0),

- 25 µL of sample, blank (sample buffer), standard (prepared in the sample buffer at concentrations ranging from 12.5-800 $\mu g.mL^{-1}$ using the BSA standard at 2 $mg.mL^{-1}$),

- 200 µL of BCA working Reagent (50 parts of BCA reagent A mixed with one part of BCA reagent B).

The plate was incubated at 37 ºC for 30 min. Then, the absorbance at 570 nm was measured in the plate reader spectrophotometer. The protein concentration in the samples was directly obtained by plotting the average of the absorbance at 570 nm for each BSA standard in function of its concentration ($\mu g.mL^{-1}$).

Protocol: Calculations

The PS uptake curves were obtained by non linear regression analysis (using GraphPad), accordingly to the following equation:

$$Uptake\ (nmol\ PS\ per\ mg\ of\ protein) = \frac{B_{max} \times [PS]}{K_d + [PS]}.$$

The B_{max} is the maximum extrapoled value of the PS uptake (nmol of PS per mg of protein) and K_d is the PS concentration needed to achieve a half maximum uptake at equilibrium.

3.2.5. Determination of intracellular photosensitizer fluorescence by fluorescence microscopy

Principle

Based on the fluorescence properties of the porphyrin and phthalocyanine based PSs, their distribution inside the cells can be evaluated by fluorescence microscopy.

Protocol

Coverslips (three coverslips per well in 12-wells culture plates) were coated with poly-L-lysine (diluted 1:10, by volume, in sterile PBS) for 1 h at RT. The coverslips were allowed to dry completely at RT. The UM-UC-3 and HT-1376 cells were plated carefully at a density of 1.8 x 10^5 cells or 3.6 x 10^5 cells per well (2 mL per well), respectively, in 12-wells culture plates for 24 h before treatment. After photosensitizer uptake and washing, cells were fixed with 4% PFA for 10 min at RT. The samples were washed with PBS (3 x 5 min). The coverslips were mounted using the VectaSHIELD mounting medium,[19] sealed with nail polish and stored at 4 ºC until visualization under the fluorescence microscope.

3.2.6. Photodynamic assays

Principle

The excitation of a potential PS (previously accumulated in cancer cells) with light at a specific wavelength induces cell toxicity, which is mediated by ROS generation. It is expected that, besides the preferential accumulation of the PS in cancer cells, they produce

[19] The mounting medium is applied on a slide and the coverslip with cells on top is added.

toxicity just after activation by light. Thus, it is important to evaluate both the PS toxicity in the absence of light and after light irradiation.

Protocol: Irradiation

After PSs incubation (as described in Part III, 3.2.3), the cells were washed twice with PBS and covered with 100 µL of fresh medium. In a dark room, the cells were irradiated for variable times with a LEDs array system emitting white light with two emission peaks at $\lambda = 450 \pm 20$ and $\lambda = 550 \pm 50$ nm. The cell culture plates were placed above the LEDs. Under these conditions, most of the light was emitted at a potency of 8.4 $mW.cm^{-2}$. After irradiation, cells were incubated for selected time points in the humidified incubator gassed with 5% CO_2 and 95% air.

3.2.7. Cell viability assays

3.2.7.1. MTT colorimetric assay

Principle

3-[4,5-dimethylthiazol-2-yl]-2,5-diphenyl-tetrazolium bromide (MTT, yellow-colored) is added directly to the medium in the wells and incubated for 2-4 h. In living cells, MTT is reduced to an insoluble formazan (giving a blue purple colour), being this reduction proportional to the mitochondrial enzyme succinate dehydrogenase activity [13].

Protocol

For the MTT colorimetric assays, the UM-UC-3, HT-1376 and CSCs HT-1376 cells were plated at a density of 3×10^4 cells per well (100 µL per well), in 96-wells culture plates for 24 h before treatment. Next, the cells were treated with the photosensitizer and the photodynamic treatment was performed, as described before (Part III, 3.2.3 and 3.2.6). Twenty four, 48, or 72 h after treatments, 50 µL of the medium was removed and 10 µL of MTT stock solution (3 $mg.mL^{-1}$ in PBS buffer) was added to each well at a final concentration of 0.5 $mg.mL^{-1}$. The plates were then wrapped in aluminium foil and incubated in the darkness at 37 ºC for 4 h. The resulting purple needle-shaped crystals were dissolved by the addition of 200 µL acidic isopropanol (0.04 M HCl in absolute isopropanol). To solubilise completely the converted dye, repetitive pipetting was applied

and the plate was stirred on an automatic plate shaker in the dark at RT. The absorbance was measured at 570 nm (using 620 nm as the background wavelength), using a plate reader spectrophotometer. The percentage of absorbance for each treated sample was normalized to that of the untreated control cells.

Calculations

For each well, the absorbance was expressed as:

$Absorbance\ 570\ nm - Absorbance\ 620\ nm.$

The results were expressed as percentage of MTT reduction:

$$MTT\ reduction\ (\%) = \frac{Absorbance\ treated\ wells}{Absorbance\ control\ wells} \times 100\%.$$

The IC_{50} values (i.e. concentration of PS that reduces cell survival by 50%) were calculated using non-linear regression analysis, sigmoidal dose-response curves (using GraphPad Prism) as shown in the equation below:

$$MTT\ reduction\ (\%) = Bottom + \frac{Top - Bottom}{1 + 10^{(log\ IC_{50} - log\ [PS]) \times Hillslope}}.$$

Herein, *Bottom* represents the maximum value of response (maximum percent of MTT reduction) and *Top* is the minimum value of response (minimum percent of MTT reduction). The *log* IC_{50} is the log of the PS concentration ([PS]) that responses midway between *Top* and *Bottom*. The *Hillslope* is the steepness of the curve.

3.2.7.2. Trypan blue assay

Principle

Trypan blue is an organic amine dye that is excluded by living cells with intact membranes, whereas dead or dying cells with compromised plasma membrane integrity take up the dye. Therefore, all the cells that exclude the dye are considered viable and appear brilliant under the microscope. By contrast, cells with damaged membranes appear with a distinctive blue color readily observed under the microscope [11].

Protocol

To check cell viability before plating the cells, they were trypsinized and resuspended in medium (as described in Part III, 3.2.1 and 3.2.2). Then, 20 µL of cell suspension and 20 µL of trypan blue stain were gently mixed, and the cells were counted using a haemocytometer. The percentage of viable cells and the concentration of viable

cells per milliliter of cell suspension were calculated. Only cells with viability above 90% were used in all experiments. To check cell viability after PDT experiments, the UM-UC-3 and HT-1376 cells were plated at a density of 8.9 x 10^4 cells per well (259 µL per well), in 48-wells culture plates for 24 h before treatment. Next, the cells were treated with the photosensitizer and the photodynamic treatment was performed, as described in Part III, 3.2.3. Twenty four, 48, or 72 h after treatments, the cell suspension was diluted in the trypan blue stain and the cells were counted.

Calculations

Viable (bright cells) and nonviable cells (cells stained in blue) were counted and summed for the total number of cells. The viability was calculated as follows:

$$Viable\ cells\ (\%) = \frac{Number\ of\ viable\ cells}{Number\ of\ total\ cells} \times 100.$$

The concentration of viable cells per milliliter in the cell suspension was calculated considering the average of viable cells (*VCs*) per each counting square, the dilution made and the volume of each counting square:[20] $\frac{Viable\ cells}{mL} = \frac{VCs \times dilution\ factor}{1 \times 10^{-4}}$.

3.2.8. Galactose blocking assays

Principle

The possible involvement of galectins (galactose binding proteins) in the uptake (and consequent phototoxicity) of PSs conjugated with galactose molecules can be indirectly assessed by "blocking" the galectin binding sites with galactose.

Protocol

The UM-UC-3 and HT-1376 cells were plated at a density of 3 x 10^4 cells per well (100 µL per well), in 96-wells culture plates for 24 h before treatment. On the following day, the cells were incubated in the presence of 50 nM galactose in PBS for 1.5 h, in an incubator at 37 ºC with 5% CO_2 and 95% air. The uptake of the galacto-conjugates was determined by fluorometry, as described in Part III, 3.2.4. The effect of galactose on cell

[20] Considering the volume of each counting square to be 0.1 mm^3, the same as 1 x 10^{-4} mL.

viability was evaluated 24 h after photodynamic therapy by the MTT viability assay, as described in Part III, 3.2.7.

3.2.9. Intracellular levels of Reactive Oxygen Species after Photodynamic assays

Principle

The ROS generation after PDT can be detected using the dichlorofluorescein (H_2DCFDA) [14] and the dihydroethidium (DHE) [15] probes, by fluorescence microscopy and fluorescence spectroscopy techniques. H_2DCFDA is able to cross the cell membrane and their acetate groups are removed by intracellular esterases, producing H_2DCF. H_2DCF reacts with several cytotoxic oxygen species producing DCF that can be used as a measure of intracellular ROS levels. DHE probe diffuses across cell membrane, exhibiting blue fluorescence. In the presence of ROS (particularly superoxide anion) this probe is oxidized to ethidium, which intercalates within the cell´s DNA, staining the nucleus with bright red fluorescence.

The intracellular fluorescence of the probes was normalized to total protein quantity.

Protocol: Reactive oxygen species evaluation by fluorimetry

The UM-UC-3 and HT-1376 cells were plated at a density of 3 x 10^4 cells per well (100 µL per well), in 96-wells black plates for 24 h before treatment. Immediately after photodynamic treatment and washings, cells were incubated with either 2 µM or 5 µM of H_2DCFDA or DHE[21] in PBS (in dark conditions) for 1 h at 37°C. The excitation and emission filters used for the H_2DCFDA probe were 485/20 nm and 528/20 nm, respectively. For the DHE probe, the excitation and emission filters used were 485/20 nm and 590/35 nm, respectively. After fluorometric measurement, cells were lysed with 1% (m/v) SDS solution in PBS (pH 7.0) and total protein concentration was determined as previously described (Part III, 3.2.4).

[21] H_2DCFDA and DHE were prepared in DMSO as stock solutions with a concentration of 5 mM, under a nitrogen atmosphere. The stock solutions were then kept in the dark at -20 ºC.

Protocol: Reactive oxygen species evaluation by fluorescence microscopy

Coverslips were coated with poly-L-lysine (diluted 1:10, by volume, in sterile PBS) for 1 h at RT. The UM-UC-3 and HT-1376 cells were plated carefully at a density of 1.8 x 10^5 cells or 3.6 x 10^5 cells per well (2 mL per well), respectively, in 12-wells culture plates for 24 h before treatment. The cells were treated with the photosensitizer and the photodynamic treatment was performed. After PDT treatments, cells were incubated with 5 μM of H_2DCFDA or DHE in PBS (in dark conditions) for 1 hour at 37°C. The cells were washed twice for 5 min each in PBS. After that, the cells were fixed in 4% PFA for 10 min at RT. The samples were washed with PBS (3 x 5 min). The coverslips were mounted using the VectaSHIELD mounting medium, sealed with nail polish and stored at 4 ºC until visualization under the fluorescence microscope.

3.2.10. Redox quenching assays

Principle

The role of type I and type II oxidative mechanisms in cell toxicity after PDT, can be evaluated using specific quenchers of $^1O_2$ (sodium azide [16] and histidine [17]) and free radical scavengers (cysteine [18]), respectively.

Protocol

The UM-UC-3 and HT-1376 cells were plated at a density of 3 x 10^4 cells per well (100 μL per well), in 96-wells black plates for 24 h before treatment. Immediately after PS uptake, the cells were washed and the redox quenchers (sodium azide, histidine and cysteine at concentration of 50 nM in growth culture medium) were added to the cells. After incubation with the redox quenchers for 10 min, the photodynamic treatment (in the presence of the redox quenchers) was performed. The effect of the presence of quenchers on cell viability was evaluated 24 h after photodynamic therapy by the MTT viability assay.

3.2.11. F-actin staining after Photodynamic assays

Principle

The changes induced by the photo-activated PS on actin microfilaments can be determined using the fluorescent conjugate tetramethylrhodamine isothiocyanate (TRITC)-labelled phalloidin[19]. Phalloidin is a fungal toxin that binds to polymeric and oligomeric forms of F-actin and stabilizes the actin filaments.

Protocol

Coverslips were coated with poly-L-lysine (diluted 1:10, by volume, in sterile PBS) for 1 h at RT. The UM-UC-3 and HT-1376 cells were plated carefully at a density of 1.8 x 10^5 cells or 3.6 x 10^5 cells per well (2 mL per well), respectively, in 12-wells culture plates for 24 h before treatment. The cells were treated with the photosensitizer and the photodynamic treatment was performed. After PDT treatments, the cells were fixed in 4% PFA for 10 min at RT. The samples were washed with PBS (3 x 5 min). To visualized F-actin staining, the cells were incubated in darkness with 0.20 µM of TRITC-phalloidin in PBS for 40 min at room temperature. After washing with PBS, coverslips were mounted using the VectaSHIELD mounting medium, sealed with nail polish and stored at 4 ºC until visualization under the fluorescence microscope.

3.2.12. Western Blotting assays

Principle

The presence of specific proteins in a complex mixture extracted from cells can be performed by Western Blotting using specific antibodies. Moreover, with this technique it is possible to quantify the levels of the proteins. For that, denaturated proteins present in the mixture are separated in a polyacrylamide gel by electrophoresis, accordingly to their size, following the methodology of Laemmli [20]. Then, the separated proteins in the gel are electrotransferred to a membrane using the method of Towbin [21] and a specific unlabeled antibody is used to stain the target antigen. After wash, a labeled secondary antibody is used to detect the presence of the primary antibody, and thus the target protein. The proteins can be visualized as bands, using the ECL (enhanced chemiluminescence) detection method. For ECL detection, the horseradish peroxidase (HRP), which is

conjugated with the secondary antibody, in the presence of hydrogen peroxide and an enhancer, catalyzes the oxidation of luminol, emitting light. The emitted light can be detected using a CCD camera for light capture.

Protocol: Sample preparation of UM-UC-3 and HT-1376 cells (adherent cells)

For immunodetection of proteins associated to cell death after PDT, the HT-1376 cells were plated at a density of 4 x 10^5 cells or 8 x 10^5 cells per well (2.5 mL per well), respectively, in 6-wells culture plates for 24 h before treatment. The cells were then treated with the photosensitizer and the photodynamic treatment was performed. After treatment, the cells were washed twice with ice-cold PBS and lysed by addition of ice-cold RIPA buffer with fresh protease inhibitors (500 µL of buffer was used per 5 x 10^6 cells, per 60 mm of Petri dish or per 75 cm^2 flask). The cell lysates were then transferred to microtubes with the help of a rubber policeman (cell scrapper) and incubated on ice during 30 min. During incubation, samples were vortexed 10 sec every 10 min.[22] The total cell lysates were centrifuged at 18,000 *x g* for 16 min, at 4 ºC. The supernatant was transferred to a new microcentrifuge tube. The supernatants were used for protein concentration determination, followed by denaturation with Laemmli buffer.

Protocol: Sample preparation of CSCs HT-1376 (cells growing in suspension)

The cells were pipetted into a fresh conical tube and placed on ice. The cells were centrifuged on low speed at 4 ºC and the medium was aspirated. Ten mL of ice cold PBS was added to the cell pellet and the tube was gently inverted to wash the cells. The cells were again centrifuged on low speed and the supernatant was aspirated. The washing and aspiration was repeated. Ice cold RIPA buffer with fresh protease inhibitors was added to the cells (500 µL of buffer was used per 60 mm of Petri dish or per 75 cm^2 flask). The cell suspension was transferred to a clean microtube and incubated on ice during 30 min. During incubation, samples were vortexed 10 sec every 10 min. The cell lysates were clarified by spinning for 16 min at 18,000 *x g*, at 4 ºC. The supernatant was transferred to a new microcentrifuge tube and the supernatants were used for protein concentration determination, followed by denaturation with Laemmli buffer.

[22] These vortex steps are important for the cell disruption.

Protocol: Determination of total protein

The protocol used for the determination of protein concentration was the same as described in Part III, 3.2.4, with some differences:

The samples were diluted in RIPA buffer 1:9 (by volume) and in a 96-wells plate, the following solutions were pipetted to each well:

- 25 µL of sample buffer: RIPA buffer,

- 25 µL of sample, blank (sample buffer), standard (prepared in the sample buffer at concentrations ranging from 12.5-800 $\mu g.mL^{-1}$ using the BSA standard at 2 $mg.mL^{-1}$),

- 200 µL of BCA working Reagent (50 parts of BCA reagent A mixed with one part of BCA reagent B).

Protocol: Sodium Dodecyl Sulfate Polyacrylamide Gel Electrophoresis and Blotting

After determination of protein concentration, the samples were denaturated with 6x Laemmli buffer. The samples were heated at 37 ºC for 30 min, or boiled during 5 min at 95 ºC. Sixty µg of protein samples was loaded on 10% or 12% polyacrylamide gels and the proteins were separated by electrophoresis. The electrophoresis was stopped when the dye front reached the bottom of the gel.

Following gel electrophoresis, the separated protein mixtures were transferred to a solid support for further analysis. The polyvinylidene difluoride membranes (PVDF) were first activated with 100% MeOH, and then soaked in Milli-Q water and equilibrated in transfer buffer. All the material used in the blotting (sponges, sheets of filter paper), as well as the gels were also equilibrated in transfer buffer. The gel and the PVDF membrane were assembled into a sandwich along with sheets of filter paper and sponges. The separated proteins were then transferred to the PVDF membranes (using ice cold transfer buffer) for 90 min under agitation, with the tank in ice (and using a cooling coil inside the tank). At the end, the baking of the membranes was performed by incubation at 50 ºC for 20 min.

Protocol: Antibodies incubations, detection and quantification

The membranes were placed into blocking buffer for 1 h at RT with gentle agitation. The membranes were incubated with the primary antibody (diluted in the blocking buffer) for 2 h at RT, under low agitation. After incubation, the membranes were rinsed in TBST

(3 x 10 min) at RT. The appropriate secondary antibody conjugated with the enzyme horseradish-peroxidase diluted 1:10,000 (v/v) in 2.5% non-fat milk (prepared in TBST) was added, and the membranes were incubated for 1 h at RT, under moderate agitation. After incubation with the secondary antibodies, the membranes were washed in TBST (3 x 10 min), with agitation. To demonstrate equivalent protein loading, all the membranes were re-probed for the protein β-actin. For the detection, the membranes were placed on the chemiluminescence detection system[23] (proteins side up), incubated with the substrate solution (1:1, by volume, mixture of luminol/enhancer and peroxide buffer) for 1 min following manufacturer instructions, and then the images were acquired. The intensity signal of the bands was quantified using the software ImageJ 1.42q and the fold change in protein levels was expressed as follows and then normalized to the control situation:

$$Fold\ change\ in\ protein\ expression = \frac{Protein\ band\ density}{\beta-actin\ band\ density}.$$

3.2.13. Immunofluorescence assays

Principle

The distribution of specific proteins through the sample can be visualized by immunocytochemistry. First, the cells are fixed to retain their shape and structure (morphology) and location of all cellular proteins and to disable intrinsic proteolytic enzymes. The cells are then permeabilized with a mild detergent, so the antibodies could have access to the cytoplasm. After that, specific unlabeled primary antibody binds to the target molecule, and the secondary antibody (covalently attached to a fluorophore) recognizes the primary antibody. At the end, the images can be obtained using a fluorescence microscope, showing the subcellular distribution of the protein of interest.

Protocol: Sample preparation, adherent cells (UM-UC-3 and HT-1376 cells)

Coverslips were coated with poly-L-lysine (diluted 1:10, by volume, in sterile PBS) for 1 h at RT. UM-UC-3 and HT-1376 cells were plated at a density of 1.8 x 10^5 cells or 3.6 x 10^5 cells per well (2 mL per well), respectively, in 12-wells culture plates for 24 h

[23] To prevent drying, the membranes were placed in a nylon transparent sheet.

before treatment. For the treatments with the PSs, the cells were treated and the photodynamic treatment was performed.

Protocol: Sample preparation, suspension cells (CSCs HT-1376)

The HT-1376 spheres growing in suspension were collected to a microtube and centrifuged at 3,300 *x g* during 5 min. The cell pellet was washed twice with warm PBS.

Protocol: Fixation, permeabilization, blocking and incubation with the antibodies

After washing with PBS, the cells were fixed in 4% PFA for 10 min at RT. The samples were washed with PBS (3 x 5 min). The cells were treated with permeabilization buffer during 10 min. Then, the cells were washed with washing buffer, for 5 min. The cells were incubated with the blocking buffer[24] for 30 min, in a humidified chamber. After blocking, the cells were incubated with the primary antibody diluted in PBST buffer during 1 h at RT, in a humidified chamber. The primary antibody solution was decanted and the samples were washed with washing buffer (3 x 5 min). The cells were incubated with the secondary antibody and DAPI (1 $\mu g.mL^{-1}$) diluted in PBST buffer for 1 h (at RT) in a humidified chamber in the dark. The cells were washed in the dark three times with the washing buffer, 5 min each wash. The coverslips were mounted using the glycergel mounting medium and sealed with nail polish. The samples were stored in an appropriate box at 4 ºC until acquisition of images by fluorescence microscopy.

[24] For the antigen CD44, the blocking buffer was goat serum. For the other antigens, the blocking buffer was BSA.

References

1. Swinehart, D. F. *The Beer-Lambert Law*. J Chem Educ, **1962**, 39(7), p. 333.
2. Spiller, W.; Kliesch, H.; Wohrle, D.; Hackbarth, S.; Roder, B. and Schnurpfeil, G. *Singlet oxygen quantum yields of different photosensitizers in polar solvents and micellar solutions*. J Porphyr and Phthalocya, **1998**, 2(2), p. 145-158.
3. Seybold, P. G. and Gouterma.M. *Porphyrins. Fluorescence Spectra and Quantum Yields*. J Mol Spectrosc, **1969**, 31(1), p. 1.
4. Oda, K.; Ogura, S. and Okura, I. *Preparation of a water-soluble fluorinated zinc phthalocyanine and its effect for photodynamic therapy*. J Photoch Photobiol, **2000**, 59(1-3), p. 20-25.
5. Zhang, Y. Z.; Zhou, B.; Zhang, X. P.; Huang, P.; Li, C. H. and Liu, Y. *Interaction of malachite green with bovine serum albumin: determination of the binding mechanism and binding site by spectroscopic methods*. J Hazard Mater, **2009**, 163(2-3), p. 1345-1352.
6. Bullous, A. J.; Alonso, C. M. A. and Boyle, R. W. *Photosensitiser-antibody conjugates for photodynamic therapy*. Photoch Photobiol Sci, **2011**, 10(5), p. 721-750.
7. Tome, J. P. C.; Neves, M. G. P. M. S.; Tomes, A. C.; Cavaleiro, J. A. S.; Soncin, M.; Magaraggia, M.; Ferro, S. and Jori, G. *Synthesis and antibacterial activity of new poly-S-lysine-porphyrin conjugates*. J Med Chem, **2004**, 47(26), p. 6649-6652.
8. Voller, A.; Bartlett, A. and Bidwell, D. E. *Enzyme Immunoassays with Special Reference to Elisa Techniques*. J Clin Pathol, **1978**, 31(6), p. 507-520.
9. Marvin, L. F.; Roberts, M. A. and Fay, L. B. *Matrix-assisted laser desorption/ionization time-of-flight mass spectrometry in clinical chemistry*. Clin Chim Acta, **2003**, 337(1-2), p. 11-21.
10. Arpino, P. J. *Combined Liquid-Chromatography Mass-Spectrometry (Lc/Ms) - a Review*. NATO ADV SCI I C-MAT, **1992**, 353, p. 253-267.
11. Freshney, R. I., *Culture of Animal Cells: A Manual of Basic Technique*. 1987: A.R. Liss.
12. Smith, P. K.; Krohn, R. I.; Hermanson, G. T.; Mallia, A. K.; Gartner, F. H.; Provenzano, M. D.; Fujimoto, E. K.; Goeke, N. M.; Olson, B. J. and Klenk, D. C. *Measurement of protein using bicinchoninic acid*. Anal Biochem, **1985**, 150(1), p. 76-85.
13. Mosmann, T. *Rapid colorimetric assay for cellular growth and survival: application to proliferation and cytotoxicity assays*. J Immunol Methods, **1983**, 65(1-2), p. 55-63.
14. Chandel, N. S.; Maltepe, E.; Goldwasser, E.; Mathieu, C. E.; Simon, M. C. and Schumacker, P. T. *Mitochondrial reactive oxygen species trigger hypoxia-induced transcription*. Proc Natl Acad Sci U S A, **1998**, 95(20), p. 11715-11720.
15. Fernandes, R.; Hosoya, K. and Pereira, P. *Reactive oxygen species downregulate glucose transport system in retinal endothelial cells*. Am J Physiol Cell Physiol, **2011**, 300(4), p. C927-936.

16. Bancirova, M. *Sodium azide as a specific quencher of singlet oxygen during chemiluminescent detection by luminol and Cypridina luciferin analogues*. Luminescence, **2011**, 26(6), p. 685-688.
17. Hara, K.; Holland, S. and Woo, J. *Effects of Exogenous Reactive Oxygen Species Scavengers on the Survival of Escherichia coli B23 during Exposure to UV-A radiation*. J Exp Microbiol Immunol, **2004**, 12, p. 62-66.
18. Aruoma, O. I.; Halliwell, B.; Hoey, B. M. and Butler, J. *The antioxidant action of N-acetylcysteine: its reaction with hydrogen peroxide, hydroxyl radical, superoxide, and hypochlorous acid*. Free Radic Biol Med, **1989**, 6(6), p. 593-597.
19. Sanz-Rodriguez, F.; Casas, A.; Gonzalez, S.; Espada, J.; Jaen, P.; Regadera, J.; Blazquez-Castro, A.; Zamarron, A.; Bagazgoitia, L.; de la Cruz, C. I. and Juarranz, A. *Preclinical photodynamic therapy research in Spain. 4. Cytoskeleton and adhesion complexes of cultured tumor cells as targets of photosensitizers*. J Porphyr and Phthalocya, **2009**, 13(4-5), p. 552-559.
20. Laemmli, U. K. *Cleavage of structural proteins during the assembly of the head of bacteriophage T4*. Nature, **1970**, 227(5259), p. 680-685.
21. Towbin, H.; Staehelin, T. and Gordon, J. *Electrophoretic transfer of proteins from polyacrilamide gels to nitrocellulose sheets: procedure and some applications*. Proc Nat Acad Sci USA, **1979**, 76, p. 4350-4354.